FRP Thermal Properties and Fire Performance for Building Exterior Applications

A Major Qualifying Project Report
Submitted to the Faculty
of the
WORCESTER POLYTECHNIC INSTITUTE
in partial fulfillment of the requirements for the
Degree of Bachelor of Science
By:

_____

Jacob Czarnowski

_____

Kristen Nich

_____

Kristina Zichelli

April 2013

Project: NAD FT12

_____

Professor Nicholas A. Dembsey, Advisor

Abstract

Fiber reinforced polymers (FRPs) are becoming more prevalent as a building material due to their versatility and ease of installation. For building exterior envelope applications, FRPs provide potential benefits relative to limited heat transmission but are also a potential hazard due to fire spread. In order to be used in exterior envelopes, sheathing materials are required by the International Building Code (IBC) to meet a range of criteria to ensure that fire cannot spread from floor to floor over the envelope. One criterion is based on the costly full-scale NFPA 285 test which measures flame height of the sheathing material when subjected to an open flame over time.

This project studied heat transfer and flame spread characteristics of five FRPs using Cone Calorimeter testing (ASTM E1354). Using data collected from the Cone and additional data gathered from thermocouples placed throughout the specimens during testing, a procedure was developed to estimate thermal properties of the FRPs during the early stages of heating when the materials have nominal inert behavior.

Using existing 2D spill plume and flame height theories, and data collected from an NFPA 285 test involving one of the five FRPs, a screening tool was created that will allow manufacturers to predict the outcome of a full-scale NFPA 285 test. The screening tool uses FRP Cone data to predict sheathing material flame height. Given the low cost of Cone testing the screening tool will allow FRP manufacturers to reduce the cost of material development.

Organization of this MQP

This MQP is a 20 page conference paper that focuses on the use of Cone Calorimeter data to estimate thermal properties of fiber reinforced polymers. Chapter 3 focuses on the estimation of the thermal conductivity and specific heat of the material based on early time Cone data. Chapter 4 focuses on the development of a flame length correlation that can be used to estimate the result of a NFPA 285 test. It also includes a proposed change to the building code as part of a capstone design exercise. Briefings with more specific information regarding the process and results that could not be covered in the conference style paper are included in the appendix.

Acknowledgements

We would like to thank the following parties, without whom, we would not have been able to complete this project:

Kreysler and Associates – for supplying testing materials and allowing us to see test results, without which, this project would not be possible

Creative Pultrusions – for supplying testing materials

Professor Dembsey – for advising our project; without his guidance, we would never had been able to complete this project

Randy Harris – for his assistance in the WPI fire lab, as well as for coordinating with everyone to schedule testing

Authorship

Paper

Abstract – Jacob, Kristen, Kristina

Introduction – Jacob and Kristen

Background – Jacob, Kristen, Kristina

Property Estimation – Jacob

285 Flame Length Correlations - Kristen

Conclusion – Jacob and Kristen

Appendices

Semi-Infinite Solid Brief – Kristina

Property Estimation Brief - Jacob

Flame Length Correlations Brief - Kristen

Building Code Update Brief - Kristen

Raw Cone Data - Jacob, Kristen, Kristina

Table of Contents

Abstract 1
Organization of this MQP 1
Acknowledgements 2
Authorship 3
1.0 INTRODUCTION 5
2.0 LITERATURE REVIEW 6
2.1 Fire Test Standards 6
2.2 International Building Code Requirements 7
2.3 Existing 2D Spill Plume Theory 8
3.0 FRP PROPERTY ESTIMATION 8
3.1 Semi-Infinite Solid Method 8
3.2 Finite Difference Method 9
Limitations 9
Model Verification 10
3.3 Error in the Temperature Measurements 10
3.4 Procedure and Results 10
Boundary Condition 1 11
Boundary Condition 2 12
Boundary Condition 3 14
3.5 Comparison of Results 15
4.0 NFPA 285 SCREENING TOOL 16
4.1 Development of Calibration Model 16
4.2 Development of Test Model 18
4.3 Pyrolysis Zone Estimations 20
4.4 Proposed Building Code Update 21
5.0 CONCLUSIONS 22
REFERENCES 24
APPENDIX A: SEMI-INFINITE SOLIDS PROPERTY ESTIMATION BRIEFING 25
APPENDIX B: PROPERTY ESTIMATION BRIEFING 31
APPENDIX C: NFPA 285 FLAME LENGTH CORRELATIONS BRIEFING 63
APPENDIX D: BUILDING CODE MODIFICATIONS BRIEFING 92
APPENDIX E: RAW CONE DATA 95

1.0 INTRODUCTION

The use of Fiber Reinforced Polymers (FRPs) as an exterior sheathing material is a relatively new market that has been steadily growing in recent years. The advantages of this material include the wide customizability of the product, the ease of installation, and the low environmental impact it has in comparison to that of other building materials. However, as a result of this new application, it has not been tested as thoroughly as traditional building materials. Although FRP envelope systems have passed tests to allow them to be used for construction applications in accordance with building codes such as the International Building Code (IBC), the need exists for further research to determine their thermal properties and their behavior when ignited. This project sought to use information from a standardized bench scale test, the Cone Calorimeter Test (ASTM E 1354) to determine thermal properties of these materials, as well as to model the fire performance of FRPs. The project included the development of two different tools which accomplished these goals. The first is a property estimation tool which uses early time Cone data from before the sample has undergone any extensive degradation due to pyrolysis. The second tool is used to predict the result of a NFPA 285 test (Standard Fire Test Method for Evaluation of Fire Propagation Characteristics of Exterior Non-Load-Bearing Wall Assemblies Containing Combustible Components) based on a quasi-two dimensional spill plume model for the test.

The thermal property estimation tool uses heat transfer modeling compared to data from thermocouples placed throughout the sample in order to estimate the thermal conductivities and specific heats of each sample. To model the heat transfer, both an analytical solution (semi-infinite solids) and a numerical solution (explicit finite differences) are used to calculate a temperature distribution throughout the depth of the sample. Three thermocouples are then placed throughout the sample to gather exact temperature data throughout the sample. Finally, the thermal properties of each model are iteratively changed until the estimated temperature distribution matches the exact temperature distribution from the thermocouples. These values represent the estimated thermal properties for the particular material.

The NFPA 285 prediction tool uses proven two-dimensional spill plume theory to develop equations that will model the temperature at various heights in the plume above the test burners based on heat release rate per unit length. This tool will allow manufacturers to predict whether a material will comply with NFPA 285 before performing the test and risking having to bear the heavy economic penalties associated with testing of a material that does not comply. In addition, tools for predicting the dimensions of the pyrolysis area of the specimen in the NFPA 285 test were developed using heat release rate per unit area data gathered from Cone testing. Finally, an update to the building code was proposed which includes a pass/fail prediction curve. This curve was created through calculation of the maximum allowable heat release rate per unit length of the burning wall in a NFPA 285 test. This tool will allow code users to predict the pass/fail status of their material based on knowledge of the heat release rate per unit area and pyrolysis height.

2.0 LITERATURE REVIEW

2.1 Fire Test Standards

The ASTM E 1354 Cone Calorimeter Test is a bench scale test that uses a constant incident heat flux to heat a horizontal sample to ignition (ASTM E 1354, 2011). Before and after ignition, observations are recorded and heat release rate and mass loss data are collected. The data leading up to ignition is not typically used, but has potential to be analyzed to discover thermal properties of the sample.

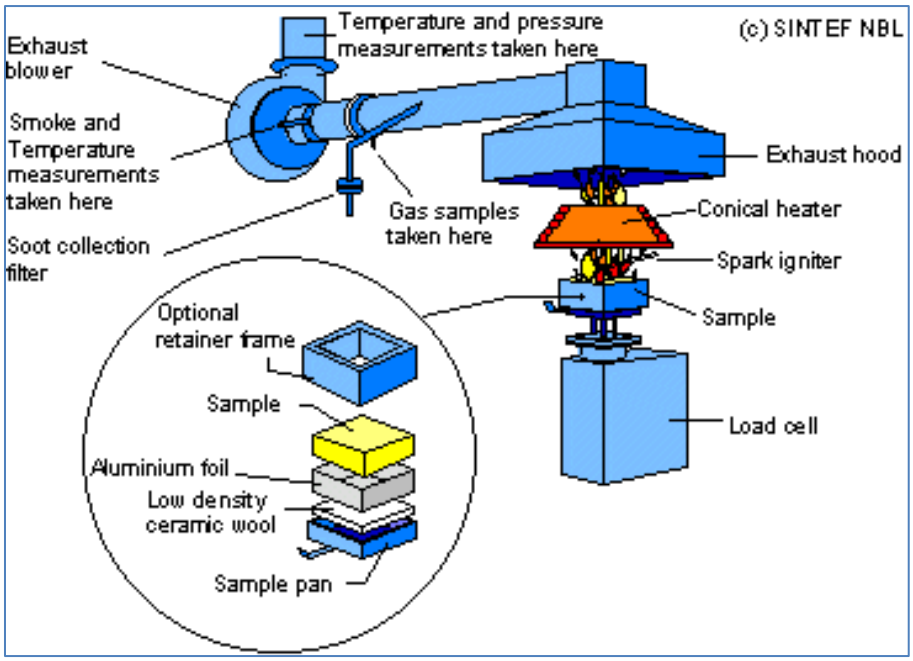

Figure 2.1.1: Diagram of Cone Calorimeter (SINTEF).

Figure 2.1.1 depicts a typical cone calorimeter like the one used in this project. The sample is prepared as shown in the zoomed in portion of the diagram, and placed on the load cell. The spark igniter is placed over the sample and a shutter separating the heater from the sample is opened. The igniter is removed when sustained flaming occurs. The Cone test is versatile, as samples can be tested in a horizontal or vertical position, and at various irradiance levels. Samples are typically 0.1016 meters by 0.1016 meters (4 inches by 4 inches), but other sizes can be tested (ASTM E 1354, 2011).

The NFPA 285 test is a full-scale fire test intended to determine if a material is safe for use in building construction based on its flame propagation characteristics (NFPA 285, 2012). If manufacturers could predict their material's performance based on the test's acceptance criteria, which is written with a pass/fail approach, they could reduce costs by testing only materials which are sure to pass. This project focused on the test specimen performance criteria for the exposed face material of the wall assembly, as stated in the NFPA 285 test standard.

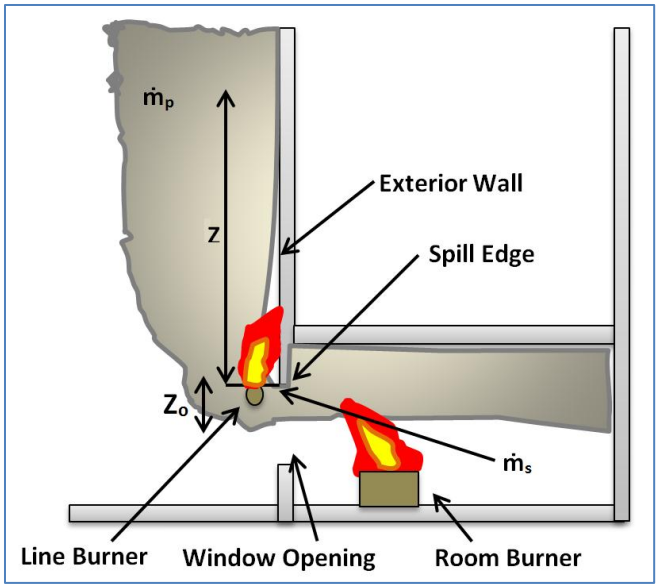

Figure 2.1.2: Diagram of NFPA 285 test geometry

Figure 2.1.2.1.2 shows the general configuration of the NFPA 285 test. The test specimen is a two-story structure that includes two compartments. The first story room includes one window opening. Two gas burners are used during the test; one inside the first story room and one line burner centered horizontally at the top of the window opening (see Figure 2.1.2). The test apparatus is calibrated to determine the gas flow rate necessary for each burner to reach the required temperatures and heat fluxes. Thermocouples installed on the sample are used to record temperature data at different locations on the wall (NFPA 285, 2012).

The 30 minute test includes six time steps, each 5 minutes long. At the start of the test, the gas supply for the room burner is turned on, and the burner is ignited. After the first 5 minute time step, the window line burner is ignited. At the end of the 30 minute test, both gas supplies are turned off.

The test is videotaped, and temperature data and visual observations are recorded. Temperatures at each thermocouple location and gas flows of the burners are recorded at a minimum of every 15 seconds and the video, temperature data collection, and visual observations are stopped only when 10 minutes have passed after the gas supply is turned off, even if residual burning has stopped (NFPA 285, 2012).

A material complies with the acceptance criteria of NFPA 285 if flame propagation is limited both vertically and horizontally as prescribed. A main requirement for acceptance, which this project focused on, is that the temperature at a height of 3.05 m (10 feet) does not exceed 537.8°C (1000°F), indicating that flames do not reach this height (NFPA 285, 2012).

2.2 International Building Code Requirements

The building industry is a highly regulated field which uses code and standards to ensure the safety of buildings. All aspects of a construction project must comply with these codes and standards in order to be legally built and approved for occupancy. One example of a building code is the International Building Code (IBC) which is a prescriptive building code widely used by jurisdictions throughout the United States, as well as many other countries (International Building Code, 2012). It is produced by the International Code Council (ICC) and is updated every three years. As stated above, the IBC is

prescriptive, and different locations use amended versions based on what the authority having jurisdiction (AHJ) requires, in order to ensure appropriate, relevant requirements.

Chapter 26 of the 2012 IBC is devoted to defining the acceptable use of plastic building materials and includes a section regarding the exterior use of FRPs. According to section 2603.5.5, FRPs to be used as the exterior envelope of a building of any type of construction must pass the criteria of the NFPA 285 test. The one exception is if the building is less than 40 feet high with fire blocking installed. Therefore, it is important for many material developers to be able to pass this test so that their product may be installed on the exterior of buildings (International Building Code, 2012).

2.3 Existing 2D Spill Plume Theory

For the purposes of this project, the geometry of the NFPA 285 test was considered to be nominally two-dimensional. Therefore, 2D spill plume theory was used in the research and development of our NFPA 285 test model. Experimentation with line burner plumes, which can be considered two-dimensional, was conducted by Li-Ming Yuan and G. Cox in 1996, and the results of this experiment suggested that the plume above a line fire could be divided into 3 regions: continuous flame, intermittent flame, and thermal plume (Yuan & Cox, 1996). The general form of the equation for these regions includes change in centerline temperature of the plume and a normalized height above the burner based on heat release rate per unit length, as follows:

$$\Delta T_m = B\left(\frac{z}{Q_l^{2/3}}\right)^{2n-1} \qquad 2.3.1$$

In the theory presented by Yuan and Cox, the constant, B, and exponent, 2n-1, are adjusted to different values in order to reflect the 3 regions of the line burner plume. A similar theory and equation was used to develop the model for the NFPA 285 test.

3.0 FRP PROPERTY ESTIMATION

In order to learn more about the thermal characteristics of FRPs and better utilize early time Cone data, two tools were created to estimate the thermal conductivity (k) and specific heat (C_p) in a sample during a test. Both tools use thermocouple data from thermocouples that were installed on the samples during the test. These thermocouples were installed on the surface, at ½ the depth, and finally the back face of the sample. The test data used were tests which were run with the Cone set to 50 kW/m^2. Two different tests were run and the data was averaged. These averages for the thermocouple data were then used to estimate the properties for each sample. The first tool is a simplified model which uses a semi-infinite solid analysis of the FRP and compares the temperature distribution within the sample during the test to the thermocouple data. The second tool is a more complex version which uses a one dimensional finite difference analysis of the temperature distribution in the sample and also compares it to thermocouple data. When the temperatures for the prediction (semi-infinite or finite difference method) matched the temperatures of the thermocouples, the values for k and C_p were considered to be correct.

3.1 Semi-Infinite Solid Method

The first property estimation method uses a semi-infinite solids analysis to model the material. The semi-infinite solid boundary condition assumes a constant heat flux at the surface with convective and radiative cooling. The equation, as defined by Carslaw and Jaeger, 1965 is:

$$T = T_o + \frac{\dot{q}''}{h_{tot}} erfc\left(\frac{x}{2\sqrt{\alpha t}}\right) - \frac{\dot{q}''}{h_{tot}} exp\left(\frac{h_{tot}}{k} + \frac{h_{tot}^2 \alpha t}{k^2}\right) erfc\left(\frac{x}{2\sqrt{\alpha t}} + \frac{h_{tot}\sqrt{\alpha t}}{k}\right) \qquad 3.1.1$$

The detailed derivation for this equation can be found in Appendix B (Carslaw and Jaeger, 1965).

3.2 Finite Difference Method

The second property estimation method uses a one dimensional finite difference analysis (Olver, 2013). The set-up of the test (as seen in Figure 3.2.1) is to place the sample on top of three ½ inch thick pieces of ceramic fiberboard. Twenty four nodes were then distributed throughout both materials. The first node is the surface of the sample, the third node is at ½ depth, the fifth node is at the interface between the sample and the fiberboard, and finally the twenty fourth node is the back face of the fiberboard.

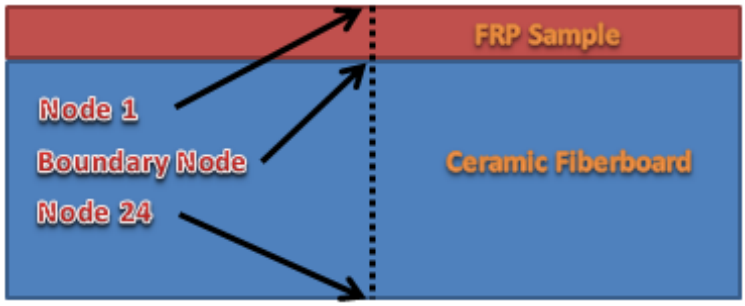

Figure 3.2.1: Node placement diagram

Two different boundary conditions for the surface node (node one) were used during the property estimation. The first was simply to use the thermocouple data from the surface of the sample as the temperature. The second boundary condition, as seen in Equation 3.2.1, involves a constant incident heat flux, as well as radiative and convective heat losses. Equation 3.1.1 uses a combined h value ($h_{total}=h_{conv}+h_{rad}$).

$$T_o^{p+1} = 2Fo\left(\frac{\Delta x \varepsilon \dot{q}''}{k} + T_{0+1}^{p} + BiT_\infty\right) + (1 - 2Fo - 2BiFo)T_o^{p} \quad 3.2.1$$

The equation for each interior node is shown in Equation 3.2.2 and only assumes conduction in and out of each node.

$$T_o^{p+1} = \mathrm{Fo}\left(T_{0-1}^{p} + T_{0+1}^{p}\right) + (1 - 2Fo)T_o^{p} \quad 3.2.2$$

The boundary condition for the back face of the fiberboard is heat loss only due to convection, as seen in Equation 3.2.3.

$$T_o^{p+1} = 2Fo\left(T_{0-1}^{p} + BiT_\infty\right) + (1 - 2Fo - 2BiFo)T_o^{p} \quad 3.2.3$$

T_o^{p+1} = Temperature at next time step [K]
F_o = Fourier number (dimensionless)
Δx = distance between nodes (0.002 m)
ε = emissivity of the sample (1)
q'' = heat flux per unit area of the cone (50 kw/m^2)
k = thermal conductivity [kW/mK]
T_{0+1}^{p} = Temperature at current time step at adjacent node [K]
Bi = Biot number (dimensionless)
T_∞ = ambient temperature [K]
T_o^{p} = Temperature at current time step [K]
T_{0-1}^{p} = Temperature at current time step at adjacent node [K]

Detailed derivations for each equation can be found in Appendix B.

Limitations

It is important to note the limitations of this estimation model, which are that it…

1. Does not assume surface degradation of sample due to pyrolysis,
2. Is only a 1 Dimensional analysis,
3. Assumes perfect conductivity between bottom of sample and fiberboard,
4. Assumes perfect conductivity between fiberboard pieces,
5. Assumes that the specimen is placed in a steel frame and placed on top of a load cell and the conduction through steel is assumed to be perfect with conductive losses to the load cell ignored.

Model Verification

When a finite difference analysis is used to solve for the temperatures in a solid, it is important to ensure that the model is written correctly. Therefore, these boundary conditions were verified using a semi-infinite solid analysis for a constant incident heat flux and convective and radiative losses (Carslaw and Jaeger, 1965) which is boundary condition 1. Figure 3.2.2 shows the solutions for the semi-infinite solid using equation 3.1.1. A detailed description of the verification, as well as the sample calculations can be found in Appendix B.

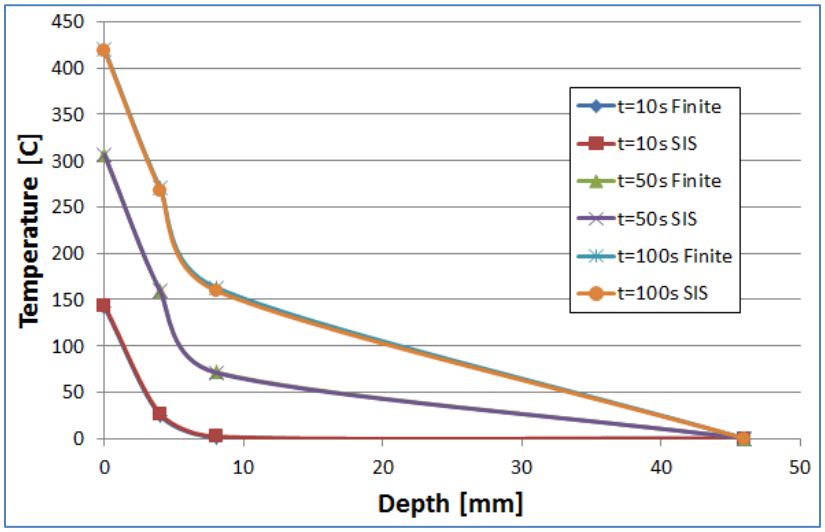

Figure 3.2.2: Temperature Profile for Model Verification (SIS stands for Semi-Infinite Solid)

Since the solutions are similar for the semi-infinite solid analysis and the finite difference analysis, it is assumed that the finite difference model was correctly modeled.

3.3 Error in the Temperature Measurements

While estimating the thermal properties of each material, it is important to note the uncertainty of the temperature measurements. The surface and back face thermocouples are both assumed to be fairly accurate (within ¼ mm), since they are located against a clearly defined surface. However, the middle thermocouple was inserted into a 1.5 mm hole that was drilled into the center of the sample, which leaves room for location error of the thermocouple due to bending of the drill bit. Therefore, in order to be as accurate as possible, a one millimeter thick dowel was inserted into each hole with a portion of the dowel outside of the hole. We then ensured that the angle of the protruding dowel was at a right angle to the side plane of the sample so that we could assume that the hole was also perpendicular to the side of the sample, and therefore at the desired depth. Finally, we inserted thermal grease into the hole with the thermocouple to ensure that the thermocouple was an accurate representation of the center of the sample. Despite these precautions, we still assume a location error of +/- one millimeter for the middle thermocouple, translating to an error of about 60 Kelvin.

3.4 Procedure and Results

Microsoft Excel software was used to run the calculations and a certain procedure was followed in order to estimate thermal properties of each sample in a consistent manner.

1. Open the Excel worksheet
2. Enter all known information such as volume and mass of the sample. The tool assumes ceramic fiberboard as a back insulation and its properties are already entered in the sheet.

3. Enter the thermocouple data from the cone calorimeter test. There should be thermocouple data for the top, middle, and bottom of the sample.
4. Assume an initial value of k and C_p to be 1 and 1000, respectively.
5. Run the "Transfer" macro (Ctrl+R) to transfer the values from the first sheet to the second sheet so they can be analyzed. Ensure that the dt is roughly 1 second. If not, the macro must be edited so it will take values for roughly each second.
6. Run the "Chart" macro (Ctrl+T) to create a graph of the thermocouple data and the temperature data from each node. If the lines for each region match, then the properties specified for k and C_p are correct.
7. If the lines do not match then run the "Clear" macro (Ctrl+E) and delete the chart
8. Navigate back to the first sheet and then adjust the values of k and C_p until the lines match up.

The three boundary conditions that were used can be seen in Table 3.4.1.

Table 3.4.1: Boundary Conditions

Boundary Condition	Model	Surface Condition	Back Face Condition
1	1-D Semi-Infinite	Constant Heat Flux with Convective and Radiative Losses	N/A
2	1-D Finite Difference	Surface Thermocouple Data	Convective Losses
3	1-D Finite Difference	Constant Heat Flux with Convective and Radiative Losses	Convective Losses

Boundary Condition 1

The temperature distribution and profile can be seen below in Figures 3.4.1 and 3.4.2, respectively. This graph is typical of the other samples that were tested. Results for property estimation using boundary condition 1 with the semi-infinite solids method are shown below in Table 3.4.2.The complete results of the other materials that were tested are listed in Appendix B.

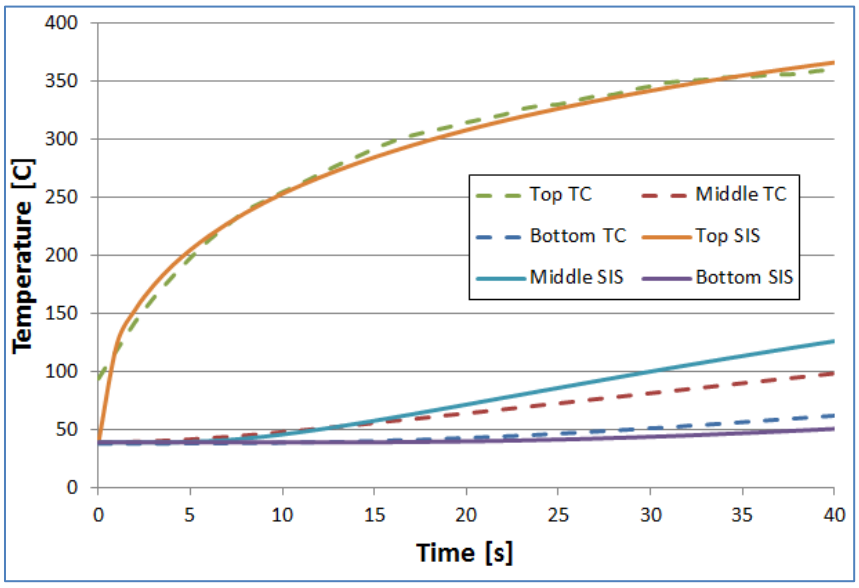

Figure 3.4.1: Temperature Distribution for Kreysler System 1, BC-1 (SIS stands for Semi-Infinite Solid)

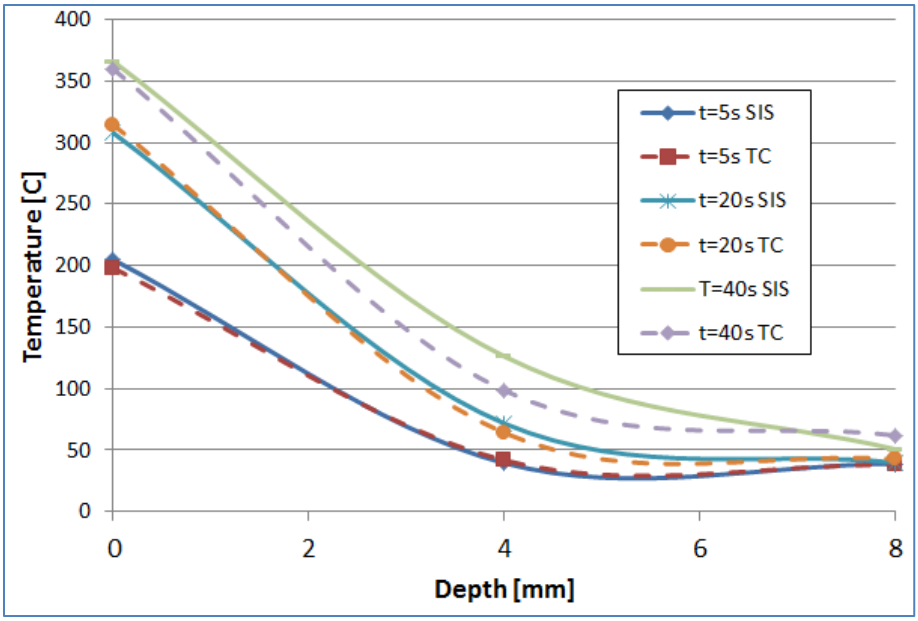

Figure 3.4.2: Temperature Profile for Kreysler System 1, BC-1 (SIS stands for Semi-Infinite Solids)

Table 3.4.2: Thermal Property Estimation Results for Boundary Condition 1

Material	Thermal Conductivity (W/m*K)	Specific Heat (J/kg*K)
Kreysler 1	0.28	700
Kreysler 2	0.3	700
CP 286	0.35	750
CP 702	0.33	750
CP 802	0.3	750

Boundary Condition 2

The temperature distribution and profile can be seen below in Figures 3.4.3 and 3.4.4, respectively. This graph is typical of the other samples that were tested. Results for property estimation using boundary condition 1 with the semi-infinite solids method are shown below in Table 3.4.3.The complete results of the other materials that were tested are listed in Appendix B.

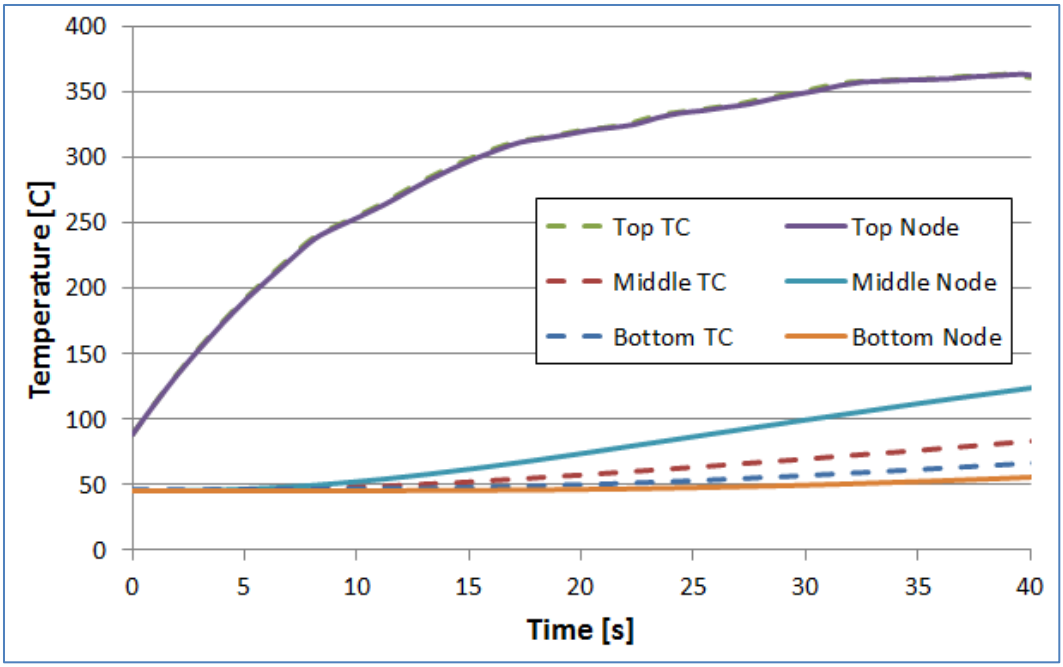

Figure 3.4.3: Temperature Distribution for Kreysler System 1, BC-2

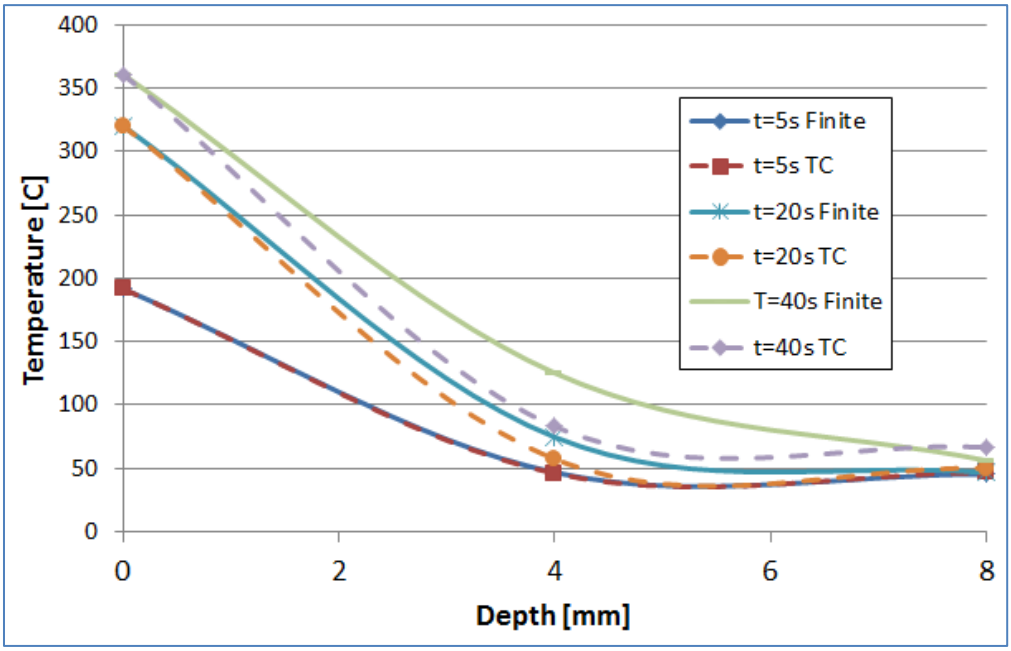

Figure 3.4.4: Temperature Profile for Kreysler System 1, BC-2

Table 3.4.3: Thermal Property Estimation Results for Boundary Condition 2

Material	Thermal Conductivity (W/m*K)	Specific Heat (J/kg*K)
Kreysler 1	0.28	800
Kreysler 2	0.26	750
CP 286	0.28	800
CP 702	0.3	800
CP 802	0.33	800

Boundary Condition 3

The temperature distribution and profile can be seen below in Figures 3.4.5 and 3.4.6, respectively. This graph is typical of the other samples that were tested. Results for property estimation using boundary condition 1 with the semi-infinite solids method are shown below in Table 3.4.4.The complete results of the other materials that were tested are listed in Appendix B.

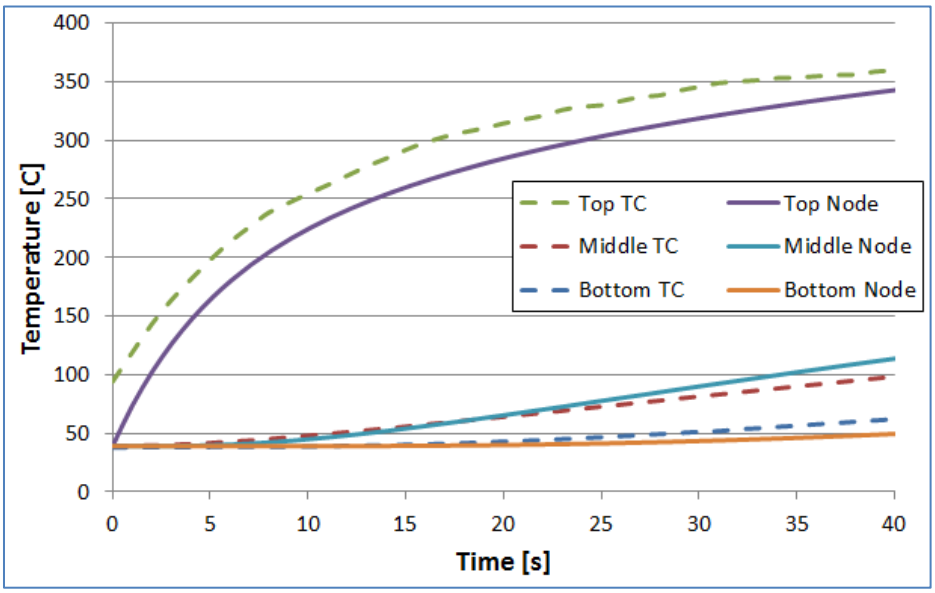

Figure 3.4.5: Temperature Distribution for Kreysler System 1, BC-3

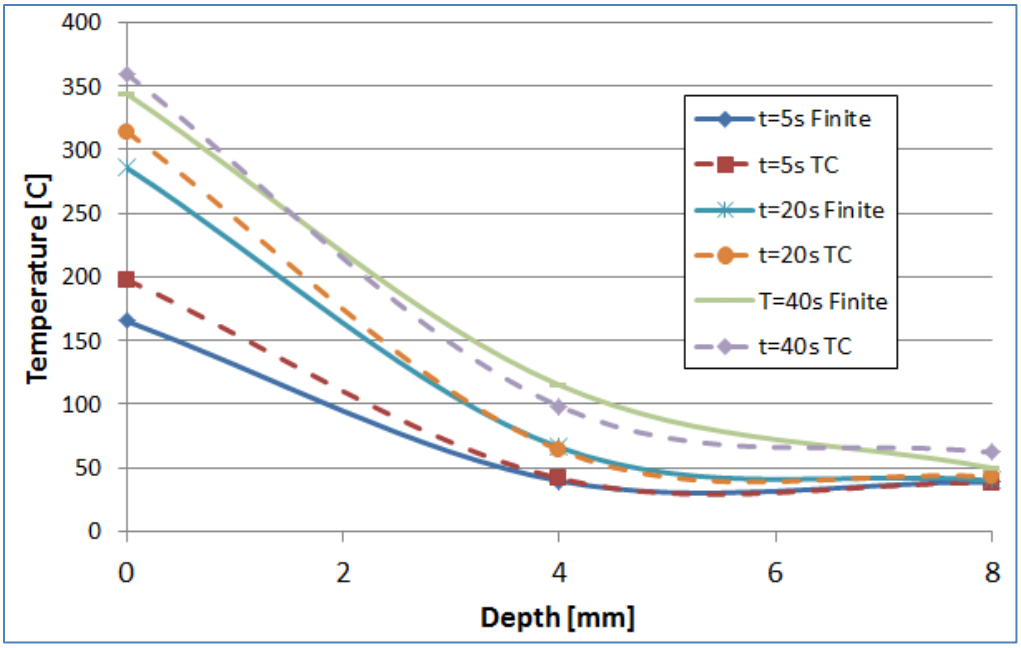

Figure 3.4.6: Temperature Profile for Kreysler System 1, BC-3

Table 3.4.4: Thermal Property Estimation Results for Boundary Condition 3

Material	Thermal Conductivity (W/m*K)	Specific Heat (J/kg*K)
Kreysler 1	0.3	800
Kreysler 2	0.22	800
CP 286	0.25	800
CP 702	0.26	800
CP 802	0.35	800

3.5 Comparison of Results

All three boundary conditions returned similar properties for each material. Thermal conductivity for each boundary condition was within 10%, for a given material. Similarly, the specific heats for each boundary condition were all within 12.5%. Without being able to test materials which have known thermal properties (which we were not able to accomplish as part of this project), we cannot know which boundary condition is the most accurate. Assuming their accuracy is similar for a given material, it is easier to judge the effectiveness based on the ease of use of each tool. Due to the fact that the semi-infinite solids calculation requires much less computational power, it is much easier and quicker to use this tool to estimate thermal properties of each material. It takes much longer to iterate on the finite difference boundary conditions due to the time it takes for the computer to be able to run each calculation. However there are advantages of the finite difference model as well. For instance, if a heterogeneous material such as a sandwich panel was being tested, then the finite difference model would be much more accurate. A sandwich panel is two pieces of exterior material, such as FRP, that are attached to a substrate material, such as foam or wood. Since the semi-infinite solid assumes that the material has the same properties throughout the depth, it cannot accurately model the change in the thermal properties the way that the finite difference method could.

4.0 NFPA 285 SCREENING TOOL

Throughout this project, a method for modeling the performance of FRPs in the NFPA 285 (NFPA 285, 2010) test was developed. This was accomplished using known two-dimensional spill plume theory and data collected during our own Cone Calorimeter testing as well as data collected during a full-scale NFPA 285 test of the same material and provided in a test report. The material tested in the Cone and the NFPA 285 test report was provided by Kreysler & Associates.

Multiple correlations regarding 2D spill plume theory were considered for the purposes of developing this model, and the one that best fit with the configuration and data values collected from the 285 test was chosen. The full explanation of the process used to determine which equations were most favorable for the purposes of this project can be found in Appendix C, and the chosen equations are as follows:

The equation 4.0.1 used for predicting the centerline temperature of the spill plume at various heights on the wall assembly is the following (NFPA 92B, 2009):

$$T_s = T_o + \frac{K_s \dot{Q}_c}{c_p \dot{m}_p} \qquad 4.0.1$$

Where $\dot{m}_p$ is the mass flow rate of the plume (kg/s) at a given height, z (meters), and is defined by the following equation 4.0.2 (Harrison, 2010):

$$\dot{m}_p = 0.08 \dot{Q}_c^{\frac{1}{3}} W^{\frac{2}{3}} (z + z_o) + 1.34 \dot{m}_s \qquad 4.0.2$$

The term $\dot{m}_s$ is the mass flow rate of the plume smoke (kg/s) at the location of the spill edge, and is defined as follows in equation 4.0.3 (Harrison, 2007):

$$\dot{m}_s = 0.025 (\dot{Q}_c W^2)^{1/3} \qquad 4.0.3$$

T_s = average plume smoke layer temperature [K]
T_o = ambient temperature (given in the 285 Test Report to be 302.5 K)
K_s = fraction of convective heat release contained in smoke layer (assumed to be 1.0)
Q_c = convective fraction of heat release rate [kW]
c_p = specific heat of the ambient air (known to be 1 kJ/kgK)
W = width of the window opening, or spill edge (known to be 1.98 m)

It is important to note that a virtual origin term (z_o) was included in Equation 4.0.2, for mass flow of the plume, which was not in the original equation. This virtual origin term was added in order to account for the differences between the truly 2D spill plume geometry that the equation was designed to model and the quasi-two-dimensional geometry that exists in the NFPA 285 test. It is also important to note that these equations apply to a far-field plume theory, and were modified during the development of the model in order to account for the near field as well.

4.1 Development of Calibration Model

Once the best equations were determined, Excel was used to graph the calibration temperature and heat release rate data provided in the test report against the theoretical spill plume line graphed using the chosen equations. The heat release rates were converted to heat release rates per unit length by dividing the values by the width of the window opening. All heat release rates were converted to heat release rates per unit length throughout the project, which was necessary given that the plume of the NFPA 285 test was being treated as a nominally two-dimensional spill plume in our calculations. Six lines were graphed on the same axes; one line for each time step of the test. A virtual origin term was used

to shift these lines so that they would collapse as closely as possible onto each other, and also line up with the theory line. The virtual origin value was different for each time step and the values were found through a trial and error experimentation process in Excel. From this graph, a model could be created based on the test calibration.

Through a derivation process that combined the plume temperature and mass flow equations, of which an extensive explanation can be found in Appendix C, the following equation 4.1.1 was developed to serve as the general form of the NFPA 285 model created in this project.

$$\Delta T = \beta \left(\frac{Z + Z_o + C}{\dot{Q}'^{2/3}} \right)^{\alpha} \qquad 4.1.1$$

ΔT = change in temperature [K] Q' = total heat release rate per unit length [kW/m]

The creation of this equation was based on the methods of Yuan and Cox (Yuan & Cox, 1996). In this equation, β, C, and α were constants that were modified in order to create the model of the NFPA 285 test. The values of β and α are dimensionless, while C has units of meters. Based on Yuan and Cox's experiments, which assume that a fire can be broken into three different regions, we also began our adjustments of the constants based on the assumption that three regions are present. These three regions were classified as continuous flame, intermittent flame, and thermal plume. We first attempted to fit the correlation to the three regions of the calibration data, and adjust the equation above by changing the exponent and constants, following the ideas of Yuan and Cox. This change of the exponent allows for variation in the slope of the fit lines for each region. Changing β allows for vertical shifts in the fit lines. The value of C is 0.46, which remains constant throughout the regions as C is simply a culmination of the constants from the original equations that equation 4.1.1 was derived from.

Using this general equation with the value of z_o (in meters) varying at each time step, three lines (one for each region) could be graphed and fit to the calibration data from the test report by changing the constants and exponent for each region. The values to create the best model were found through an extensive trial and error process. The best fit was determined to occur with the use of the following values set for the variables for the three regions, shown in Tables 4.1.1 and 4.1.2:

Table 4.1.1: Values assigned to z_o (meters) at each time step of calibration, as well as the corresponding heat release rate per unit length.

Time Step [min]	Zo [m]	Q's [kW/m]
0-5	0.6	299.44
5-10	-0.088	366.33
10-15	-0.241	406.78
15-20	-0.308	483.78
20-25	-0.335	518
25-30	-0.377	588.39

Table 4.1.2: Constants and exponents used to create the 3 regions of the calibration model.

	Beta	Alpha	C
Continuous	575	0	0.46
Intermittent	42	-0.6	0.46
Plume	8.46	-0.998	0.46

The final graph of the calibration data, theoretically calculated values, and three regions of the model was as follows in Figure 4.1.1:

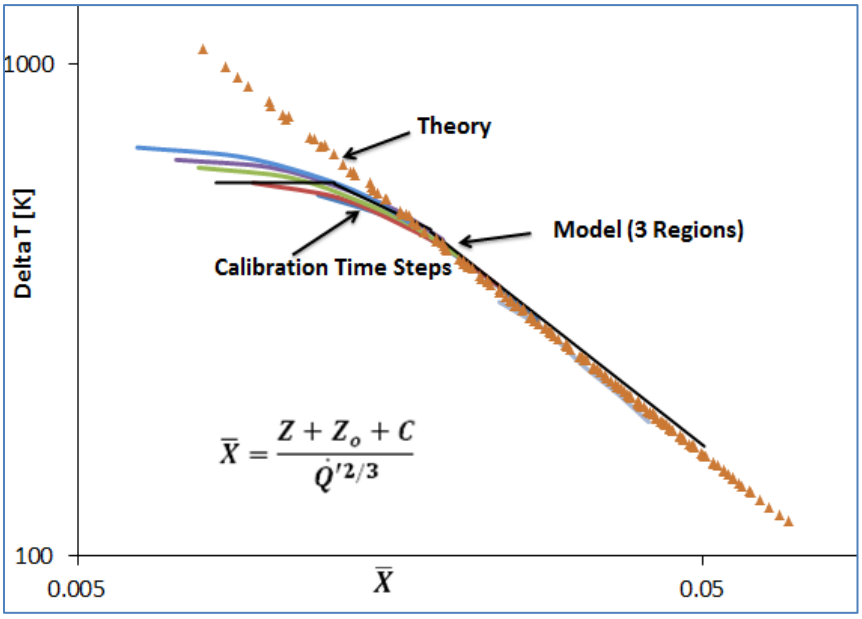

Figure 4.1.3: The final model created for the calibration of the NFPA 285 test, as well as the data for the 6 time steps and the calculated theory line.

4.2 Development of Test Model

After the calibration model was complete, a similar procedure was used to model the actual test results using the test data provided in the 285 test report. A major challenge faced in creating the test model was the estimation of the heat release rate per unit length of the burning wall. Based on data collected during Cone testing, the critical heat flux for ignition of the wall material determined to be 25 kW/m^2. Using the calibration heat flux data from the 285 test report, we found that the heat flux imposed on the wall by the burners would not be great enough to cause ignition of the wall during the first 3 time steps of the test. Therefore, heat release rates per unit length of the burning wall were estimated only for time steps 4 through 6 of the test. The process of estimating the heat release rates per unit length was completed using a trial and error approach.

The six time steps were first plotted on the same general axes as were used in the calibration graph using the temperature and source heat release rate per unit length data from the test. However, this yielded a result that was less satisfactory than the calibration graph, as the lines for the time steps were spread much farther apart across the plot. The lines were brought closer together by adding the estimated heat release rates per unit length contributed by the burning wall to the heat release rates per unit length of the source fires. The addition of these heat release rates per unit length of the burning wall caused a shift of the curves in the x-direction. The best estimated heat release rate per unit length of the burning wall for each of the 3 time steps was considered reached when the plume regions of the 3 curves were aligned.

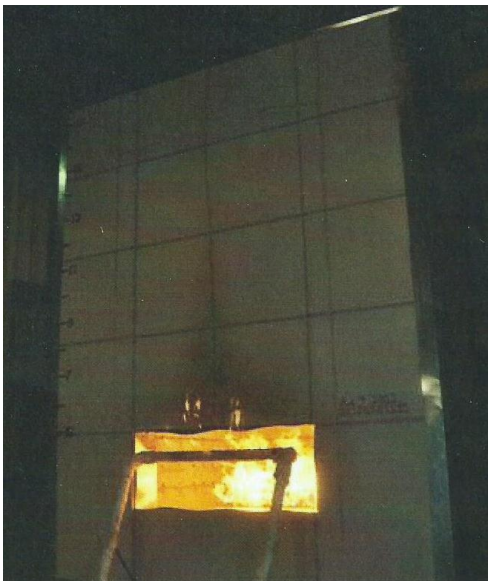

Figure 4.2.1: Test photo taken at 7 min, 45 sec. No sustained flaming yet on the wall assembly.

Figure 4.2.2: Test photo taken at 21 min, 16 sec. Sustained flaming to approximately 11-ft mark.

Although in theory the same model that was applied to the calibration data should also be applicable to the test, this was not found to be the case. The ΔT, or wall temperature minus ambient temperature, values from the test were discovered to be lesser than those from the calibration. This should not have been the case as the major difference between the calibration and test is that during the test there is a burning wall contributing to the total heat release rate, as pictured in Figures 4.2.1 and 4.2.2, which should have caused the test temperatures to be the same or greater than the calibration temperatures depending on whether the wall had yet ignited. This abnormality was explained by making an assumption that the heat release rates of the burners were not consistent between the calibration and test, and that those of the calibration were greater than those produced during the test. Due to this testing abnormality, the model was modified in order to fit the test data.

The test results were modeled by again using the principles developed by Yuan and Cox, and the model was based on the same general equation. However, since the heat release rate per unit length of the burning wall assembly now had to be added to the heat release rate per unit length of the burners, the following equation 4.2.1 was used for the test model:

$$\Delta T = \beta \left(\frac{Z + Z_o + C}{(\dot{Q}'_s + \dot{Q}'_w)^{2/3}} \right)^{\alpha} \qquad 4.2.1$$

Q'_s = heat release rate per unit length (based on the width of the window opening) from the source fires [kW/m]

Q'_w = heat release rate per unit length of the burning wall [kW/m]

Again through trial and error, the constants and exponent were adjusted in order to fit the three regions of the model to the test data. The best fit was determined to occur with the use of the following values set for the variables for each of the three regions, shown in Table 4.2.1:

Table 4.2.1: Constants and exponents used to create the 3 regions of the test model

	Beta	Alpha	C
Continuous	670	0	0.46
Intermittent	51.5	-0.6	0.46
Plume	10.4	-0.998	0.46

It is important to note that although the values assigned to the constant β differ between the calibration and test models, the constant C and exponent values of each region are the same. This demonstrates that even though the test data is not as similar to the calibration data in terms of the time step curves collapsing onto one another as would be expected; the curves are not wholly dissimilar. The three regions of both fires can be approximated as having the same slope, but are simply shifted on the plot. This shift can be accounted for by the notion that the heat release rates per unit length of the source were erroneously different during the test from those recorded during calibration.
The test data curves and the three regions of the test model were plotted as follows in Figure 4.2.3:

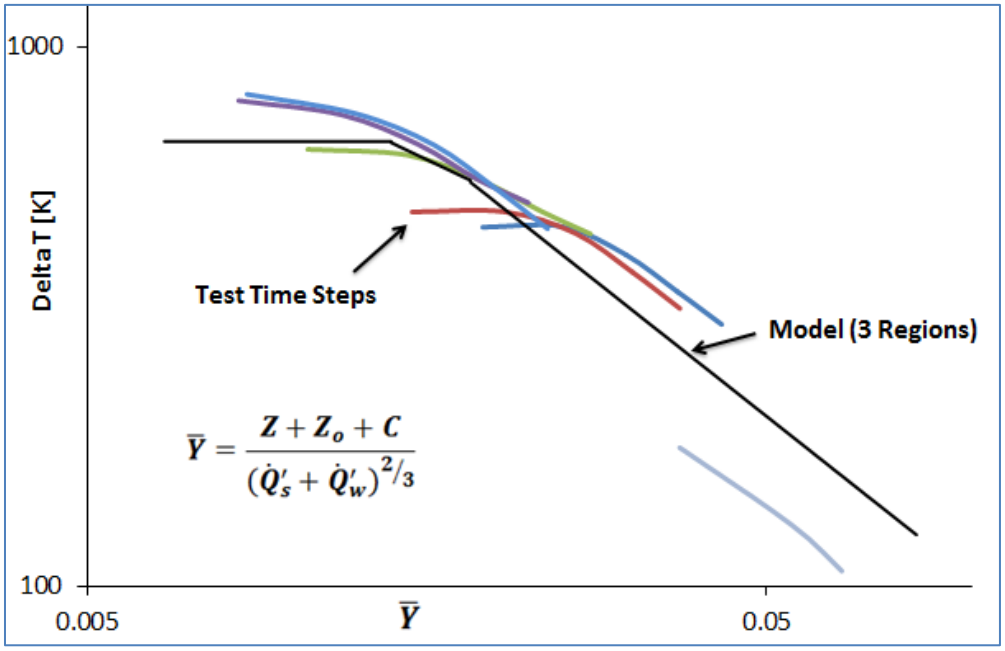

Figure 4.2.3: The final model created for the NFPA 285 test, as well as the data recorded for the 6 time steps during the test.

Although the test model may not appear to align with the test results as clearly as the calibration model aligned with the calibration data, we believe that the test model is a satisfactory representation of the data that was available at the time the project was completed.

4.3 Pyrolysis Zone Estimations

In addition to creating a test model, the estimated values for the heat release rate per unit length of the burning wall were also used in creating a method for determining characteristics of the pyrolysis zone of the NFPA 285 test. Based on knowledge that the wall is only ignited during time steps 4 through 6, heat flux data from calibration at various heights on the wall, and heat release rate per unit area data

collected from the Cone, we were able to estimate the height of pyrolysis. From photos provided in the test report, the width of the base of the pyrolysis zone could be estimated and the shape of the pyrolysis zone could be approximated as a triangle, which then allowed for calculation of the area of pyrolysis. Using this area and the peak heat release rate per unit area from the Cone of 80 kW/m^2, the heat release rate of the wall could be approximated for time steps 4 through 6 of the test. Then, considering the heat release rates per unit length of the burning wall that were estimated to create the NFPA 285 test model, a width of pyrolysis was found. This was accomplished by dividing the heat release rate of the wall by various widths in a trial and error process in order to obtain the width that would make the heat release rates per unit length being calculated equal to those that were previously estimated. It was found that the width of the pyrolysis zone, which in reality varies throughout the height of the zone, can be approximated as 1/5 the width of the base of the triangular pyrolysis area. These methods for approximation of pyrolysis dimensions would be useful tools for future estimations of the heat release rate per unit length of a burning wall in the NFPA 285 Test. For a more complete explanation of the calculations performed, please see Appendix C.

4.4 Proposed Building Code Update

The International Building Code (IBC) currently does not provide its users with prescriptive tools regarding the acceptance criteria of the NFPA 285 test. However, compliance with the criteria of NFPA 285 is mandated by the IBC for exterior wall assemblies. Using the knowledge that NFPA 285 requires flames to maintain a height of less than 3.05 meters (10 feet) above the window opening throughout the test and that the presence of flame is defined in the test standard as a temperature greater than 537.8°C (1000°F), a simple prescriptive tool was developed that, if added to the IBC, would allow users of the code to predict whether their material would comply with NFPA 285 based on knowledge of the heat release rate per unit area and pyrolysis height produced by the material.

The prescriptive tool was created by determining the heat release rate per unit length of the burning wall ($\dot{Q}'_w$) that would result in a temperature of 537.8°C (1000°F) at a height of 3.048 meters (10 feet) above the window using equation (4.2.1), where $\dot{Q}'_s$, z_o, β, C, and α are all set to be the values associated with the plume region of the model during the sixth time step of the test. This value of $\dot{Q}'_w$ represents the pass/fail threshold of the burning wall during the test.

From the threshold value for the heat release rate per unit length of the burning wall, pairs of heat release rate per unit area (Q") and pyrolysis height (x_p) were identified to create a pass/fail curve to be used as a screening tool for exterior building materials. If added to the IBC, this curve could aid users in predicting whether a material would comply with the criteria of NFPA 285 based on knowledge of Q" and x_p. The curve is shown in Figure 4.4.1 below.

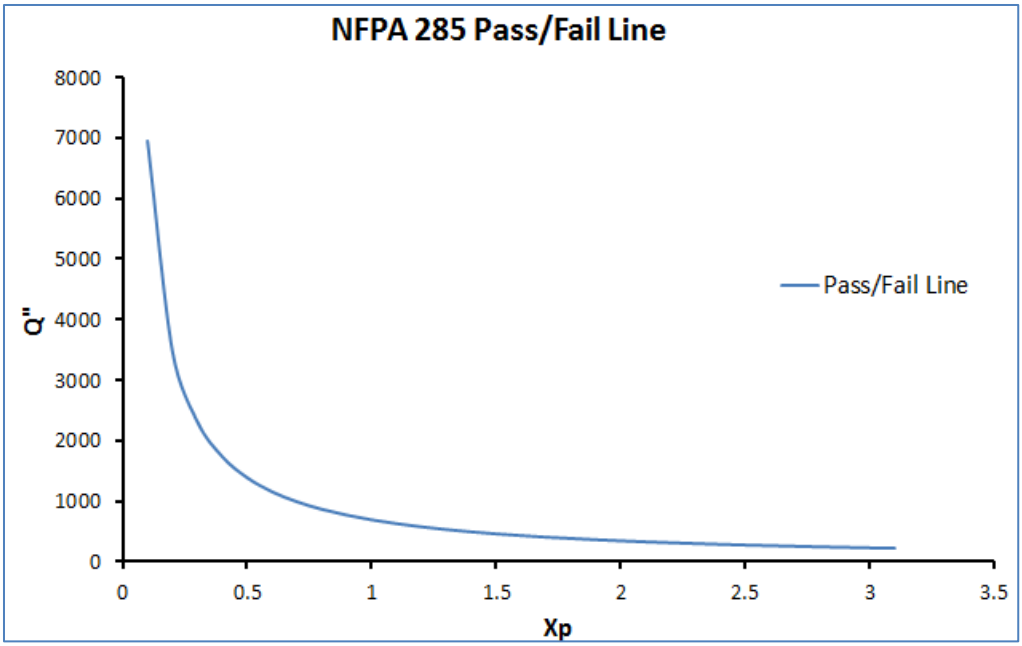

Figure 4.4.14: This graph demonstrates the prescriptive tool created to show the pass/fail curve for the NFPA 285 test. All combinations of Q" and xp that fall below the curve indicate that the material would meet the acceptance criteria of NFPA 285, while pairs falling above the curve are not likely to comply.

5.0 CONCLUSIONS

This project successfully created two tools which utilize data that is normally gathered from Cone Calorimeter tests to estimate thermal properties and predict the outcome of a NFPA 285 test. The property estimation tool only requires that 3 thermocouples are installed in addition to the normal Cone test. In using this tool, the thermal conductivity and specific heat of samples can be estimated with reasonable accuracy which may be helpful to material designers. Since the semi-infinite solid solution is similar to the finite difference solutions, at least for the samples that were tested in this project, it is much easier and faster to use the semi-infinite tool since there are much less calculations. However if different types of materials were to be tested in the Cone, such as a sandwich panel with different layers, then the finite difference analysis should be used. However there is room for improvement of this tool in the future. First of all, this project does not include the testing of materials with known thermal properties to further verify the solutions. The tool would be improved by knowing that it has accurately predicted the thermal properties of such materials. Another improvement would be to write coding language for either Excel or another computational program which automatically changes thermal properties in an iterative fashion until they are correct.

The NFPA 285 test model that was developed throughout this project can be used to aid manufacturers in predicting whether their exterior building façade materials will comply with the acceptance criteria of the NFPA 285 test. It is useful to be able to make this prediction because of the large costs associated with the test. If an exposed face material is unlikely to comply with NFPA 285, this tool could help manufacturers to know in advance and avoid the costs of the test. We believe that the NFPA 285 test model created is a satisfactory representation of the data that was available at the time the project was completed. However, a significant limitation of this project was the minimal NFPA 285 test data used to develop the model. If more data had been available, such as reports from several NFPA 285 tests

instead of just a single test, the methods could likely be improved. This is one opportunity that was identified for future students to improve the NFPA 285 test model.

The proposed building code update could also be a useful tool for materials manufacturers in the future. This supplementary tool, if added to the building code, would allow code users to predict whether their material would comply with NFPA 285 based on knowledge of the heat release rate per unit area and pyrolysis height produced by the material. The ability to predict this would be useful since compliance with the acceptance criteria of NFPA 285 is mandated by the IBC for exterior wall assemblies, but the code does not currently provide its users with prescriptive tools regarding the acceptance criteria of the NFPA 285 test.

REFERENCES

Carslaw, H. S., & Jaeger, J. C. (1959). Conduction of heat in solids. (2nd ed.). London: Oxford. Retrieved ISBN-0198533683

E1354-11b Standard Test Method for Heat and Visible Smoke Release Rates for Materials and Products Using an Oxygen Consumption Calorimeter. (2011 Edition). West Conshohocken, PA: ASTM

Guigard, S., Kindzierski, W., Harper, N. (2000). Heat Radiation from Flares. Department of Civil and Environmental Engineering, University of Alberta. http://environment.gov.ab.ca/info/library/6694.pdf

Harrison, R. (2009). Entrainment of Air into Thermal Spill Plumes. *Department of Civil and Natural Resources Engineering, University of Canterbury*. http://ir.canterbury.ac.nz/handle/10092/2865

Harrison, R., & Spearpoint, M. (2010). Physical Scale Modeling of Adhered Spill Plume Entrainment. *Fire Safety Journal*, *45*(3), 149-158. http://dx.doi.org/10.1016/j.firesaf.2010.02.005

Harrison, R., & Spearpoint, M. (2007). A Review of Simple Entrainment Calculation Methods for the Thermal Spill Plume. *International Journal on Engineering Performance-Based Fire Codes, 9*(4), 142-153. http://www.bse.polyu.edu.hk/researchCentre/Fire_Engineering/summary_of_output/journal/IJEPBFC/V9/p142-153.pdf

International Building Code. (2012 Edition). Washington DC: International Code Council.

NFPA 92B: Standard for Smoke Management Systems in Malls, Atria, and Large Spaces. (2009 Edition). Quincy, MA: NFPA.

NFPA 285: Standard Fire Test Method for Evaluation of Fire Propagation Characteristics of Exterior Non-Load-Bearing Wall Assemblies Containing Combustible Components. (2012 Edition). Quincy, MA: NFPA.

Olver, P. J. (n.d.). Retrieved from http://www.math.umn.edu/~olver/pd_/nfd.pdf

Quintiere, J. (2006). *Fundamentals of Fire Phenomena.* Chichester, West Sussex, England: John Wiley & Sons Ltd. ISBN-13 978-0-470-09113-5 (HB)

SFPE Handbook of Fire Protection Engineering. (2002). *Burning Wall and Ceilings*. (3rd ed.). Qunicy, MA: National Fire Protection Association.

SINTEF. (2005). *ISO 5660-1:1993: The Cone Calorimeter Test*. Retrieved from http://www.sintef.no/home/Building-and-Infrastructure/SINTEF-NBL-as/Key-projects-and-topics/Fire-testing-of-railway-seats/ISO-5660-11993-THE-CONE-CALORIMETER-TEST/

Southwest Research Institute. (2012). *Fire Performance Evaluation of a Wall Assembly Tested in Accordance with NFPA 285*. (SwRI Project No. 01.16918.01.615). San Antonio, Texas.

Yuan, L., Cox, G. (1996). An Experimental Study of Some Line Fires. *Fire Safety Journal*, *27*, 123-139.

APPENDIX A: SEMI-INFINITE SOLIDS PROPERTY ESTIMATION BRIEFING

Semi-Infinite Solids

A semi-infinite solid is a "simple geometry for which analytical solutions may be obtained" (Incropera 6th 283). Samples in the cone calorimeter are considered to have one face during the test, and data after edge burning begins is disregarded. A semi-infinite solid is considered to have one surface, with the assumption that the other surfaces extend to infinity. The sample being tested in the NFPA 285 test can also be considered a semi-infinite solid. Both tests are considered to test semi-infinite solids, so the results of each can be compared, and potentially be used to predict the outcome of each other.

For semi-infinite solids, change in temperature is transient, one-dimensional conduction, which allows us to analyze ideal situations in order to make correlations. One useful example of this is the ability to find the surface temperature history of a semi-infinite solid under a constant surface heat flux using the equation below:

$$q^* = \frac{1}{2}\sqrt{\frac{\pi}{Fo}} \text{ where } Fo = \frac{\alpha t}{L^2}$$

q* - dimensionless conduction heat rate
Fo - Fourier number, the ratio of the heat conduction rate to the rate of thermal energy storage in a solid (dimensionless)
α – thermal diffusivity (m^2/s)
t – time (s)
L – length (m)

In the cone calorimeter and the NFPA 285 Test, a constant surface heat flux is applied to the sample being tested, so this equation can be used to relate information found during the cone test to the results of the NFPA 285 Test.

When looking at data from a cone calorimeter test, the sample can be considered semi-infinite until the back face heats up. In the investigations that are explained below, data past the time when the back face thermocouple became 10°C hotter was disregarded, to represent a semi-infinite solid as accurately as possible.

Note about Data Analyzed

The methods explained below were used to estimate temperature at different times and depths for Kreysler Sample 1, using data from two separate thermocouple tests of the sample. The graph below shows the data from the tests, with an average. Based on the graph, the thermocouple test can be considered repeatable enough to use for the analysis.

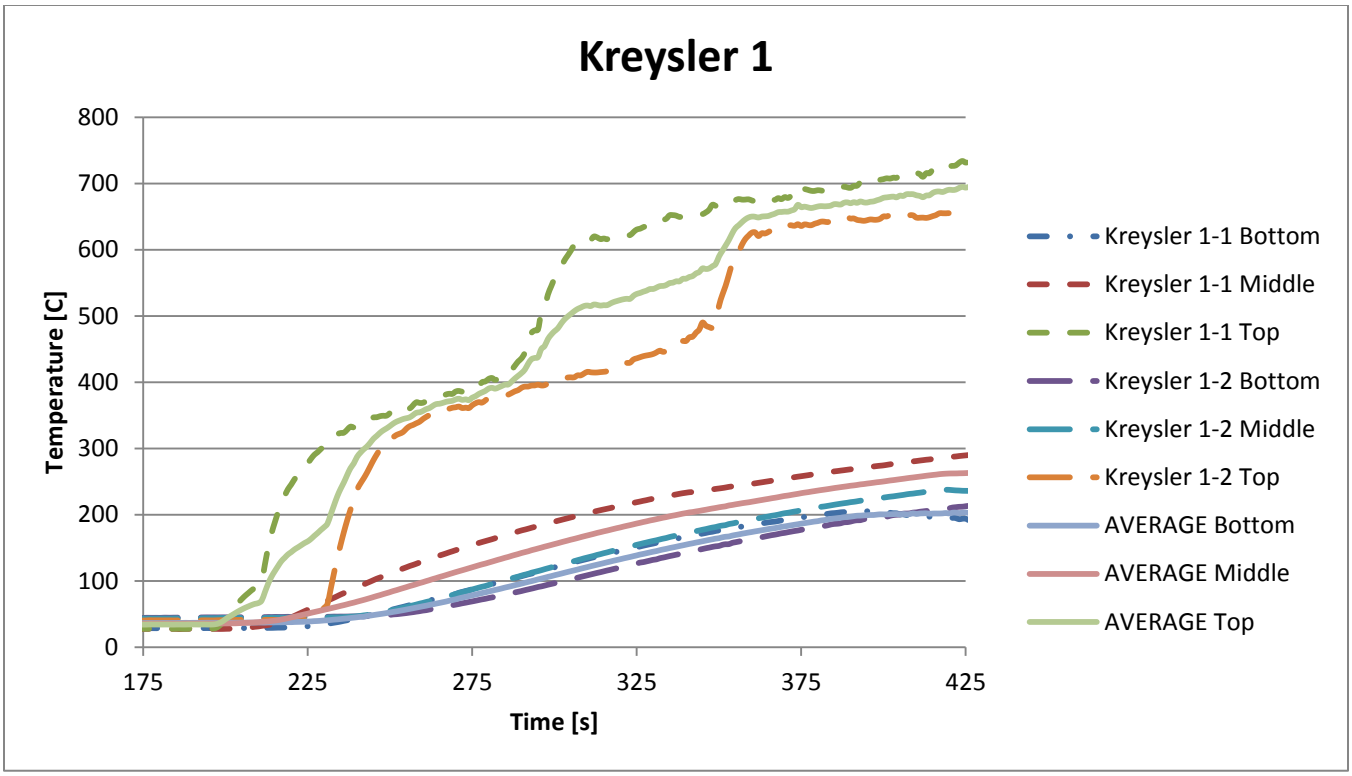

Property Estimation Method

The boundary conditions explained below were used with Microsoft Excel for parameter estimation of thermal conductivity and specific heat. An iterative direct method was applied, and results were graphed for comparison with data from the Cone test.

Constant Temperature Boundary Condition

This boundary condition was used as a "test method" to familiarize myself with the process.

The equation representing constant temperature is

$$\frac{T(x,t) - T_s}{T_i - T_s} = \text{erf}\left(\frac{x}{2\sqrt{\alpha t}}\right)$$

For this method, T_s is surface temperature, which is constant. Temperature of ignition was used as the value for surface temperature because it is the maximum surface temperature that can be considered while still using test data from an inert material. As expected, this method does not represent the cone calorimeter test well. The estimated values for the top surface thermocouple (x=0) during the first 33 seconds after the shutter is opened are all equal to the temperature of ignition, due to the arrangement of the equation. The values for the thermocouple at a depth of x=4mm start at 25 K and go to 162 K, and the values for the thermocouple at a depth of x=8mm range from 25 K to 40 K.

Cone Boundary Condition – Constant Net Heat Flux with Newtonian Cooling

Before applying this equation, it looks like it emulates an ideal cone calorimeter test the best. The equation represents a constant net surface heat flux with Newtonian cooling. The cone test applies a constant heat flux, but the heat flux at the surface is not constant, due to the air between the cone heater and the surface of the sample being tested, so the equation needs to be altered slightly to account for that. Newtonian cooling occurs because there is air in the room where the test is being conducted, and some of it is pulled over the sample and into the cone.

The equation representing constant surface heat flux is

$$T(x,t) - T_i = \frac{2q_o^{"}(\alpha t/\pi)^{1/2}}{k}\exp\left(\frac{-x^2}{4\alpha t}\right) - \frac{q_o^{"}x}{k}erfc(\frac{x}{2\sqrt{\alpha t}})$$

The equation for Newtonian cooling is

$$q" = h(T_s - T_\infty)$$

To account for cooling, q_o"

$$q_o^{"} = \epsilon q_i^{"} - CHF$$

where CHF (critical heat flux) is the minimum heat flux for ignition, as explained in the SFPE Handbook by Tewarson. For this project, the minimum heat flux was considered to be the incident heat flux at which flashing occurred on the sample, even if sustained flaming did not occur.

Unfortunately, this method was not as effective as it seemed it could be. To achieve temperature curves at different depths similar to the curves of the thermocouple data from the cone test, the values of thermal conductivity and specific heat were 30 W/mK and 80 J/kgK respectively. Not only are the values extremely different from expected values (around 0.3 W/mK and 800 J/kgK), the curves are not even very similar to those from the test, as can be seen in the figure below.

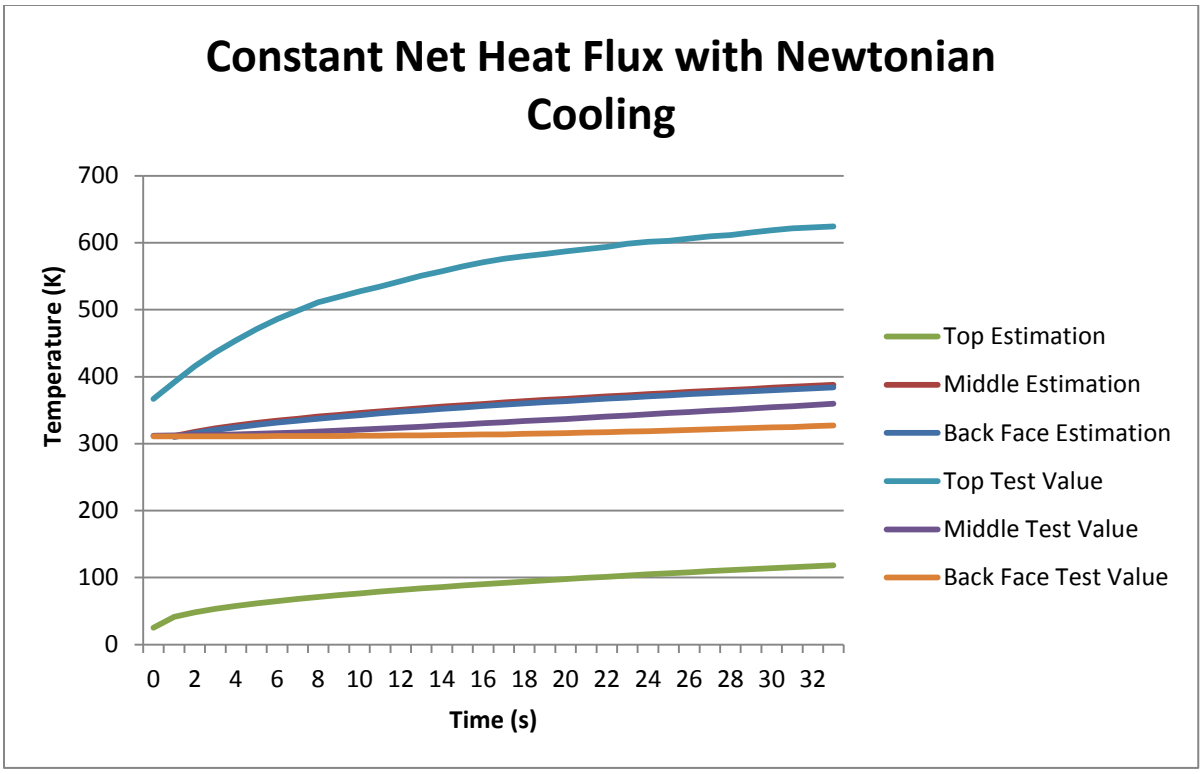

Radiation at the Surface

This method represents a heat source being placed on the sample, which seems like a good representation of the cone test.

The equation used for this method is:

$$T(x,t) - T_i = \frac{\dot{q}''}{h}\left[erfc\left(\frac{x}{2\sqrt{\alpha t}}\right) - \exp\left(\frac{\bar{h}}{k}x + (\frac{\bar{h}}{k})^2 \alpha t\right) erfc\left(\frac{x}{2\sqrt{\alpha t}} + \frac{\bar{h}}{k}\sqrt{\alpha t}\right)\right]$$

Using the same values as for the method above results in curves that are similar to the curves from the thermocouple data, even though the values are very unlikely. The graph below shows both sets of curves.

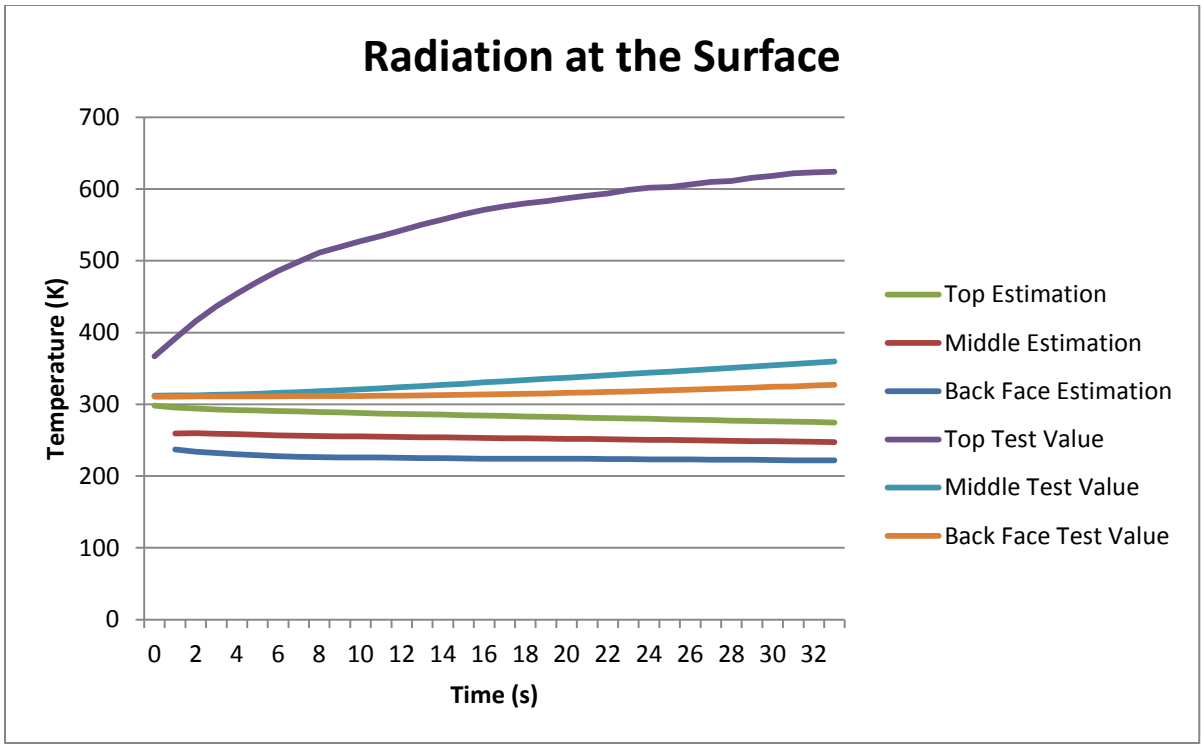

Conclusion

Unfortunately, the equations explained in this brief did not accurately determine thermal properties for the samples analyzed. The Property Estimation Brief by Jacob Czarnowski explains a more accurate approach.

References

Carslaw, H. S., & Jaeger, J. C. (1959). Conduction of heat in solids. (2nd ed.). London: Oxford. Retrieved ISBN-0198533683

Incropera, F.P., DeWitt, D.P., Bergman, T.L., & Lavine, A.S. (2007). *Fundamentals of Heat and Mass Transfer.* Danvers, MA: John Wiley & Sons, Inc. ISBN 0471457280

Quintiere, J. (2006). *Fundamentals of Fire Phenomena.* Chichester, West Sussex, England: John Wiley & Sons Ltd. ISBN-13 978-0-470-09113-5 (HB)

SFPE Handbook of Fire Protection Engineering. (2002). *Burning Wall and Ceilings*. (3rd ed.). Qunicy, MA: National Fire Protection Association.

APPENDIX B: PROPERTY ESTIMATION BRIEFING

1.0 INTRODUCTION

A tool is being developed which can use information from a standardized bench scale test, the Cone Calorimeter Test (ASTM E 1354) to determine thermal properties of materials (ASTM E 1354, 2011). It utilizes early time Cone data from before the sample has undergone any extensive degradation due to pyrolysis. Moreover, this tool assumes that the sample is inert with constant thermal properties. One-dimensional heat transfer modeling is compared to data from thermocouples placed throughout the sample in order to estimate the thermal conductivities and specific heats of each sample. To model the heat transfer, both an analytical solution (semi-infinite solids) and a numerical solution (explicit finite differences) are used to calculate a temperature distribution throughout the depth of the sample. Three thermocouples are then placed throughout the sample to gather exact temperature data throughout the sample. Finally, the thermal properties of each model are iteratively changed until the estimated temperature distribution matches the exact temperature distribution from the thermocouples. These values represent the estimated thermal properties for the particular material.

2.0 BACKGROUND AND METHODOLOGY

In order to learn more about the thermal characteristics of FRPs and better utilize early time Cone data, two tools were created to estimate the thermal conductivity (k) and specific heat (C_p) in a sample during a test. Both tools use thermocouple data from thermocouples that were installed on the samples during the test. These thermocouples were installed on the surface, at ½ the depth, and finally the back face of the sample. The test data used were tests which were run with the Cone set to 50 kW/m^2. Two different tests were run and the data was averaged. These averages for the thermocouple data were then used to estimate the properties for each sample. The first tool is a simplified model which uses a semi-infinite solid analysis of the FRP and compares the temperature distribution within the sample during the test to the thermocouple data. The second tool is a more complex version which uses a one dimensional finite difference analysis of the temperature distribution in the sample and also compares it to thermocouple data. When the temperatures for the prediction (semi-infinite or finite difference method) matched the temperatures of the thermocouples, the values for k and C_p were considered to be correct.

2.1 The Semi-Infinite Solid Method

The first property estimation method uses a semi-infinite solids analysis to model the material. A semi-infinite solid is, “an idealized body that has a single plane surface and extends to infinity in all directions” (ECourses, Transient Heat Conduction in Semi-Infinite Solids). An illustrated model of this is shown below in Figure 2.1.1.

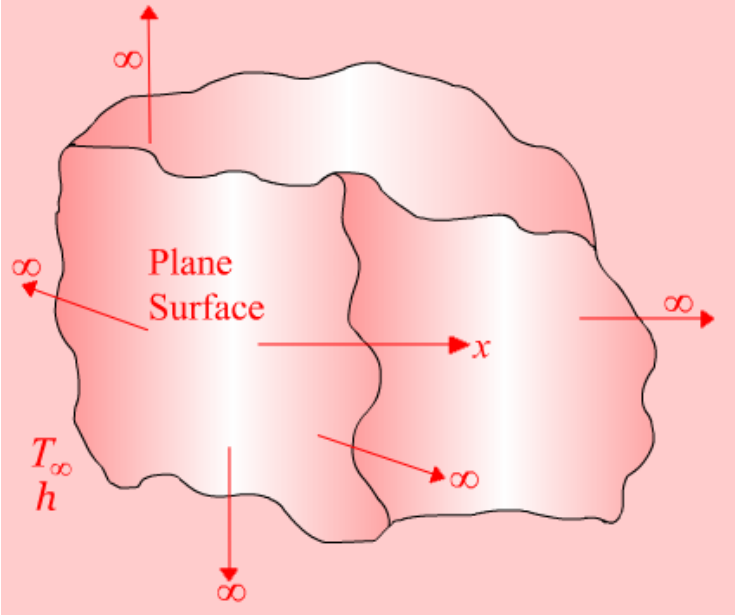

Figure 2.1.1: Schematic of a Semi -Infinite Body (ECourses, Transient Heat Conduction in Semi-Infinite Solids)

The semi-infinite solid model is used to describe temperatures in a body close to the surface as a result of those thermal conditions. In general, to be considered semi-infinite when subjected to one-dimensional heat conduction the following relation must be true (which holds for each sample that was tested as part of this project) (Rathore, 2011):

$$\frac{\delta}{2\sqrt{\alpha t}} \geq 0.5 \qquad 2.1.1$$

For this project, the surface condition was modeled as a constant incident heat flux with convective and radiative cooling. Therefore to describe the temperatures in the body we use the general equation which is given by Carslaw and Jaeger (Carslaw & Jaeger, 1965) as:

$$f(t) = A \qquad \frac{\partial v}{\partial t} = k\frac{\partial^2 v}{\partial x^2} \qquad \frac{-\partial v}{\partial t} + hr \neq hf(t)$$

$$v = Aerfc\left(\frac{x}{2\sqrt{kt}}\right) - Aexp(hx + h^2kt)erfc\left(\frac{x}{2\sqrt{kt}} + h\sqrt{kt}\right)$$

Where $\qquad v = T - T_o \quad k = \frac{k}{\rho C_p} = \alpha\frac{\partial T}{\partial t} = \alpha\frac{\partial^2 T}{\partial x^2}$

$$\frac{-\partial v}{\partial t} + hv = hf(t)$$

$$-k\frac{\Delta T}{C_p} \neq q" - h(T - T_o)$$

$$\frac{\Delta T}{L} = \frac{\epsilon''}{k} - \frac{h}{k}(T - T_o)$$

$$\frac{q''}{k} = hA \qquad h = \frac{h_{tot}}{k} \qquad A = \frac{\epsilon''}{h_{tot}}$$

$$T = T_o + \frac{\dot{q}''}{h_{tot}} erfc\left(\frac{x}{2\sqrt{\alpha t}}\right) - \frac{\dot{q}''}{h_{tot}} exp\left(\frac{h_{tot}}{k} + \frac{h_{tot}^2 \alpha t}{k^2}\right) erfc\left(\frac{x}{2\sqrt{\alpha t}} + \frac{h_{tot}\sqrt{\alpha t}}{k}\right) \quad 2.1.2$$

2.2 The Finite Difference Method

When an analytical solution for conduction in a solid is not available, the finite different method can be used to determine the temperature distribution at discrete points in a solid. This method works by subdividing the surface into equal sized areas. A grid is then "drawn" over the surface with intersections of the grids placed in the center of each area. These points, called nodes, are used to describe the temperatures of each area. The smaller the areas are, the more there will be and therefore the more accurate the solution will be. For transient problems, there are two forms of the finite difference solutions, the explicit and implicit forms, however the explicit form is the only one that will be discussed here (Fundamentals of Heat and Mass Transfer 2011). In order to determine material properties using this method, we are using thermocouples to measure the temperature throughout the test. Thermocouples will be placed on the top surface, bottom surface and interior of the sample. The thermocouples used were Omega brand K type 30 gauge thermocouples with glass braid insulation. For the calculations in this brief, the top surface thermocouple was placed on the surface and the wire was bent slightly to keep it touching the surface throughout the test. The bottom surface thermocouple was taped to the bottom of the sample using foil tape. To insert the interior thermocouple, a hole was drilled in the center of the sample 0.75 inches deep with a 1.5 mm drill bit. To ensure the hole was drilled straight into the sample, a 1mm drill bit was inserted and the angle of the emerging bit was measured with respect to the side of the sample to ensure it was 0 degrees. This check ensured that the drill bit did not deviate from the center of the sample, placing the interior thermocouple closer to one of the surfaces which would give incorrect temperature information. The hole was then filled with omegatherm thermally conductive paste (to ensure the thermocouple would accurately measure the sample temperature) and the thermocouple was then inserted in the hole.

The explicit form uses the previous time to calculate the temperature of a node at the next time step using known temperatures. Therefore the explicit method is said to be a forward-difference approximation to the time derivative and is independent of the temperatures of other nodes at the same time step. Although this method is simple, its limitation is that the time step must be less than a certain number, dependent on Delta-x and other system parameters, which is called the stability criterion. If this stability criterion rule is not upheld, the numerical solution will diverge from the true solution. The boundary condition at the surface of the sample was defined in two different ways. First, the thermocouple data from the surface thermocouple was used to drive the finite differences. The second method was using a constant heat flux with convective and radiative cooling which will be derived in the next section. For interior nodes, energy storage was simply conduction in and out of a particular node. Finally the back surface of the sample was modeled using only a convective cooling term.

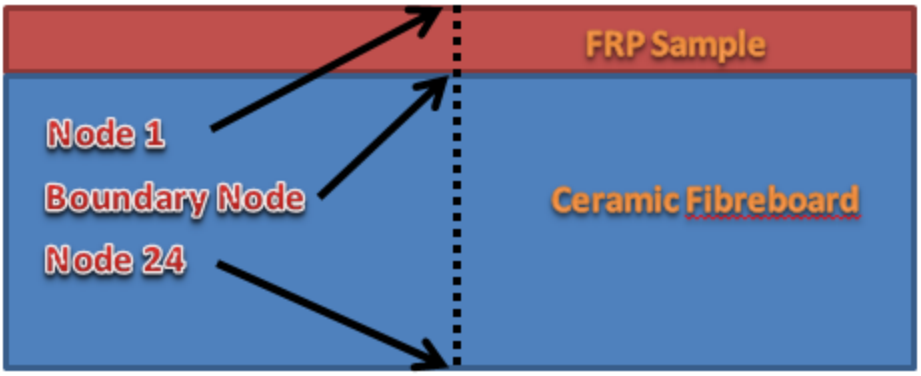

Figure 2.2.1: Node Diagram

Figure 2.2.1 depicts the one-dimensional system of nodes that are used in the finite difference analysis. The boundary node is node 5 and the middle node for the sample is node 3. The distance between the nodes is 2mm for Kreysler and Associates samples and 1.5 mm for Creative Pultrusions (CP) samples. That is because the Kreysler samples are 8mm thick and the CP samples are all 6 mm thick.

The Surface Node

Increase in Internal Energy = Radiation into Node - Convection out of Node - Conduction out of Node

$$\rho A C_p \frac{\Delta x^2}{2}\left(\frac{T_o^{p+1}-T_o^p}{\Delta t}\right) = \varepsilon \dot{q}''\mathrm{A} - \mathrm{hA}(T_o^p - T_\infty) - \mathrm{kA}\left(\frac{T_o^p - T_{o+1}^p}{\Delta x}\right)$$

$$T_o^{p+1} - T_o^p = \frac{2\varepsilon \dot{q}''\Delta t}{\rho C_p \Delta x} - \frac{2\mathrm{h}\Delta t}{\rho C_p \Delta x}\left(T_o^p - T_\infty\right) - \frac{2\mathrm{k}\Delta t}{\rho C_p \Delta x^2}(T_o^p - T_{o+1}^p)$$

$$Fo = \frac{\alpha \Delta t}{\Delta x^2} \text{ and } \alpha = \frac{k}{\rho C_p} \text{ so...}$$

$$Fo = \frac{\mathrm{k}\Delta t}{\rho C_p \Delta x^2} \text{ and } Bi = \frac{h\Delta x}{k}$$

$$BiFo = \frac{h\Delta t}{\rho C_p \Delta x}$$

$$T_o^{p+1} = T_o^p + \frac{2\Delta \mathrm{x}}{k}\varepsilon \dot{q}''\mathrm{Fo} - 2\mathrm{BiFo}\left(T_\mathrm{o}^p - T_\infty\right) - 2\mathrm{Fo}(T_o^p - T_{o+1}^p)$$

$$T_o^{p+1} = 2Fo\left(\frac{\Delta x \varepsilon \dot{q}''}{k} + T_{0+1}^p + BiT_\infty\right) + (1 - 2Fo - 2BiFo)T_o^p \quad 2.2.1$$

$$\text{Where } \mathrm{Fo}(1 + \mathrm{Bi}) \leq \frac{1}{2} \text{ to remain stable}$$

The Fourier number is conceptually the ratio of heat conduction rate to the rate of thermal energy storage and is used to characterize transient heat conduction problems (Rohsenow et al. 1985). The alpha term is known as the thermal diffusivity and this number is a measure of the thermal inertia of an object (Tye, 1969)

The Interior Nodes

Increase in Internal Energy = Conduction into Node - Conduction out of Node

$$\rho A C_p \Delta x \left(\frac{T_o^{p+1}-T_o^p}{\Delta t}\right) = \mathrm{kA}\left(\frac{T_{o-1}^p-T_o^p}{\Delta x}\right) - \mathrm{kA}\left(\frac{T_o^p-T_{o+1}^p}{\Delta x}\right)$$

$$T_o^{p+1} - T_o^p = \frac{\mathrm{k}\Delta t}{\rho C_p \Delta x}\left(\frac{T_{o-1}^p-T_o^p}{\Delta x}\right) - \frac{\mathrm{k}\Delta t}{\rho C_p \Delta x}\left(\frac{T_o^p-T_{o+1}^p}{\Delta x}\right)$$

$$T_o^{p+1} = T_o^p + \frac{\mathrm{k}\Delta t}{\rho C_p \Delta x^2}\left(T_{o-1}^p - T_{o+1}^p\right) - \frac{2\mathrm{k}\Delta t}{\rho C_p \Delta x^2}\left(T_o^p\right)$$

$$Fo = \frac{\alpha \Delta t}{\Delta x^2} \text{ and } \alpha = \frac{k}{\rho C_p} \text{ so...}$$

$$Fo = \frac{\mathrm{k}\Delta t}{\rho C_p \Delta x^2}$$

$$T_o^{p+1} = \mathrm{Fo}\left(T_{0-1}^p + T_{0+1}^p\right) + (1-2Fo)T_o^p \qquad 2.2.2$$

$$\mathrm{Fo} \leq \frac{1}{4} \text{ To remain stable}$$

The Back Surface Node

Increase in Internal Energy = Conduction into Node - Convection out of Node

$$\rho A C_p \frac{\Delta x^2}{2}\left(\frac{T_o^{p+1}-T_o^p}{\Delta t}\right) = \mathrm{kA}\left(\frac{T_{o-1}^p-T_o^p}{\Delta x}\right) - \mathrm{hA}\left(T_o^p - T_\infty\right)$$

$$T_o^{p+1} - T_o^p = \frac{2\mathrm{k}\Delta t}{\rho C_p \Delta x^2}\left(T_{o-1}^p - T_o^p\right) - \frac{2\mathrm{h}\Delta t}{\rho C_p \Delta x}\left(T_o^p - T_\infty\right)$$

From Equation 1.3, $BiFo = \frac{h\Delta t}{\rho C_p \Delta x}$

$$T_o^{p+1} = T_o^p + 2\mathrm{Fo}\left(T_{o-1}^p - T_o^p\right) - 2\mathrm{BiFo}\left(T_\mathrm{o}^p - T_\infty\right)$$

$$T_o^{p+1} = 2Fo\left(T_{0-1}^p + BiT_\infty\right) + (1 - 2Fo - 2BiFo)T_o^p \qquad 2.2.3$$

2.3 Model Limitations

It is important to note the limitations of this estimation model, which are that it…

1. Does not assume surface degradation of sample due to pyrolysis,
2. Is only a 1 Dimensional analysis,
3. Assumes perfect conductivity between bottom of sample and fiberboard,
4. Assumes perfect conductivity between fiberboard pieces,
5. Assumes that the specimen is placed in a steel frame and placed on top of a load cell and the conduction through steel is assumed to be perfect with conductive losses to the load cell ignored.

2.4 Model Verification

In order to ensure accuracy of the finite difference model and the boundary conditions for each node, a semi-infinite analysis using equation 2.1.2 was conducted. The temperature distribution and profile can be seen below in Figures 2.4.1 and 2.4.2, respectively. As the graphs show, the results for the semi-infinite solid and the finite difference method are similar, meaning the finite difference boundary condition equations were correctly derived. The semi-infinite solution starts to drop below the finite difference solution towards the higher times because the semi-infinite solution assumes that conduction continues throughout the solid. However the finite difference equation is modeled to start losing heat to convection at a certain point, which is a smaller loss than conduction. If the finite differences would have been modeled to continue losing heat due to conduction at the back face, then the solution for each would be equal.

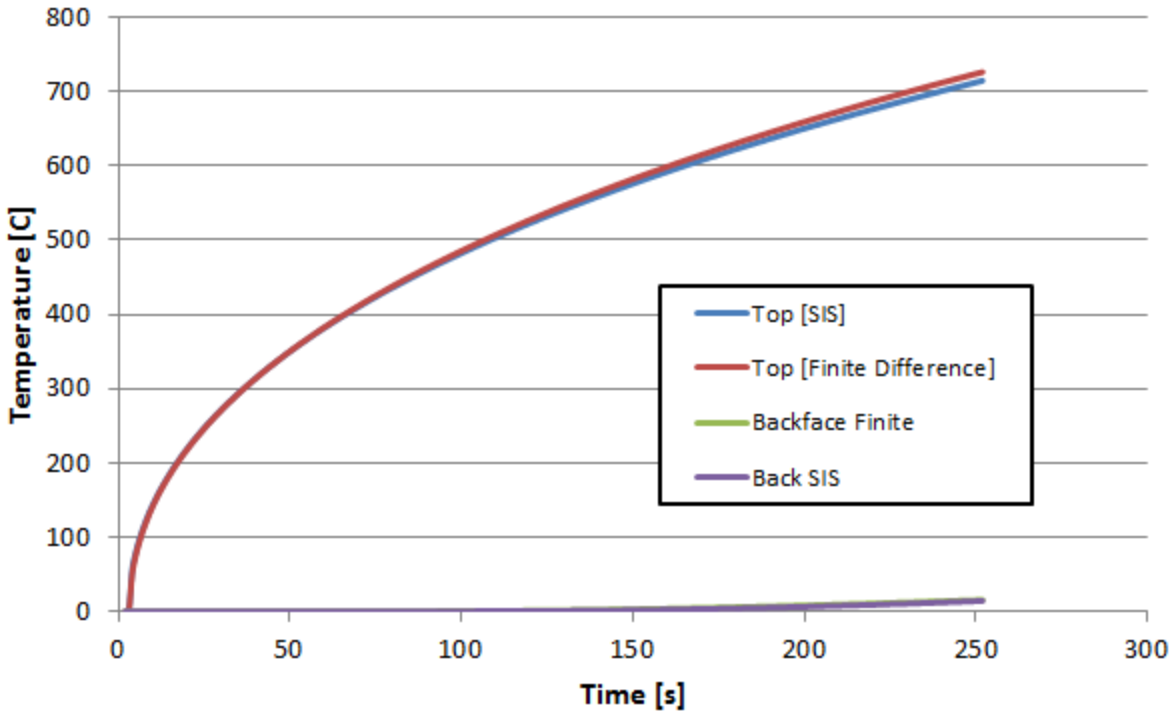

Figure 2.4.1: Temperature Distribution for Model Verification (SIS stands for Semi-Infinite Solid)

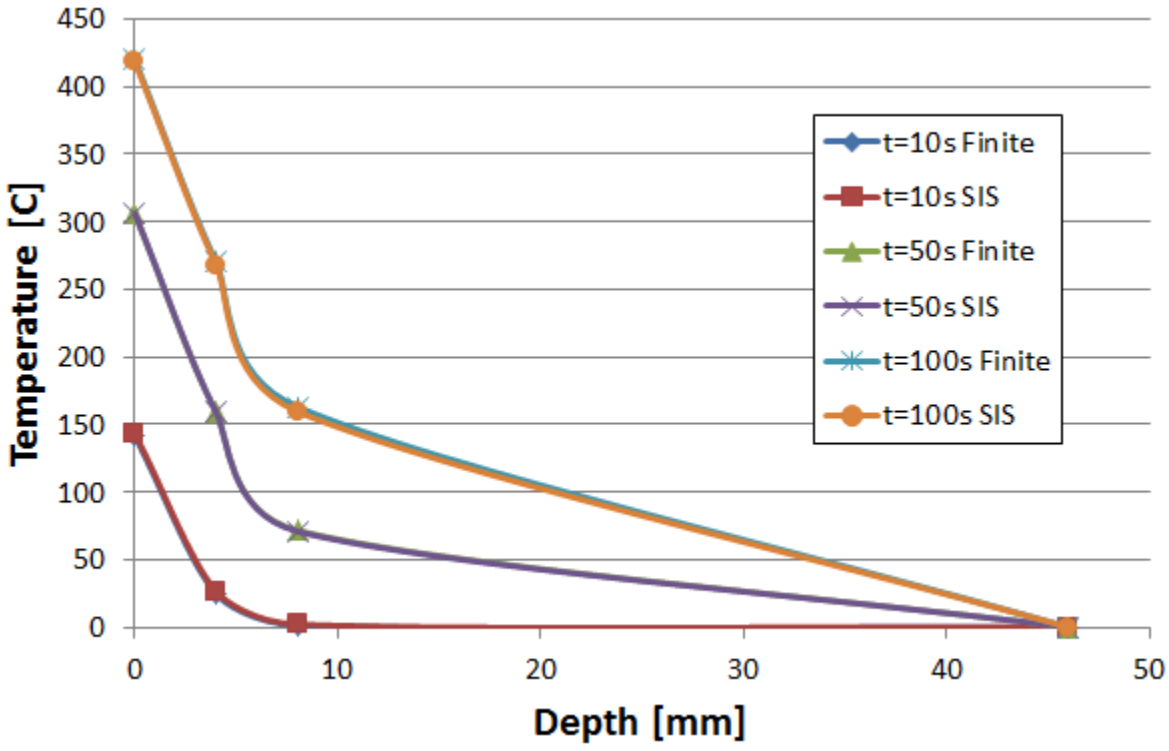

Figure 2.4.2: Temperature Profile for Model Verification (SIS stands for Semi-Infinite Solid)

3.0 PROPERTY ESTIMATION PROCEDURE

Microsoft Excel was used to calculate the temperature distributions for the different samples for each of the three boundary conditions. These samples were all exposed to 50 kW/m^2 for the tests. For the finite difference methods, 24 nodes were programmed in to comprise the sample and the 1.5 inches of ceramic fiberboard insulation. In order to determine the material properties, a chart was generated in excel and the material properties were changed until the plotted calculated values lined up with the thermocouple data.

3.1 Calculations

A sample calculation can be found in Property Estimation Sample Calculations at the end of this brief.

3.2 Property Estimation Process

The procedure that was used to estimate the thermal properties in each material using the semi-infinite solid method is as follows:

1. Open the Excel worksheet
2. Enter all known information such as volume and mass of the sample.
3. Enter the thermocouple data from the cone calorimeter test. There should be thermocouple data for the top, middle, and bottom of the sample.
4. Assume an initial value of k and C_p to be 1 and 1000, respectively.
5. If the lines for the estimated and TC values match up, they are correct, otherwise…
6. Adjust the values of k and C_p until the lines match up.

The process is similar for the finite difference and is as follows:

9. Open the Excel worksheet
10. Enter all known information such as volume and mass of the sample. The tool assumes ceramic fiberboard as a back insulation and its properties are already entered in the sheet.
11. Enter the thermocouple data from the cone calorimeter test. There should be thermocouple data for the top, middle, and bottom of the sample.
12. Assume an initial value of k and C_p to be 1 and 1000, respectively.
13. Run the “Transfer” macro (Ctrl+R) to transfer the values from the first sheet to the second sheet so they can be analyzed. Ensure that the dt is roughly 1 second. If not, the macro must be edited so it will take values for roughly each second.
14. Run the “Chart” macro (Ctrl+T) to create a graph of the thermocouple data and the temperature data from each node. If the lines for each region match, then the properties specified for k and C_p are correct.
15. If the lines do not match then run the “Clear” macro (Ctrl+E) and delete the chart
16. Navigate back to the first sheet and then adjust the values of k and C_p until the lines match up.

4.0 RESULTS

For each of the samples that were tested (see Table 4.0.1), there are temperature distributions and temperature profiles for each boundary condition. A table is included as well which shows the estimated thermal properties for each sample. The results will be discussed in section 4.6.

Table 4.0.5: Boundary Conditions

Boundary Condition	Model	Surface Condition	Back Face Condition
1	1-D Semi-Infinite	Constant Heat Flux with Convective and Radiative Losses	N/A
2	1-D Finite Difference	Surface Thermocouple Data	Convective Losses
3	1-D Finite Difference	Constant Heat Flux with Convective and Radiative Losses	Convective Losses

4.1 Kreysler System 1

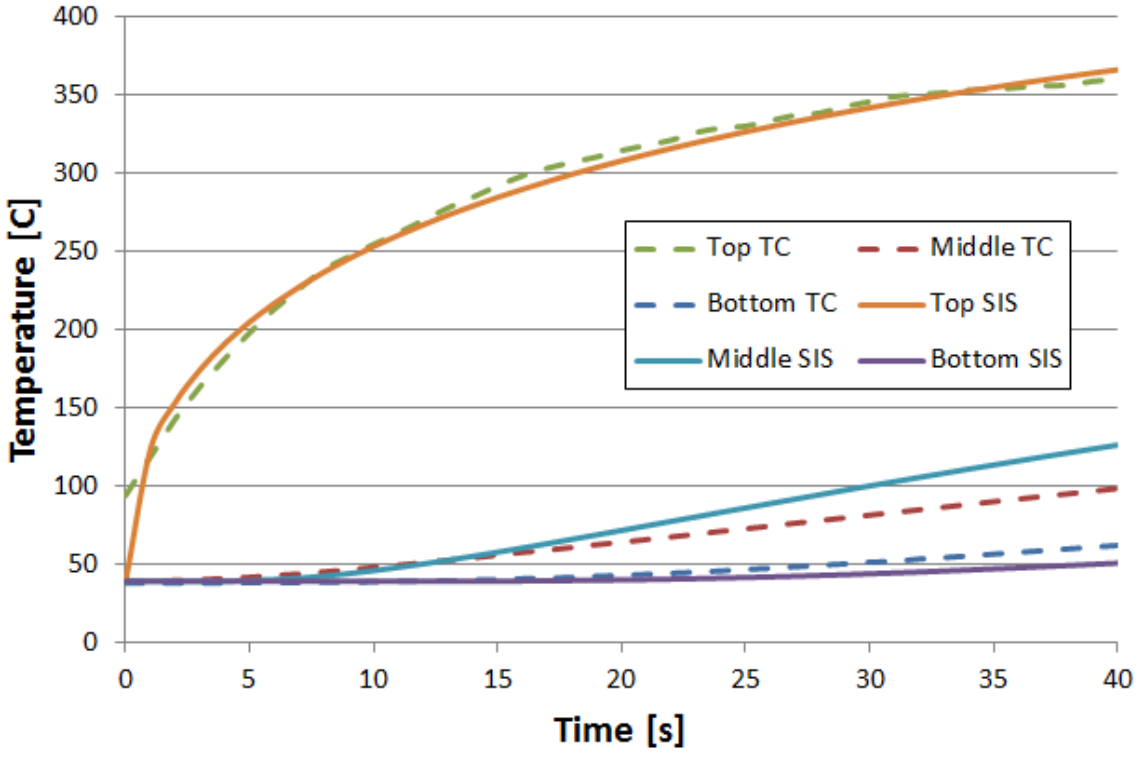

Figure 4.1.1: Boundary Condition 1 Temperature Distribution (SIS stands for Semi-Infinite Solid)

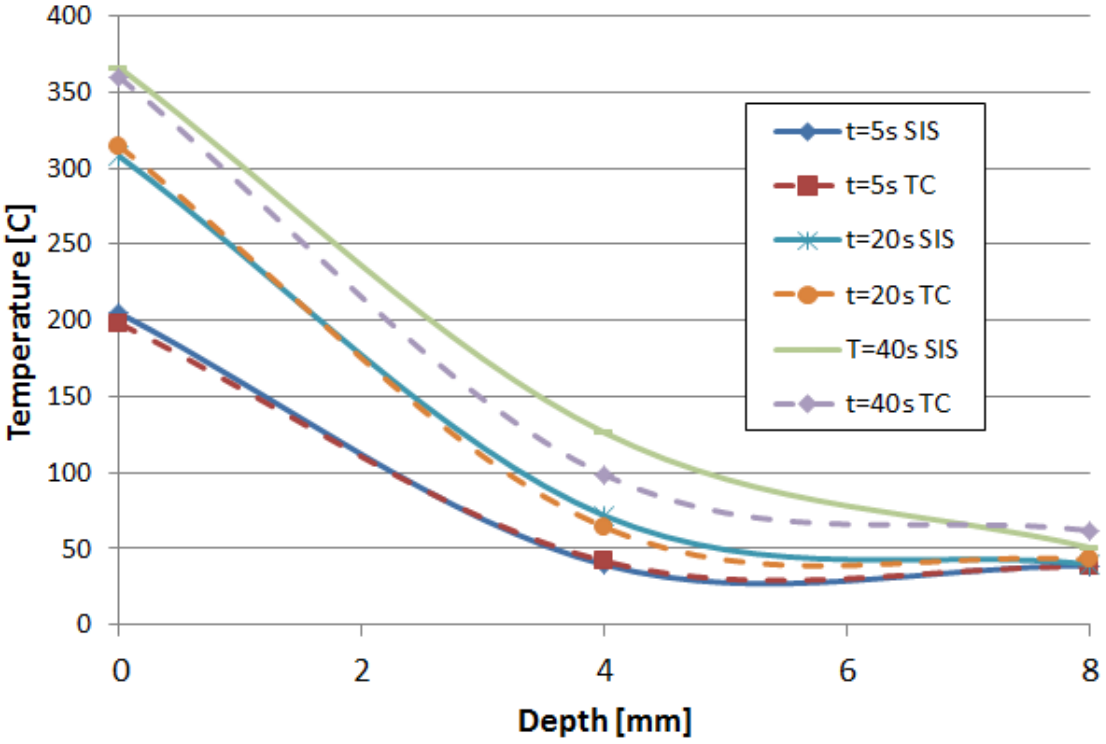

Figure 4.1.2: Boundary Condition 1 Temperature Profile (SIS stands for Semi-Infinite Solid)

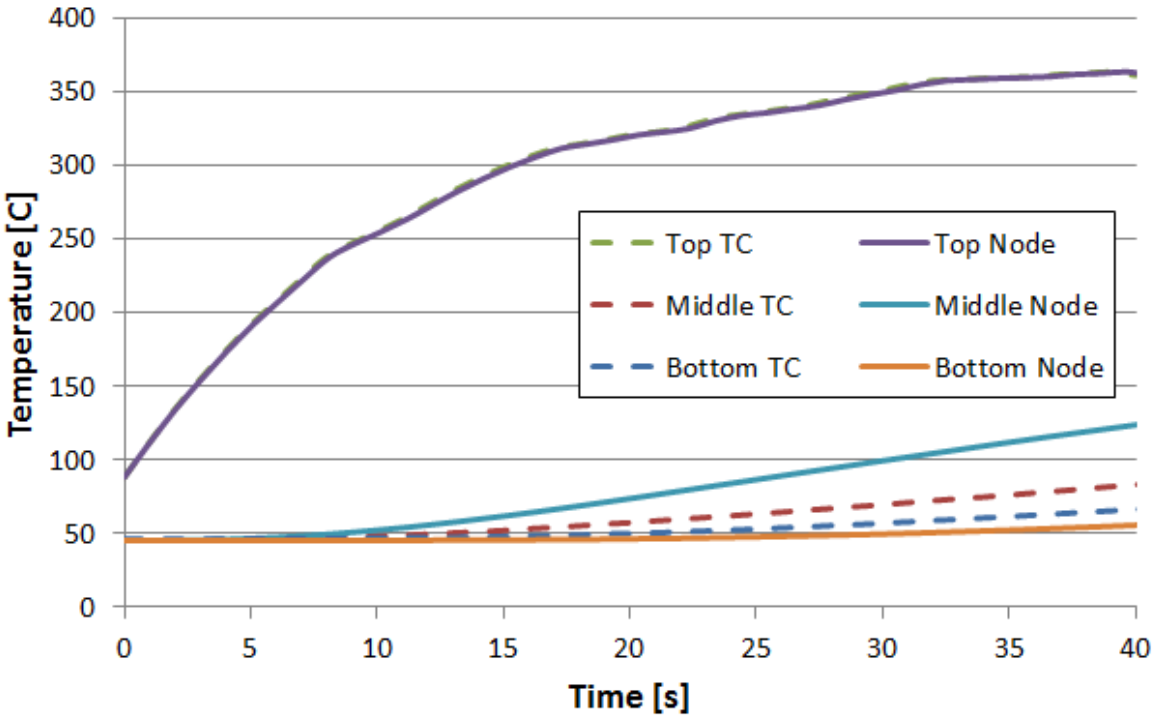

Figure 4.1.3: Boundary Condition 2 Temperature Distribution

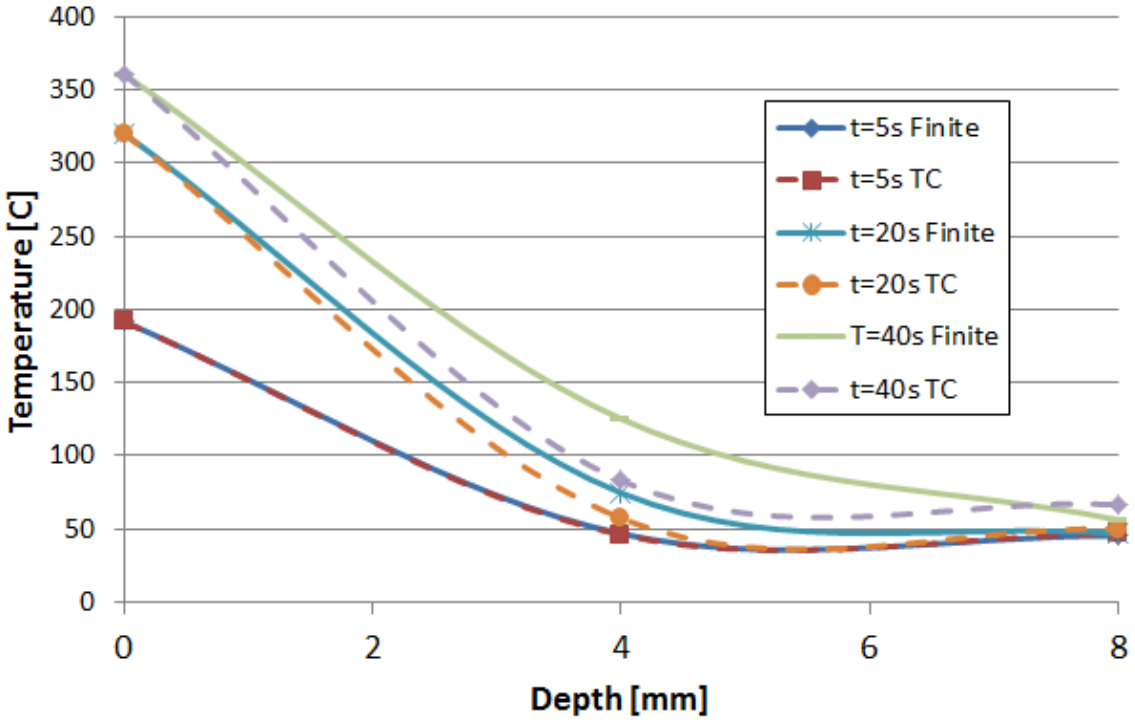

Figure 4.1.4: Boundary Condition 2 Temperature Profile

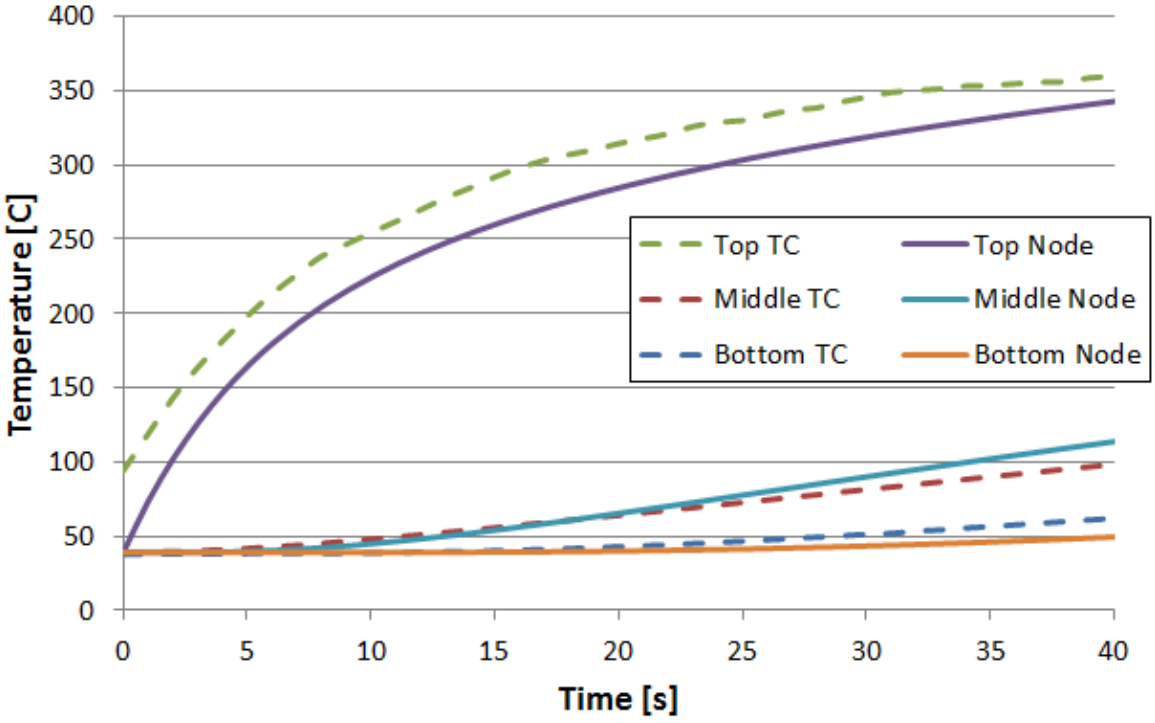

Figure 4.1.5: Boundary Condition 3 Temperature Distribution

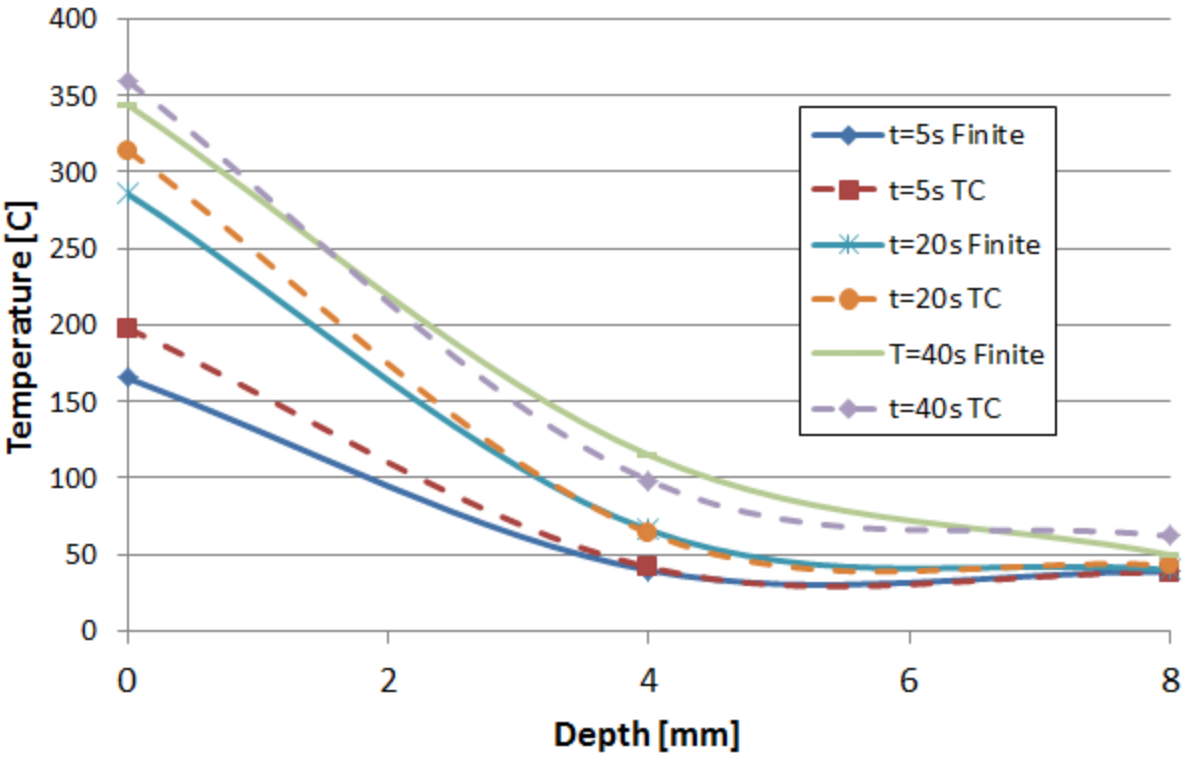

Figure 4.1.6: Boundary Condition 3 Temperature Profile

Table 4.1.1: Estimated Properties for Kreysler System 1

Kreysler System 1		
Boundary Condition	Thermal Conductivity (W/m*K)	Specific Heat (J/kg*K)
1	0.28	700
2	0.28	800
3	0.3	800

4.2 Kreysler System 2

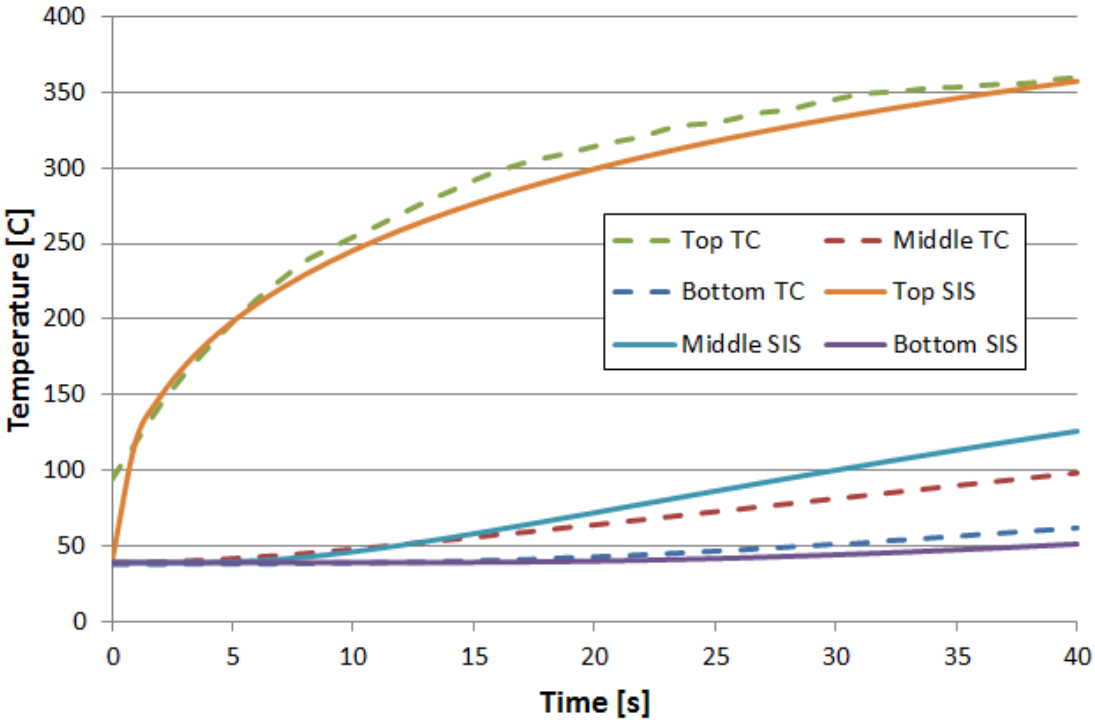

Figure 4.2.1: Boundary Condition 1 Temperature Distribution (SIS stands for Semi-Infinite Solid)

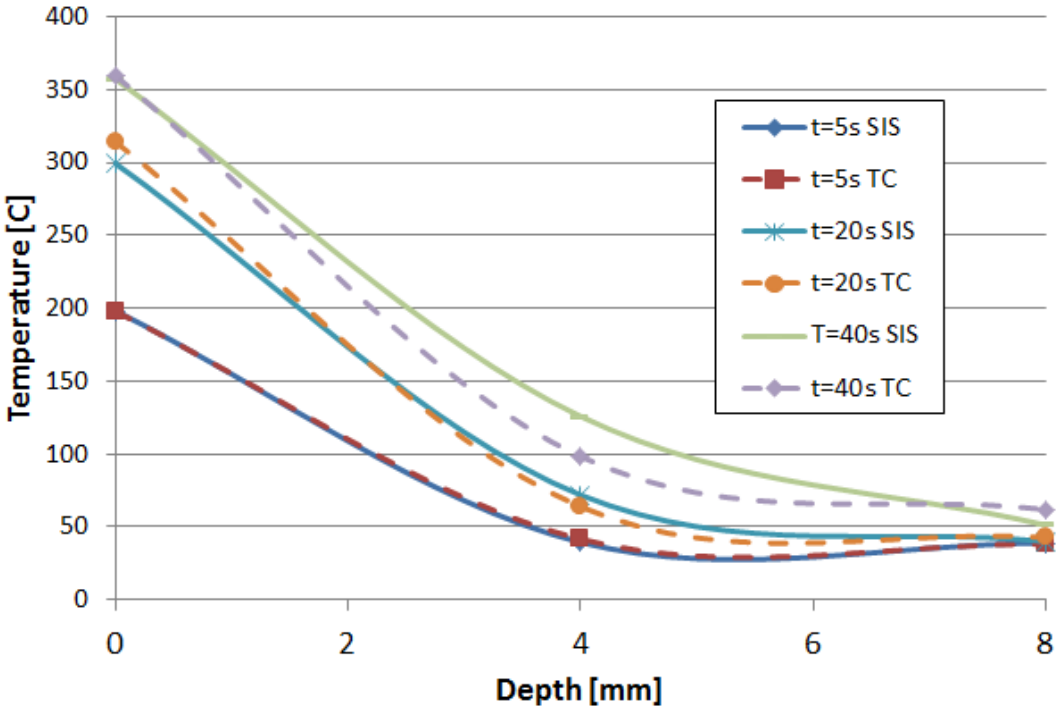

Figure 4.2.2: Boundary Condition 1 Temperature Profile (SIS stands for Semi-Infinite Solid)

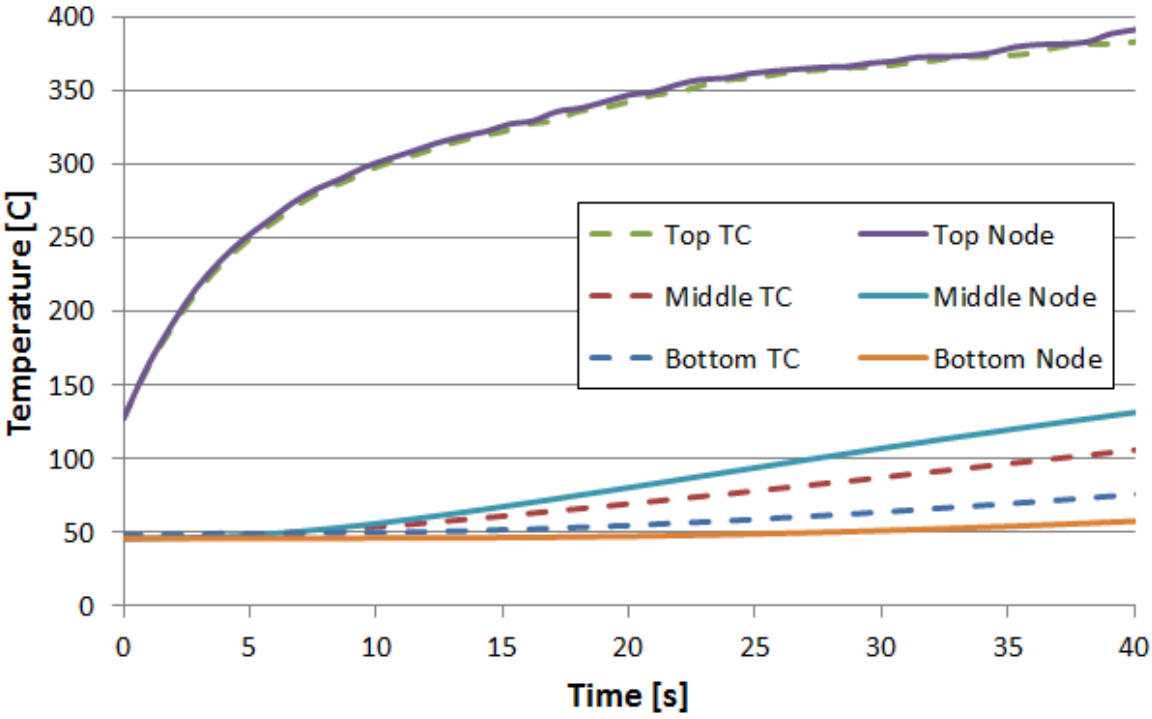

Figure 4.2.3: Boundary Condition 2 Temperature Distribution

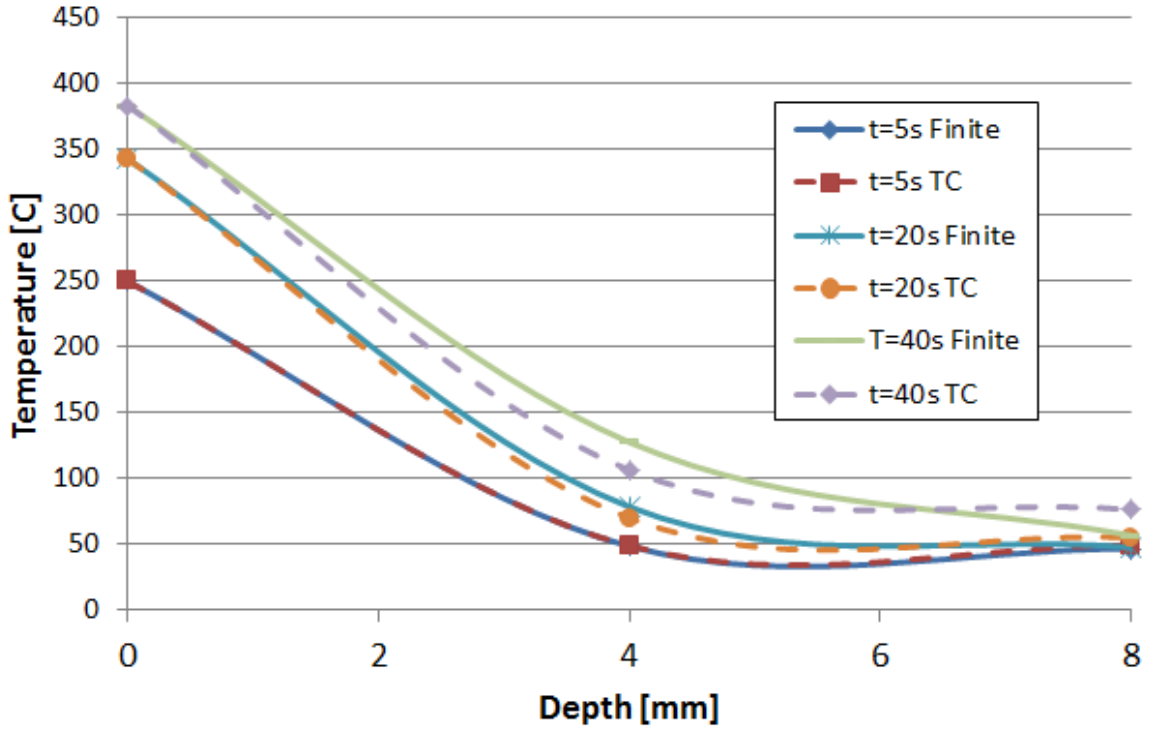

Figure 4.2.4: Boundary Condition 2 Temperature Profile

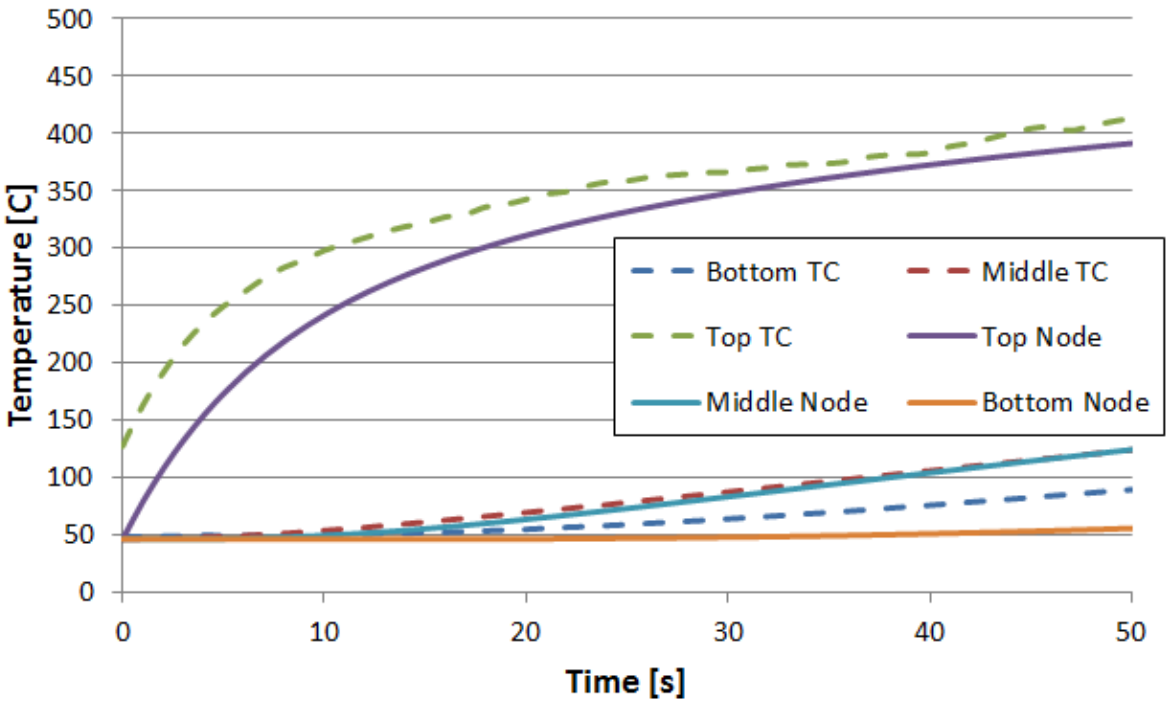

Figure 4.2.5: Boundary Condition 3 Temperature Distribution

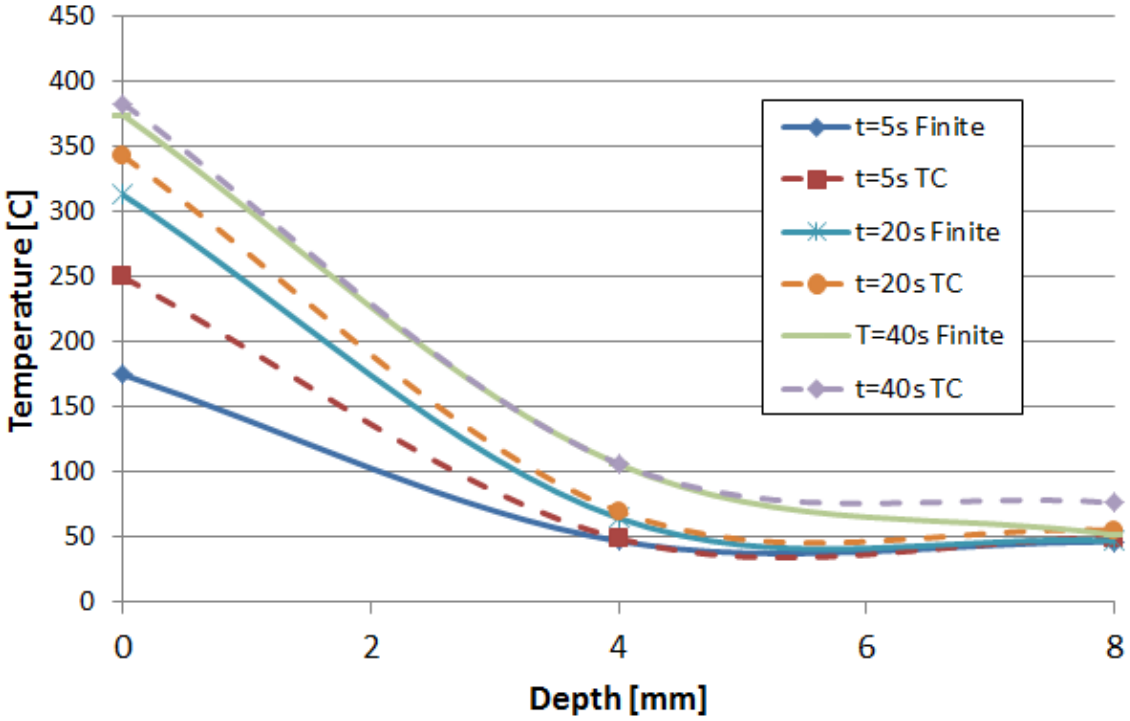

Figure 4.2.6: Boundary Condition 3 Temperature Profile

Table 4.2.1: Estimated Properties for Kreysler System 2

Kreysler System 2		
Boundary Condition	Thermal Conductivity (W/m*K)	Specific Heat (J/kg*K)
1	0.3	700
2	0.26	750
3	0.22	800

4.3 CP 802

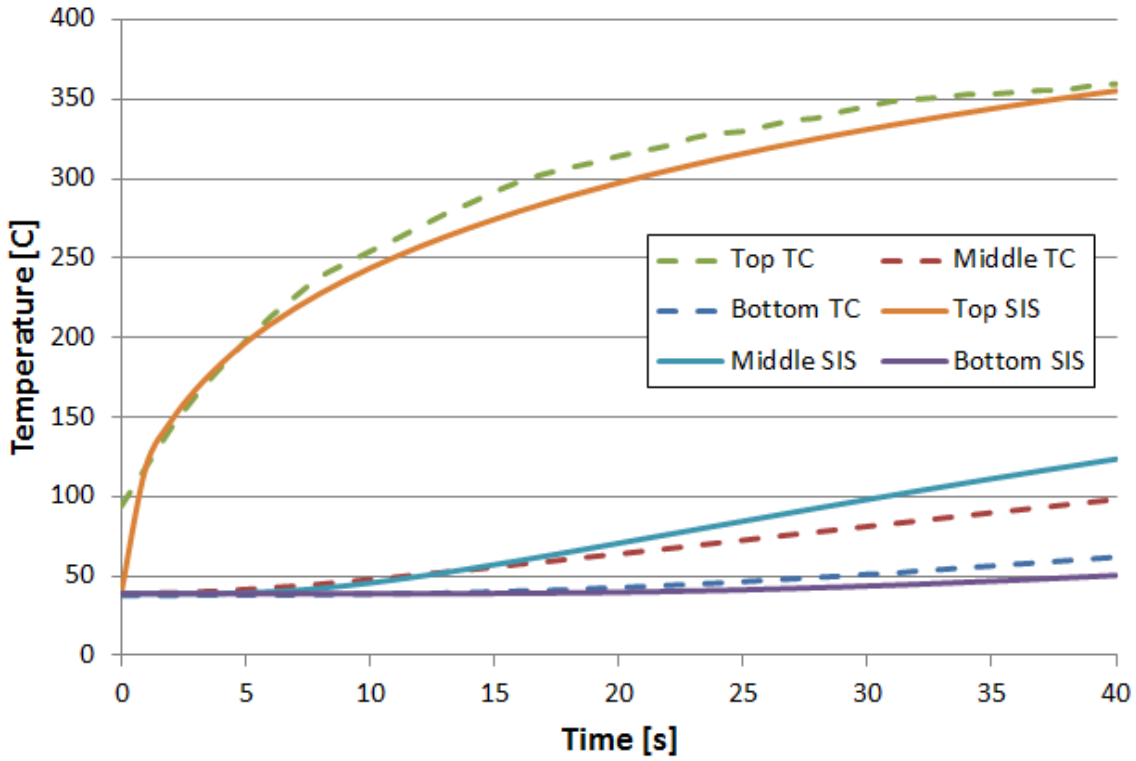

Figure 4.3.1: Boundary Condition 1 Temperature Distribution (SIS stands for Semi-Infinite Solid)

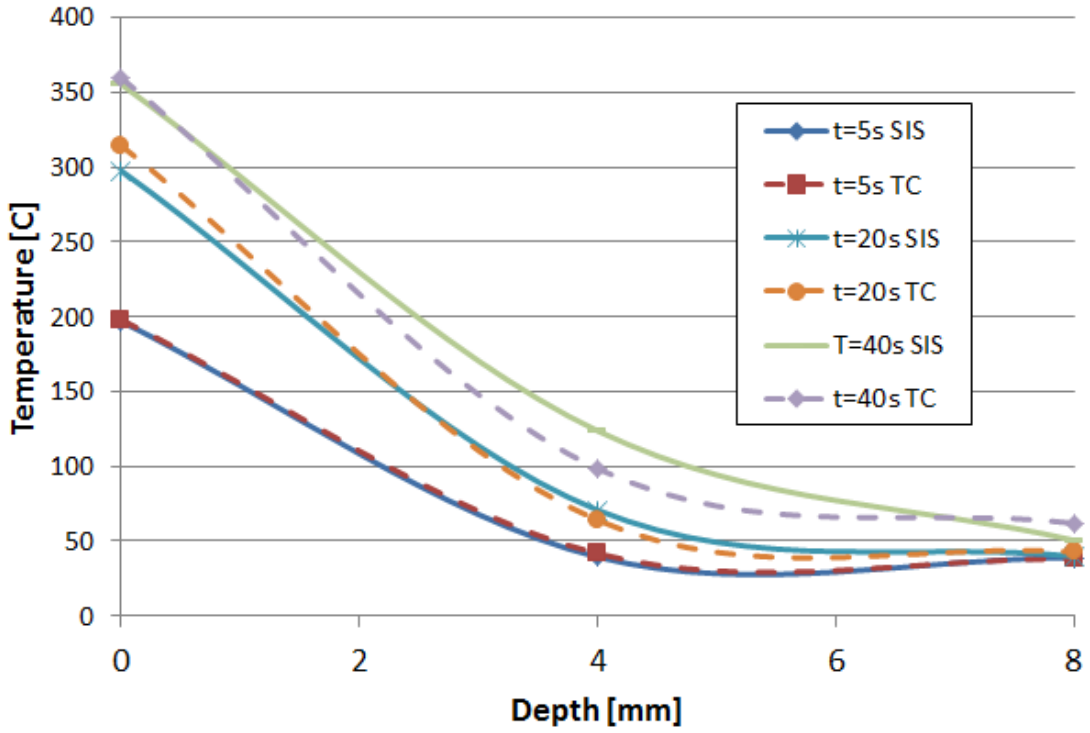

Figure 4.3.2: Boundary Condition 1 Temperature Profile (SIS stands for Semi-Infinite Solid)

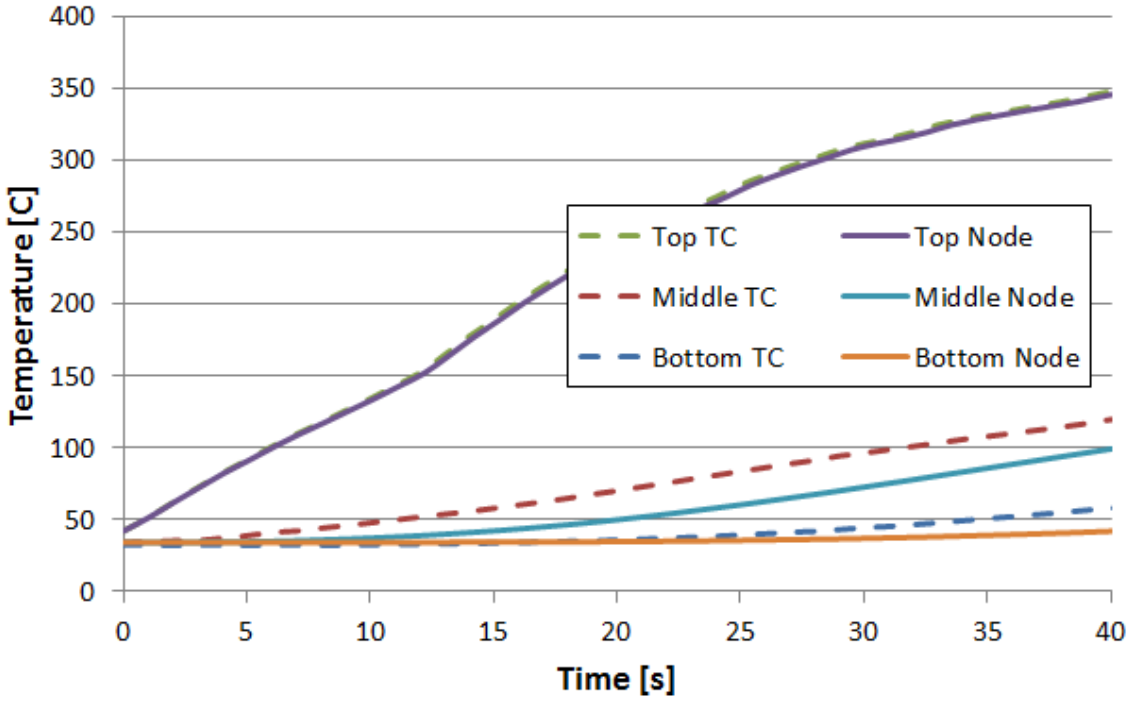

Figure 4.3.3: Boundary Condition 2 Temperature Distribution

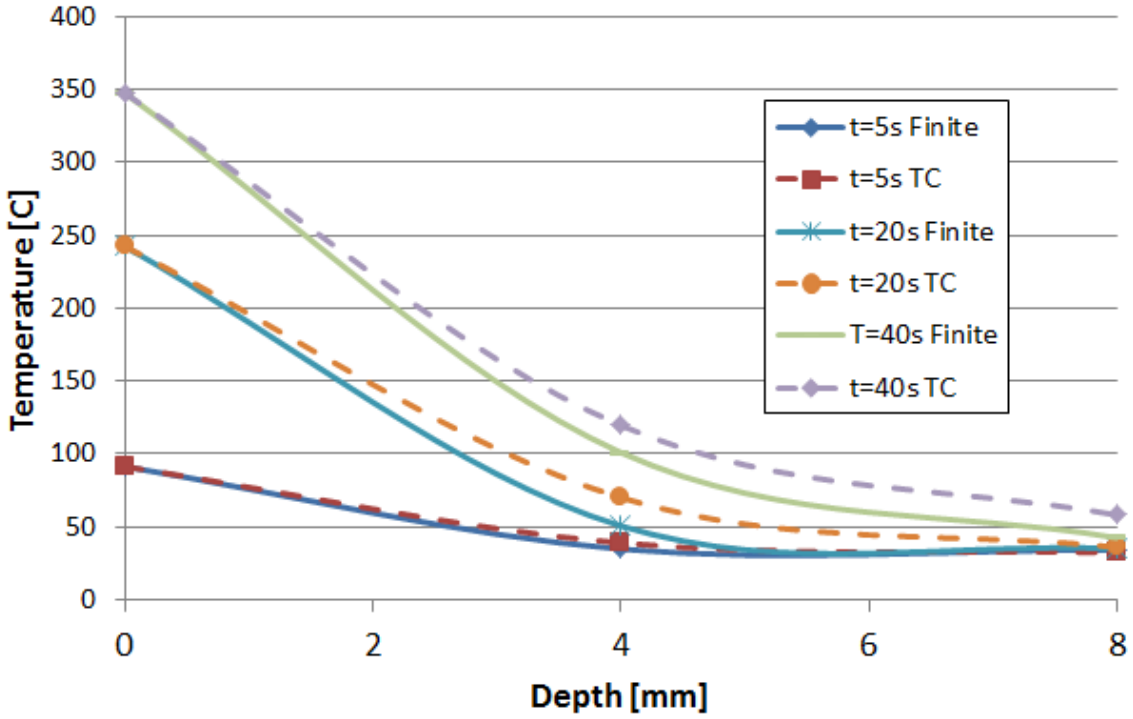

Figure 4.3.4: Boundary Condition 2 Temperature Profile

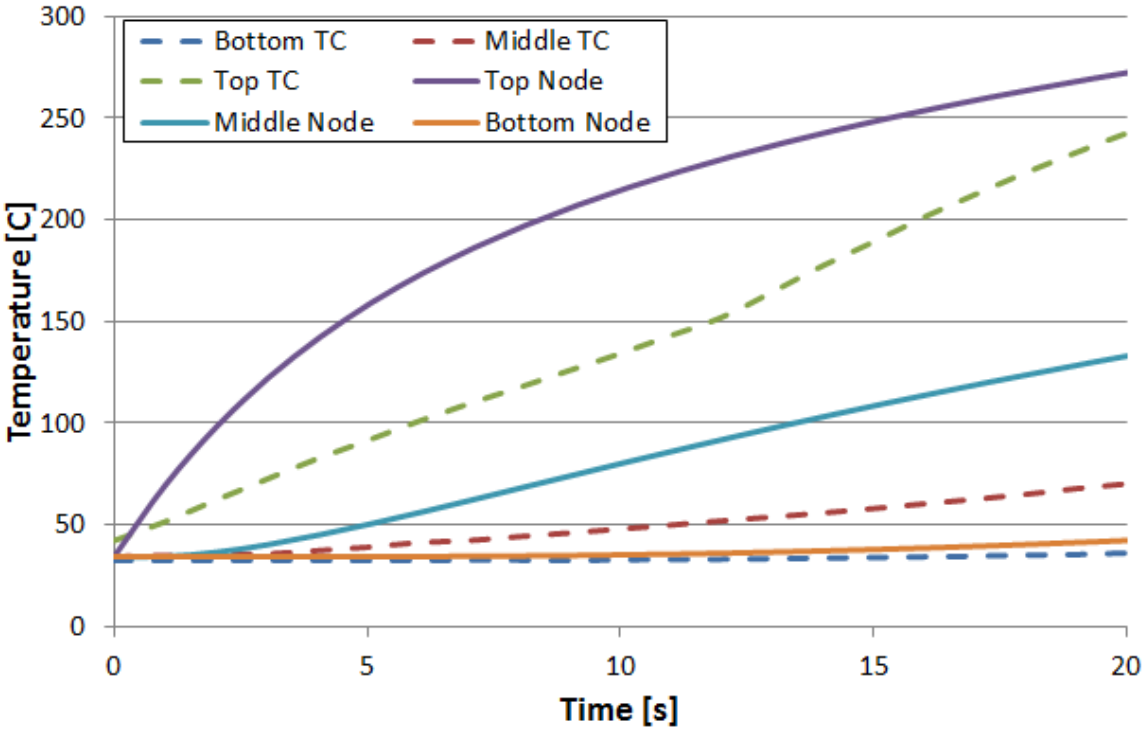

Figure 4.3.5: Boundary Condition 3 Temperature Distribution

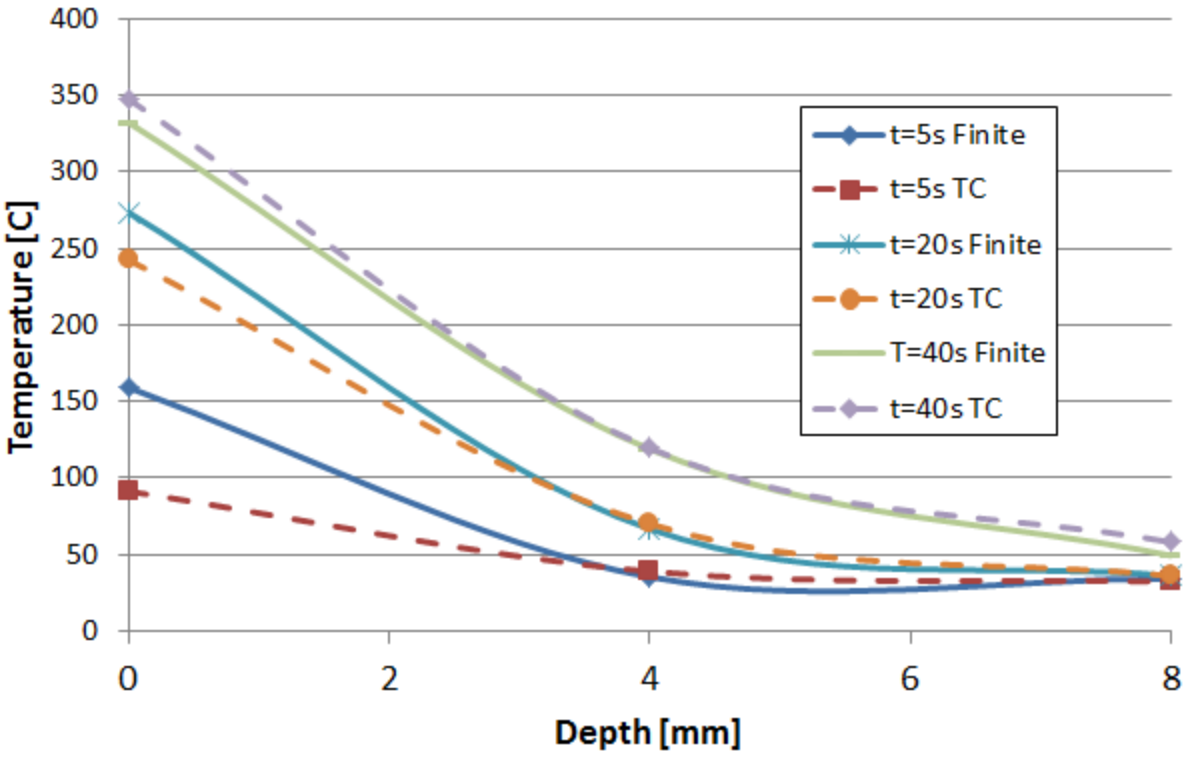

Figure 4.3.6: Boundary Condition 3 Temperature Profile

Table 4.3.1: Estimated Properties for CP 802

CP 802		
Boundary Condition	Thermal Conductivity (W/m*K)	Specific Heat (J/kg*K)
1	0.3	750
2	0.33	800
3	0.35	800

4.4 CP 702

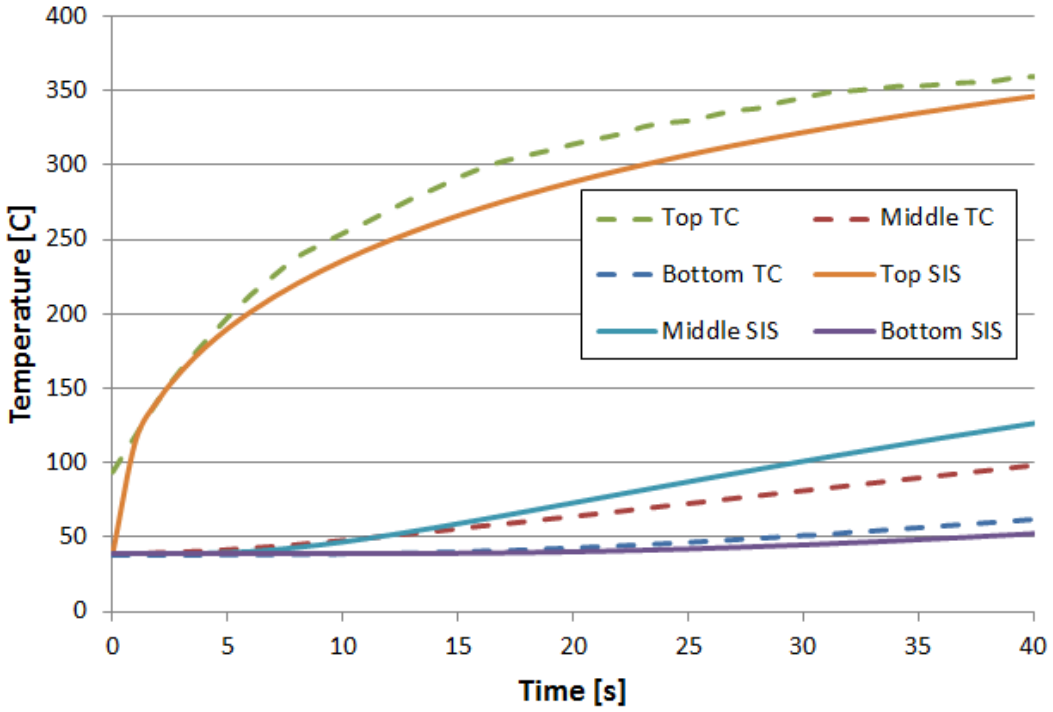

Figure 4.4.15: Boundary Condition 1 Temperature Distribution (SIS stands for Semi-Infinite Solid)

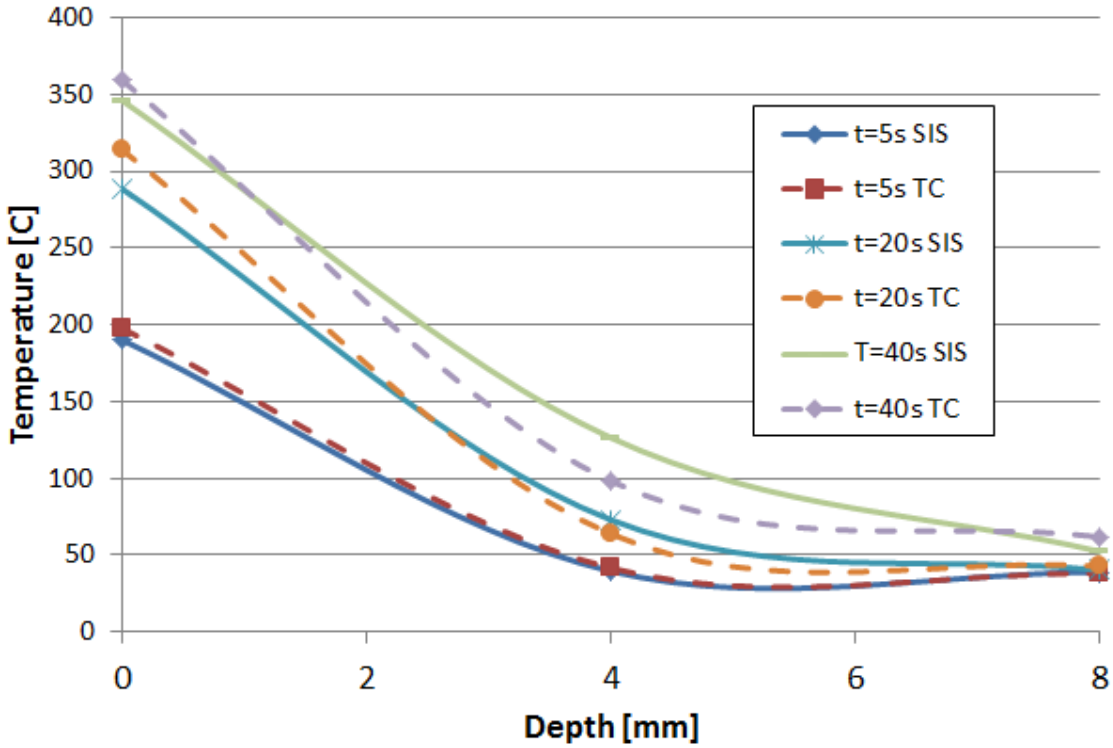

Figure 4.4.2: Boundary Condition 1 Temperature Profile (SIS stands for Semi-Infinite Solid)

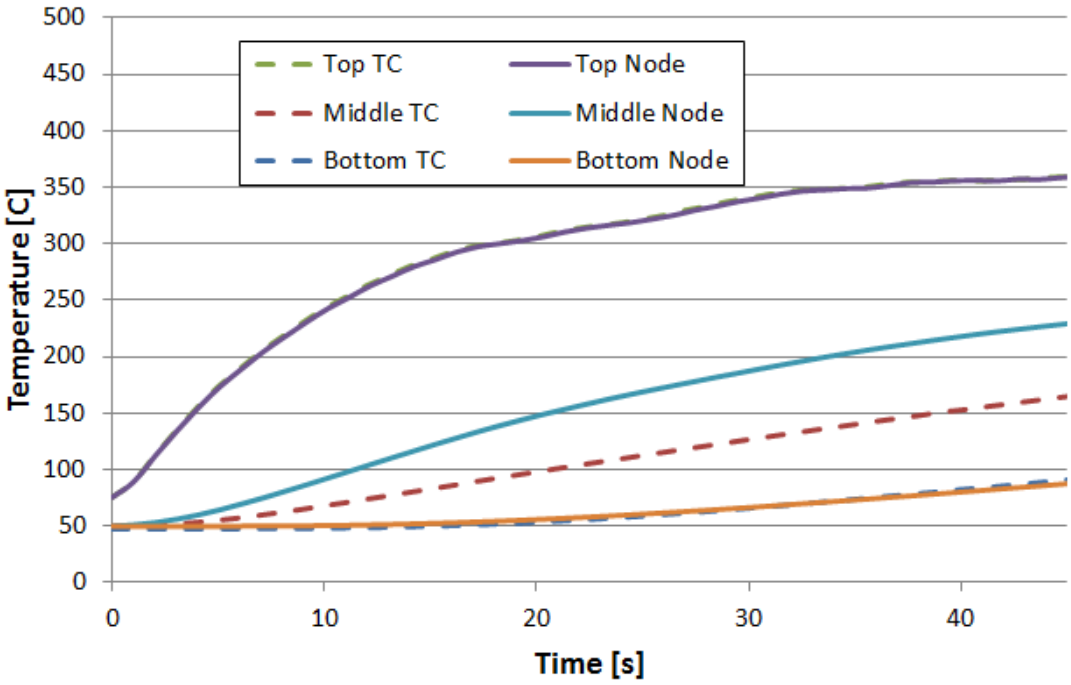

Figure 4.4.3: Boundary Condition 2 Temperature Distribution

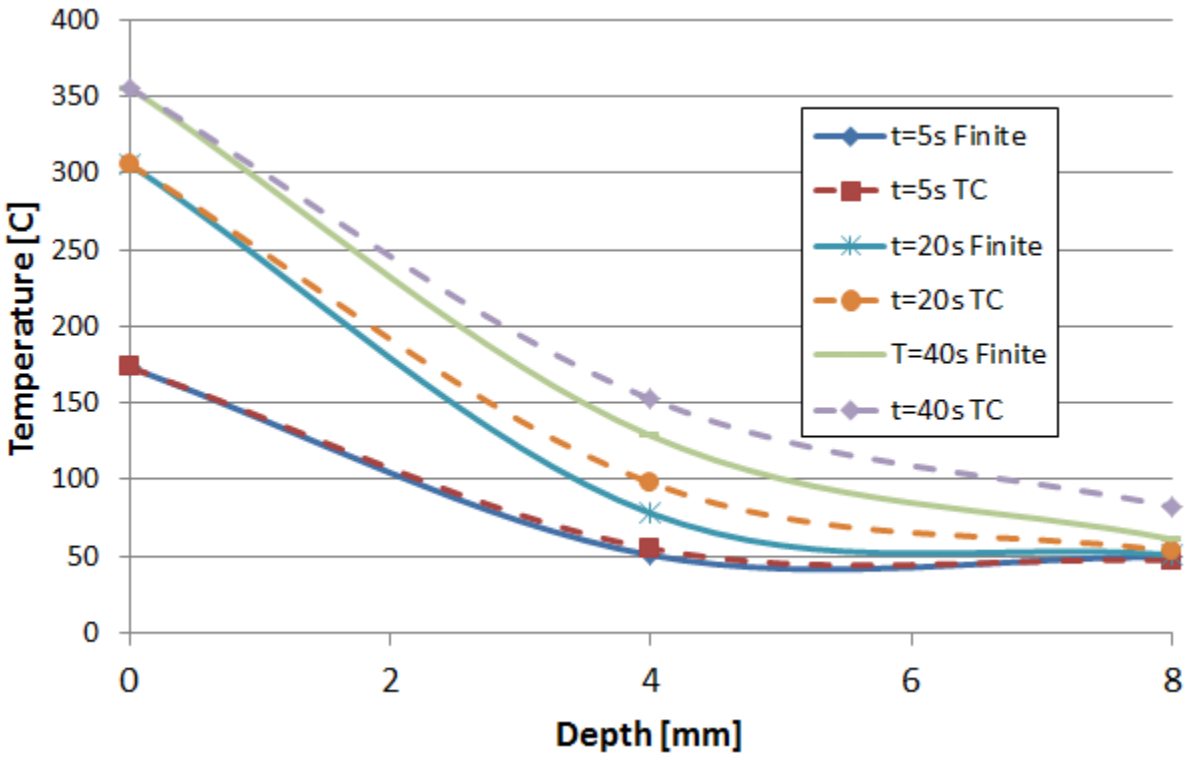

Figure 4.4.4: Boundary Condition 2 Temperature Profile

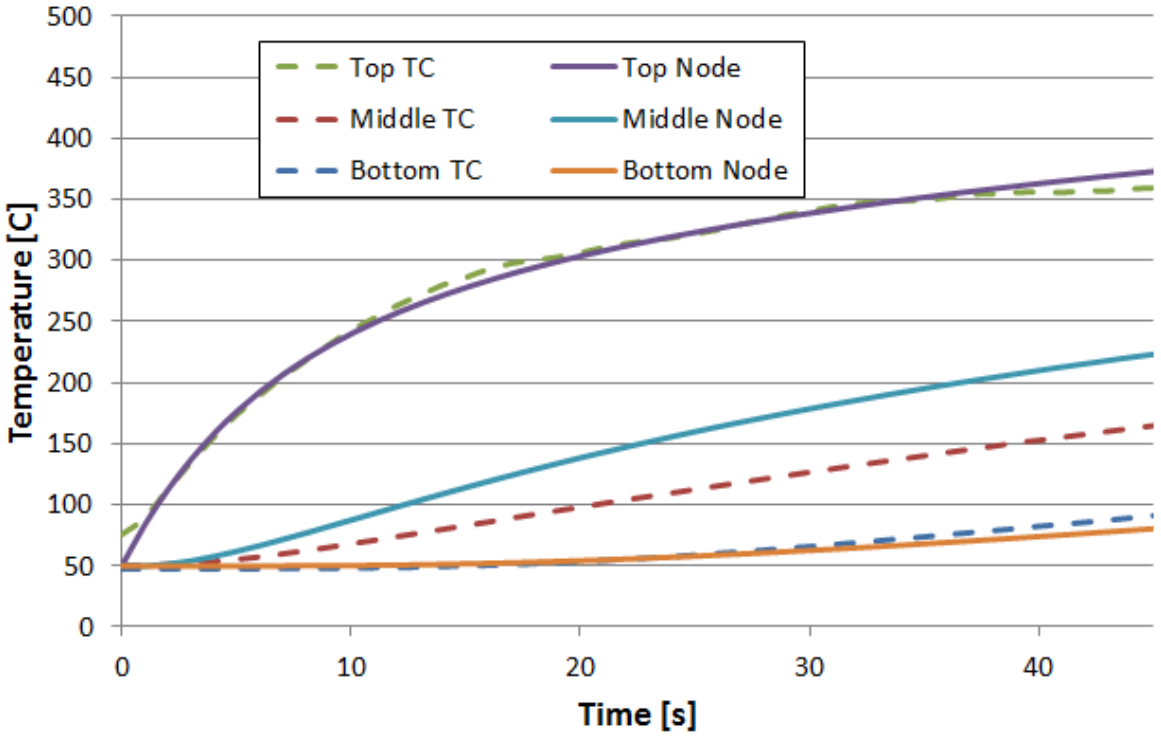

Figure 4.4.5: Boundary Condition 3 Temperature Distribution

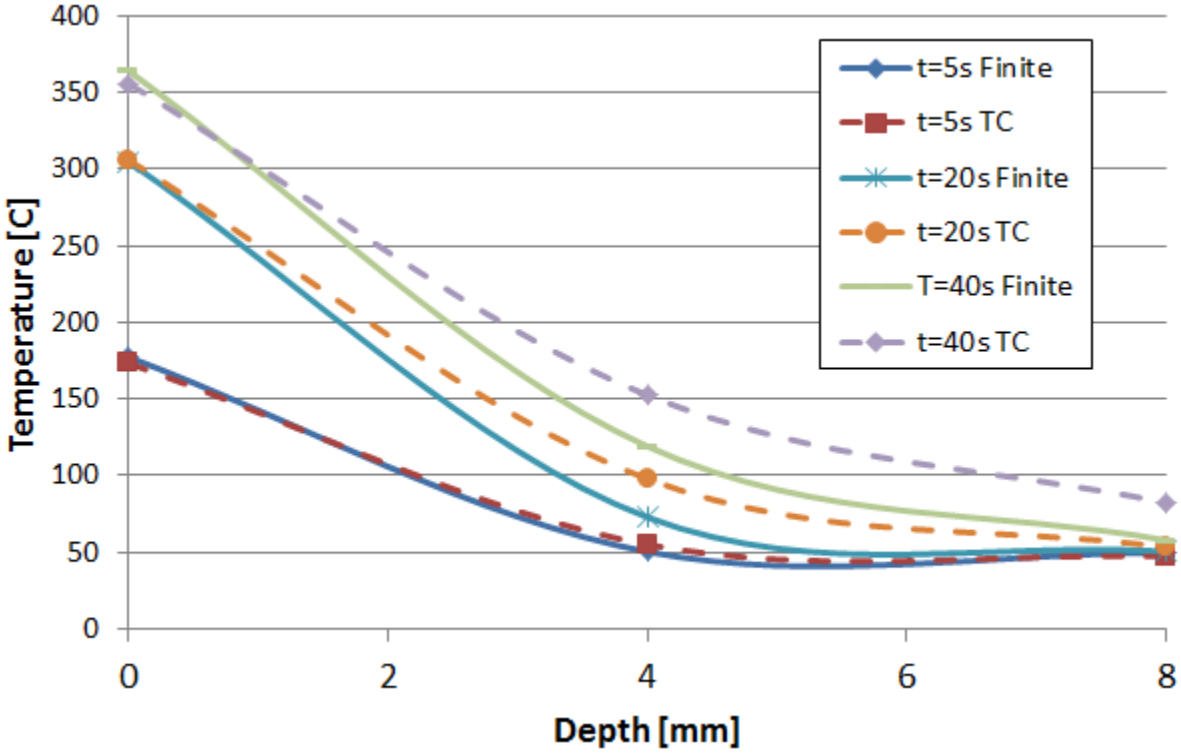

Figure 4.4.6: Boundary Condition 3 Temperature Profile

Table 4.4.1: Estimated Properties for CP 702

CP 702		
Boundary Condition	Thermal Conductivity (W/m*K)	Specific Heat (J/kg*K)
1	0.33	750
2	0.3	800
3	0.26	800

4.5 CP 286

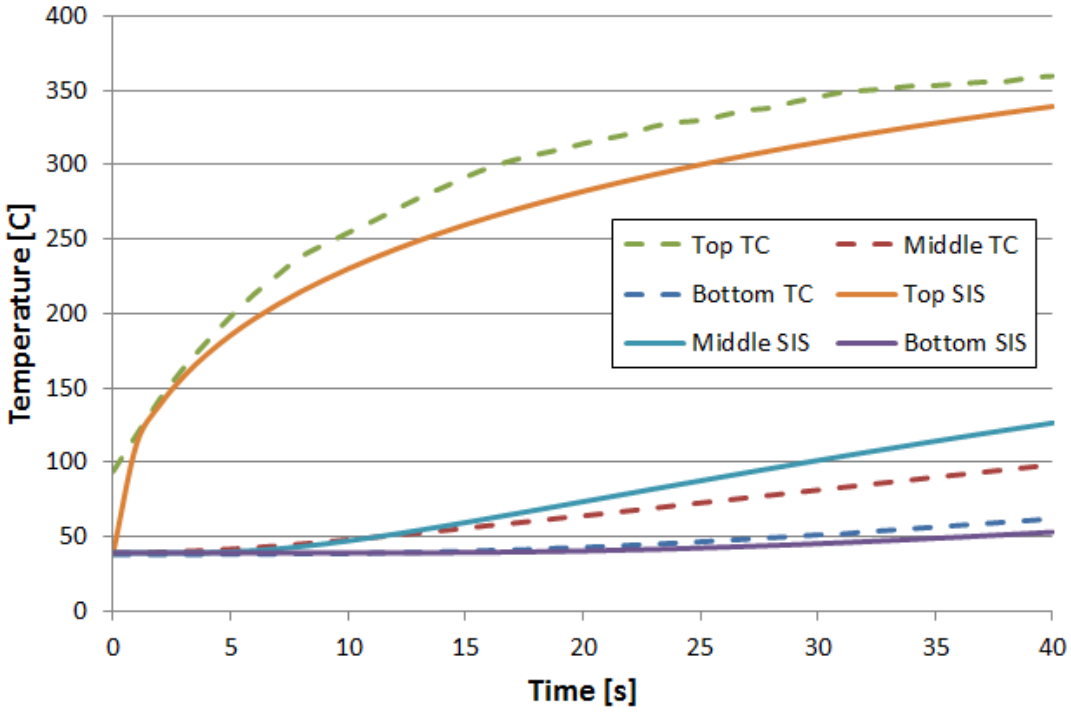

Figure 4.5.1: Boundary Condition 1 Temperature Distribution (SIS stands for Semi-Infinite Solid)

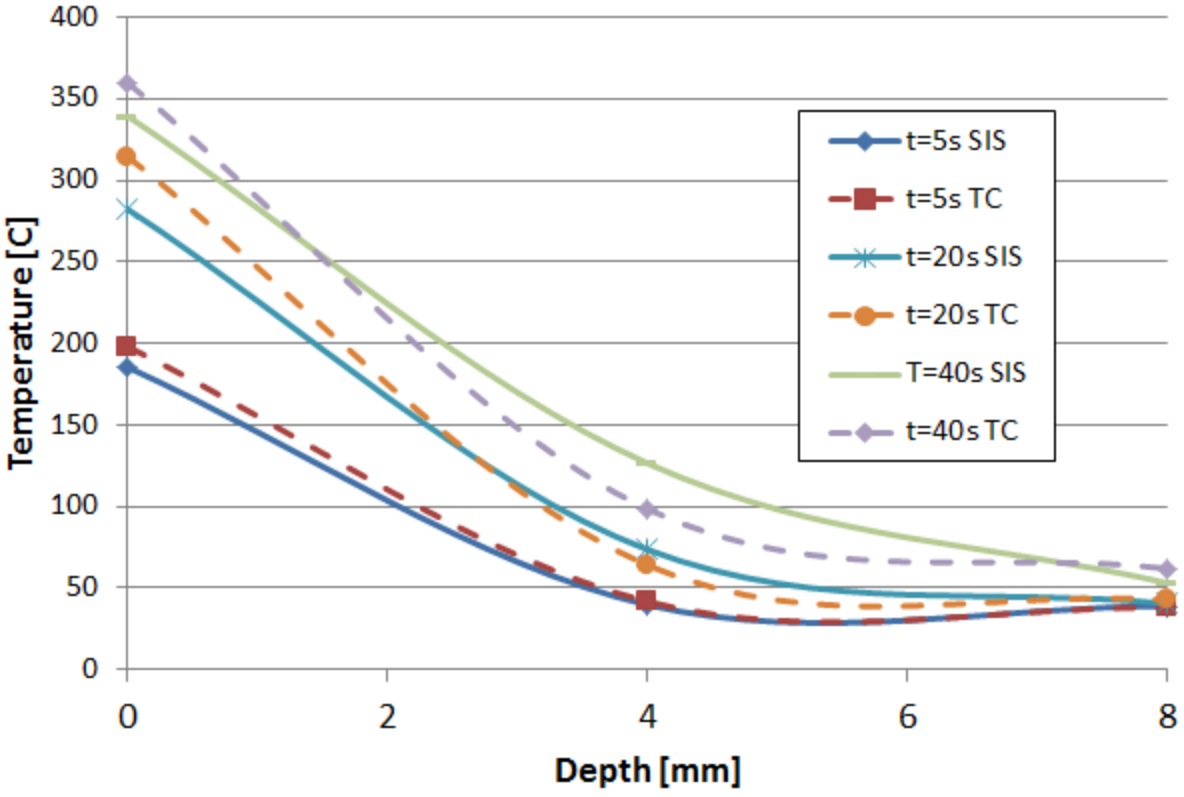

Figure 4.5.2: Boundary Condition 1 Temperature Profile (SIS stands for Semi-Infinite Solid)

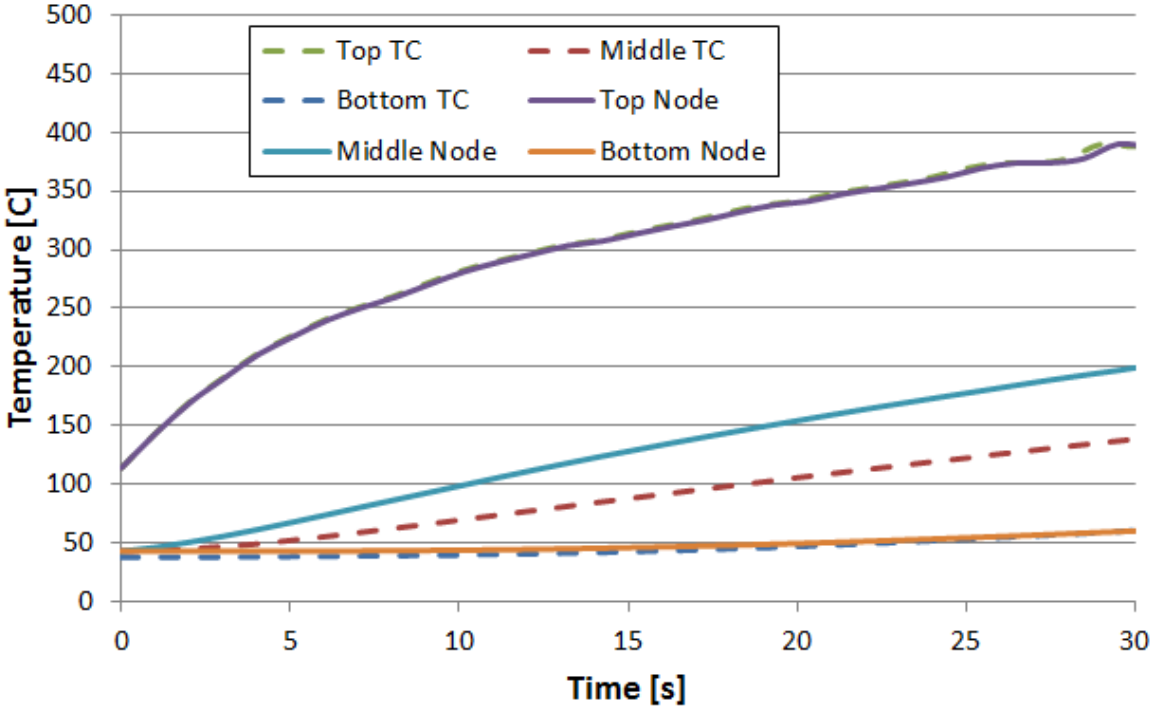

Figure 4.5.3: Boundary Condition 2 Temperature Distribution

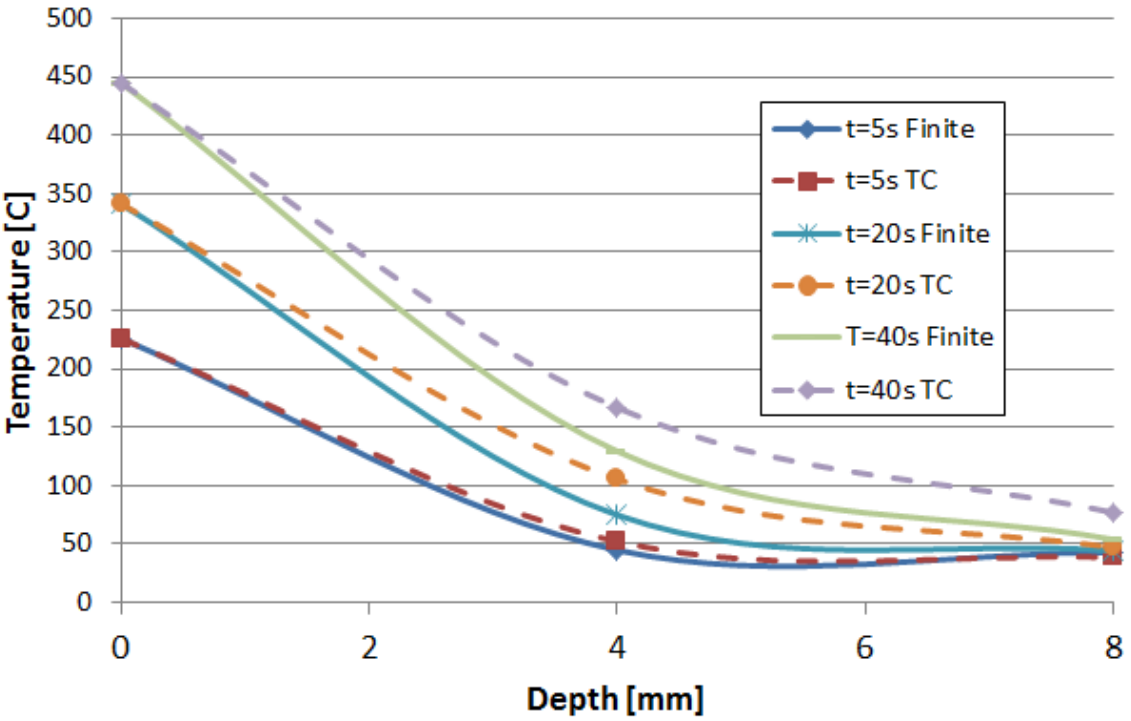

Figure 4.5.4: Boundary Condition 2 Temperature Profile

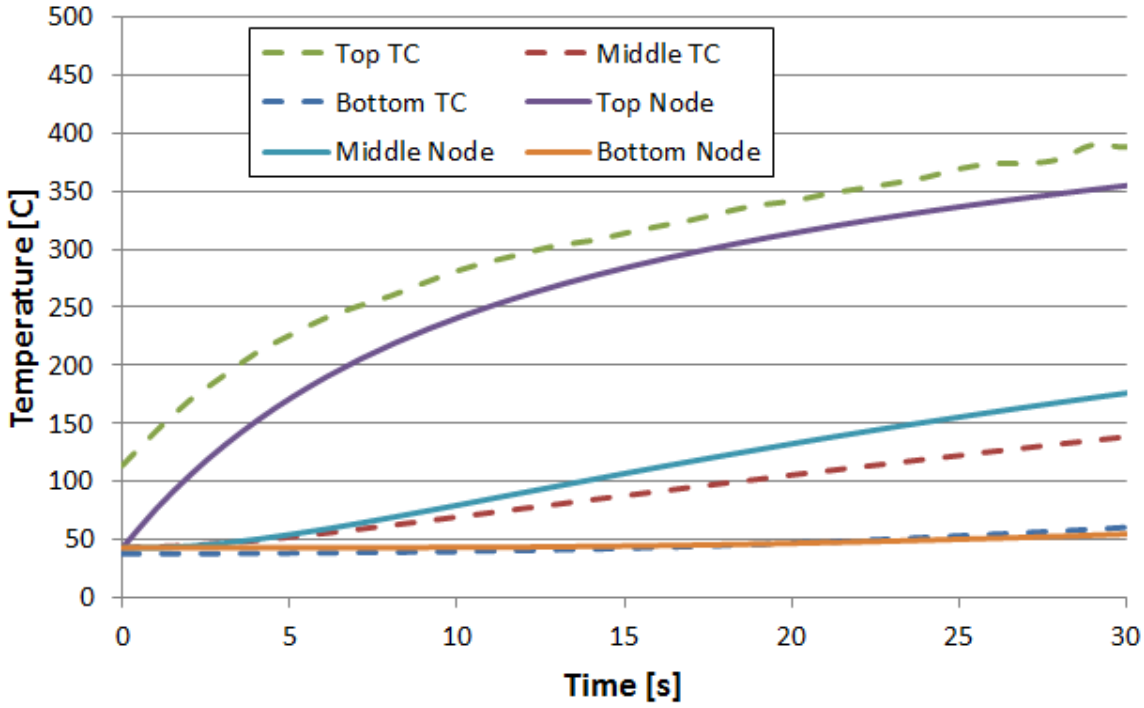

Figure 4.5.5: Boundary Condition 3 Temperature Distribution

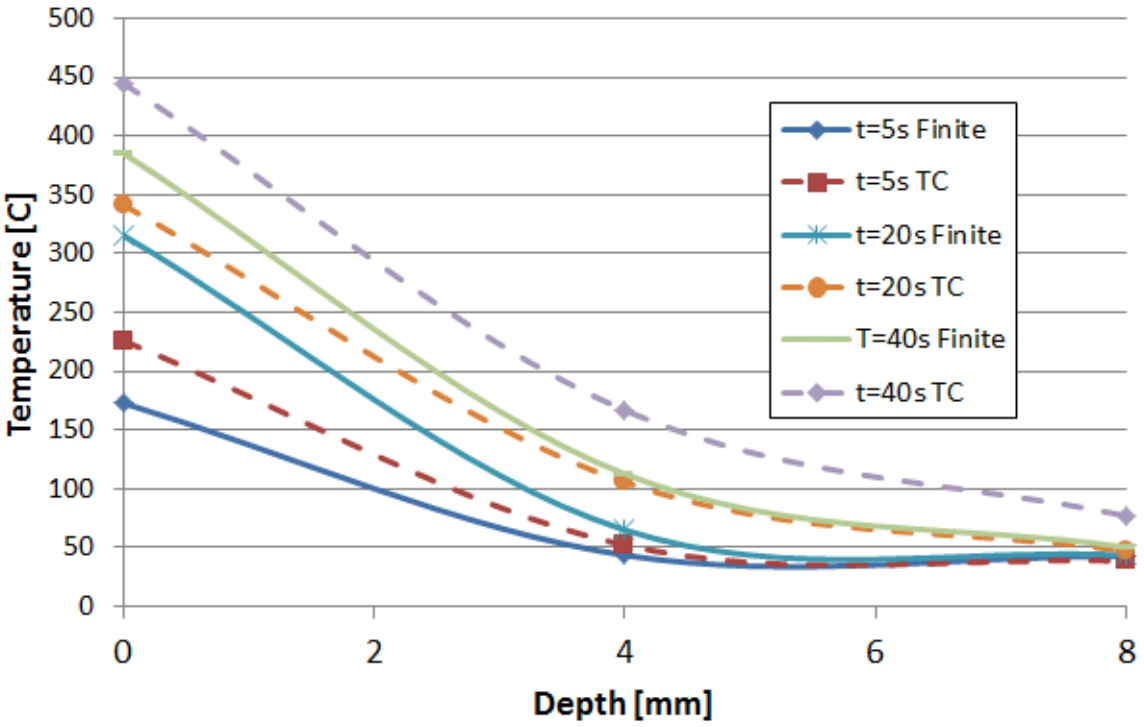

Figure 4.5.6: Boundary Condition 3 Temperature Profile

Table 4.5.1: Estimated Properties for CP 286

CP 286		
Boundary Condition	Thermal Conductivity (W/m*K)	Specific Heat (J/kg*K)
1	0.35	750
2	0.28	800
3	0.25	800

4.6 RESULTS

A summary of the thermal properties can be seen below in Table 4.0.1.

Table 4.0.1: Summary of Estimated Thermal Properties

	BC 1		BC 2		BC 3	
System	Thermal Conductivity (W/m*K)	Specific Heat (J/kg*K)	Thermal Conductivity (W/m*K)	Specific Heat (J/kg*K)	Thermal Conductivity (W/m*K)	Specific Heat (J/kg*K)
1	0.28	700	0.28	800	0.3	800
2	0.3	700	0.26	750	0.22	800
286	0.35	750	0.28	800	0.25	800
702	0.33	750	0.3	800	0.26	800
802	0.3	750	0.33	800	0.35	800

All three boundary conditions returned similar properties for each material. Thermal conductivity for each boundary condition was within 10%, for a given material. Similarly, the specific heats for each boundary condition were all within 12.5%. Without being able to test materials which have known thermal properties (which we were not able to accomplish as part of this project), we cannot know which boundary condition is the most accurate. Assuming their accuracy is similar for a given material, it is easier to judge the effectiveness based on the ease of use of each tool. Due to the fact that the semi-infinite solids calculation requires much less computational power, it is much easier and quicker to use this tool to estimate thermal properties of each material. It takes much longer to iterate on the finite difference boundary conditions due to the time it takes for the computer to be able to run each calculation. However there are advantages of the finite difference model as well. For instance, if a heterogeneous material such as a sandwich panel was being tested, then the finite difference model would be much more accurate. A sandwich panel is two pieces of exterior material, such as FRP, that are attached to a substrate material, such as foam or wood. Since the semi-infinite solid assumes that the material has the same properties throughout the depth, it cannot accurately model the change in the thermal properties the way that the finite difference method could.

5.0 CONCLUSION

A tool that can utilize data that is normally gathered from Cone Calorimeter tests to estimate thermal properties was successfully created. The property estimation tool only requires that 3 thermocouples are installed in addition to the normal Cone test. In using this tool, the thermal conductivity and specific heat of samples can be estimated with reasonable accuracy which may be helpful to material designers. Since the semi-infinite solid solution is similar to the finite difference solutions, at least for the samples that were tested in this project, it is much easier and faster to use the semi-infinite tool since there are much less calculations. However if different types of materials were to be tested in the Cone, such as a sandwich panel with different layers, then the finite difference analysis should be used. However there is room for improvement of this tool in the future. First of all, this project does not include the testing of materials with known thermal properties to further verify the solutions. The tool would be improved by knowing that it has accurately predicted the thermal properties of such materials. Another improvement would be to write coding language for either Excel or another computational program which automatically changes thermal properties in an iterative fashion until they are correct.

REFERENCES

ASTM E1354-11b Standard Test Method for Heat and Visible Smoke Release Rates for Materials and Products Using an Oxygen Consumption Calorimeter. (2011 Edition). West Conshohocken, PA: ASTM

Carslaw, H. S., & Jaeger, J. C. (1959). Conduction of heat in solids. (2nd ed.). London: Oxford. Retrieved ISBN-0198533683

"Convective Heat Transfer." *Convective Heat Transfer*. The Engineering Toolbox, n.d. Web. 17 Dec. 2012.

"How to Determine the "R" Value." *Professional Equipment*. Professional Equipment, n.d. Web. 17 Dec. 2012.

Incropera, Frank P., and David P. Dewitt. *Fundamentals of Heat and Mass Transfer*. Vol. 7. Jefferson City: John Wiley and Sons, 2011. Print.

Incropera, Frank P., David P. Dewitt, Theodore L. Bergman, and Adrienne S. Lavine. *Fundamentals of Heat and Mass Transfer*. 6th ed. N.p.: John Wiley & Sons, 2007. Print.

Rathore, M. M. *Engineering Heat Transfer*. 2nd ed. N.p.: Jones and Bartlett Learning, 2011. Print.

Rohsenow, W. M., Hartnett, J. P. and Ganic, E. N. (1985) *Handbook of Heat Transfer*, 2nd ed., McGraw-Hill, New York.

Rowlett, Russ. "A Dictionary of Units of Measurement." *Units: R*. University of North Carolina at Chapel Hill, 25 Apr. 2002. Web. 17 Dec. 2012.

"Transient Heat Conduction in Semi-Infinite Solids." *TRANSIENT HEAT CONDUCTION IN SEMI-INFINITE SOLIDS*. ECourses, n.d. Web. 15 Feb. 2013. <http://ecourses.vtu.ac.in/nptel/courses/Webcourse-contents/IIT%20Bombay/Heat%20and%20Mass%20Transfer/Conduction/Module%204/main/4.5.html>.

Tye, R. P. (1969) *Measurement of Thermal Conductivity*, Vols 1 and 2, Academic Press, New York.

PROPERTY ESTIMATION SAMPLE CALCULATIONS

1.0 INPUTS

Δx (distance between nodes)= 0.002 m

K, sample (initial guess of the thermal conductivity) = 0.001kW/mK

Cp,air (specific heat of air)=1kJ/kgK

Cp,sample (initial guess of the sample specific heat) =1kJ/kgK

Mass, sample = 0.1481 kg

Width, sample = 0.1016 m

Thickness, sample = 0.008 m

T, ambient = 30 K

Q" (heat flux per unit area of the Cone)= 50 kW/m^2

Mass, Fiberboard = 0.05 kg

Width, Fiberboard = 0.1016 m

Thickness, Fiberboard = 0.0381 m

K, fiberboard (thermal conductivity of the fiberboard)= 0.0001 kW/mK

e,sample (emissivity of the sample) = 1

h (convective and radiative combined coefficient) = 0.080 kW/m^2K

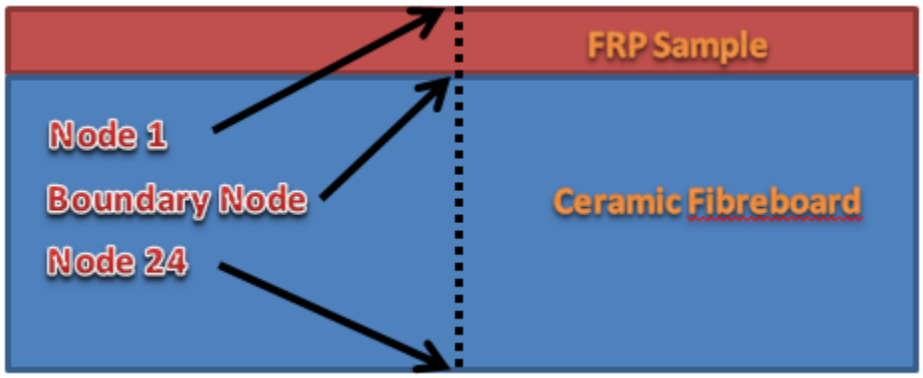

Figure 1: Node Diagram

2.0 INTERMEDIATE CALCULATIONS

2.1 Calculations for Sample

$$\text{Volume} = \text{Width}^2\text{Thickness} = 0.1016^2\,(0.008) = 8.26 \times 10^{-5}\ m^3 \quad (1)$$

$$\text{Density} = \text{Mass/Volume} = \rho = 0.1481/8.26 \times 10^{-5}\ m^3 = 1793.4 \quad (2)$$

$$\text{Thermal Diffusivity} = K/\rho C_p = \alpha = 0.001/(1793.4*1) = 5.58 \times 10^{-7} \quad (3)$$

$$Fo = \alpha * dt/\Delta x^2 \quad (4)$$

The value of dt should be as large as possible to reduce calculation time of the property estimation time. With the initial guess, the value of the Fo,Fiberboard will be greater, so dt will depend upon that value.

$$Qmin=e*Sigma*(Tig^4-Tinf^4)-hconv*(Tig-Tinf) \quad (5)$$

$$25000=1*5.67E-8*(Tig^4-303^4)-20*(Tig-303) \quad (6)$$

$$Tig= 901.5\ C \quad (7)$$

$$Qnet=e*Sigma*(T^2-Tinf^2)*(T-Tinf)*(T-Tinf) \quad (8)$$

$$hrad= e*Sigma*(T^2-Tinf^2)*(T-Tinf) \quad (9)$$

$$hrad=5.67E-8*(901.5^2+303^2)*(901.4+303) \quad (10)$$

$$hrad=61.8\ W/m^2K \quad (11)$$

$$hrad+hconv=htot \quad (12)$$

$$htot=61.8+20 \quad (13)$$

$$htot=81.8\ W/m^2K \quad (14)$$

2.2 Calculations for Fiberboard

$$\text{Volume} = \text{Width}^2\text{Thickness} = 0.1016^2\,(0.0381) = 3.93 \times 10^{-4}\ m^3 \quad (15)$$

$$\text{Density} = \text{Mass/Volume} = \rho = 0.05/3.93 \times 10^{-4}\ m^3 = 127.1 \quad (16)$$

$$\text{Thermal Diffusivity} = K/\rho C_p = \alpha = 0.0001/(127.1*1) = 7.87 \times 10^{-7} \quad (17)$$

$$Fo = \alpha * dt/\Delta x^2 \text{ where } Fo <= 0.25 \quad (18)$$

Therefore…

$$(Fo*\Delta x^2)/\alpha = dt \quad => \quad 0.25*(0.002)^2/7.87 \times 10^{-7} = 1.27\ s \quad (19)$$

$$\text{And } Fo = 0.25 \quad (20)$$

Continuing to find Fo for the sample…

$$Fo,sample = 5.58 \times 10^{-7}(1.27)/0.002^2 = 0.177 \quad (21)$$

3.0 FINITE DIFFERENCES

Node 1, the surface node, will be modeled using a constant net heat flux with radiative and convective cooling.

$$T_o^{p+1} = 2Fo(xeq''/k+T_1^p +Bi*Tamb)+(1-2*Fo-2*Bi*Fo)*T_o^p \quad 22$$

$$Bi=h*\Delta x/k = (0.0818*0.002)/0.001 = 0.348 \quad 23$$

$$T_o^{p+1} =2*.177*(.002*1*50/.001+30+.16*30)+(1-2*.177-2*.16*.177)*30 \quad 24$$

$$T_o^{p+1} = 65.16\ C \quad 25$$

For Nodes 2-23 all calculations are similar, this calculation will be specifically for node 2, but they are all similar.

$$T_m^{p+1} = Fo(T_{m+1}^p + T_{m-1}^p)+(1-2*Fo)*T_m^p \quad 26$$

$$T_m^{p+1} = 0.177*(30+30)+(1-2(0.177))*30 \quad 27$$

$$T_m^{p+1} = 30\ C \quad 28$$

Node 24, the back face, will be modeled using only convective losses

$$T_o^{p+1} = 2Fo(T_1^p +Bi*Tamb)+(1-2*Fo-2*Bi*Fo)*T_o^p \quad 29$$

Properties for this node are based on the fiberboard because the node is in that region.

$$Bi=h*\Delta x/k = (0.0818*0.00)/0.0001 = 0.348 \quad 30$$

$$T_o^{p+1} = 2(0.25)*(30+0.17*30)+(1-2*(0.25)-2*0.17*(0.25))*30 \quad 31$$

$$T_o^{p+1}=26 \quad 32$$

4.0 MODEL VERIFICATION

$$T_o^{p+1} =To+(q/h)*ERFC(x/(2*SQRT(a*t)))-(q/h)*EXP(((h/k)*0)+((h^2)*a*t)/k^2)*ERFC((x/(2*SQRT(a*t)))+((h *SQRT(a*t))/k)) \quad 33$$

$$T_o^{p+1}= 0+(50/.017)*ERFC(0/(2*SQRT(6.95E-7*1)))-(50/.017)*EXP(((.017/.001)*0)+((.017^2)*6.95E-7*1)/.001^2)*ERFC((0/(2*SQRT(6.95E-7*1)))+((.017*SQRT(6.95E-7*1))/.001)) \quad 34$$

$$T_o^{p+1} = 55.58\ C \quad 35$$

APPENDIX C: NFPA 285 FLAME LENGTH CORRELATIONS BRIEFING

A major goal of this project was to develop a method for relating tests performed on fiber reinforced polymers (FRPs) using the Cone Calorimeter (ASTME 1354) to NFPA 285 Tests performed on the same FRPs. More specifically, the group aimed to develop a correlation that would allow data gathered through Cone testing to predict the fire performance of the FRPs that would be observed during an NFPA 285 Test of the same FRP material.

Flame length is a characteristic of the tests that is useful to be able to predict because of the nature of the acceptance criteria of the NFPA 285 Test. The NFPA 285 test is designed to evaluate the flame propagation on a wall assembly when subjected to an open flame (from natural gas burners) over time for duration of 30 minutes. In order for a material to comply with the criteria of the test, the flames must not exceed a height of 10 feet above the top of the window opening in the wall assembly used in the test at any point in time. As the small scale Cone Calorimeter test is much less costly when compared to the large scale NFPA 285 test, it would be beneficial to be able to predict the length of the flames using cone calorimetry so that compliance in accordance with the NFPA 285 test criteria may be predicted before the costly large scale test is performed. A screening tool that would provide the ability to predict flame height accurately could save FRP manufacturers a great deal of money, time, and valuable resources if they were able to know that a material they had created would not likely meet the acceptance criteria of the NFPA 285 test, and can be used as an aid in material development.

Flame Height Correlation

A potential method identified for accomplishing the goal of predicting flame height involves the use of a flame length correlation for line fires. This correlation will be based off of the following, which has been applied to wall fire tests in other research experiments. The following correlation, proposed by Delichatsios (SFPE, 2002), is as follows:

$$L_f = 0.052\dot{Q}'^{\frac{2}{3}} \qquad (1)$$

where Q' is the heat release rate per unit length of burning wall (kW/m) and L_f is in meters (SFPE Handbook 2-281).

This simple correlation requires knowledge of the heat release rate per unit length in order to find the flame length. However, the data gathered during Cone testing provides heat release rate per unit area (kW/m^2), which cannot be used in this correlation without prior manipulation.

The method for assessing the usefulness of this correlation involved comparing the flame lengths calculated using the equation above with the actual flame lengths that are gathered from the NFPA 285 Test results for one of the FRP wall assemblies, *Fireshield 285*, which were provided by Kreysler & Associates. This information was inferred from the test report using the temperature values that were collected at various heights up the wall assembly using thermocouples during the test. The NFPA 285 Test Standard defines the presence of a flame as being any point at which the temperature exceeds 1000°F (538°C). These known flame lengths were then plotted and compared to the plotted flame length values that were calculated using the equation above.

The heat release rate per unit area values collected from the Cone Calorimeter testing that the team performed on the same material as were tested in the NFPA 285 Test must be manipulated to be in the form of heat release rate per unit length in order to be used in the equation above. To accomplish this,

we initially multiplied the measured heat flux by the length of the pyrolysis zone, x_p, of the fire going up the wall. To estimate this length, we used the photographs provided in the NFPA 285 Test report. Since the pyrolysis length changed throughout the test, a value was estimated for each time step of the test, but was assumed to remain constant at the estimated value throughout the given time step. From the photographs, we estimated the following values of x_p for each time step:

Table 1: Pyrolysis heights based on test report photos.

Time [min]	Xp [ft]	Xp [m]
0-5	0	0
5-10	0	0
10-15	0.5	0.1524
15-20	2	0.6096
20-25	4	1.2192
25-30	1	0.3048

From the estimated pyrolysis lengths for each time step, as given above, the heat release rate per unit length of the burning wall, Q'_w, could then be estimated by multiplying the heat release rate per unit area values gathered from the Cone tests by x_p. For this application, we used the peak heat release rate per unit area from the Cone, which was determined to be 80 kW/m^2. This provides the following estimated values of Q':

Table 2: Heat release rates per unit length based on calibration data, estimated pyrolysis heights, and data collected during Cone tests.

Total Q'	
Time [min]	Q' [kW/m]
0-5	299.4444444
5-10	366.3333333
10-15	418.9697778
15-20	532.5457778
20-25	615.536
25-30	612.7728889

Once the heat release rate per unit area was converted to heat release rate per unit length, this resulting heat release rate was intended to account for the burning wall portion of the NFPA 285 test. The calculated value was combined with the prescribed heat release rates per unit length of the room and window burners. The heat release rates per unit length of the burners were calculated by dividing the known heat release rates from calibration given in the test report by the width of the window opening in the wall assembly, which was also considered to be the width of the burner flames. The total heat release rates per unit length of the burners and burning wall were then used in the flame length equation to predict the height of the flames. The predicted heights were then compared to the actual heights of the flames that were derived from the temperatures recorded in the test report. From the comparison, constants could be altered or added to the equation if needed to better fit it to the experimental test values to create a more accurate equation to be used for the prediction of flame heights in future testing.

A first attempt at comparing the theoretically calculated values to the experimental calibration data and also experimental test data did not yield a desirable result. It was decided that the equations would need more manipulation, perhaps through adding a constant or modifying the exponent of the heat release rate per unit length, in order to fit it to the experimental data. The initial attempt was plotted and provided the following results:

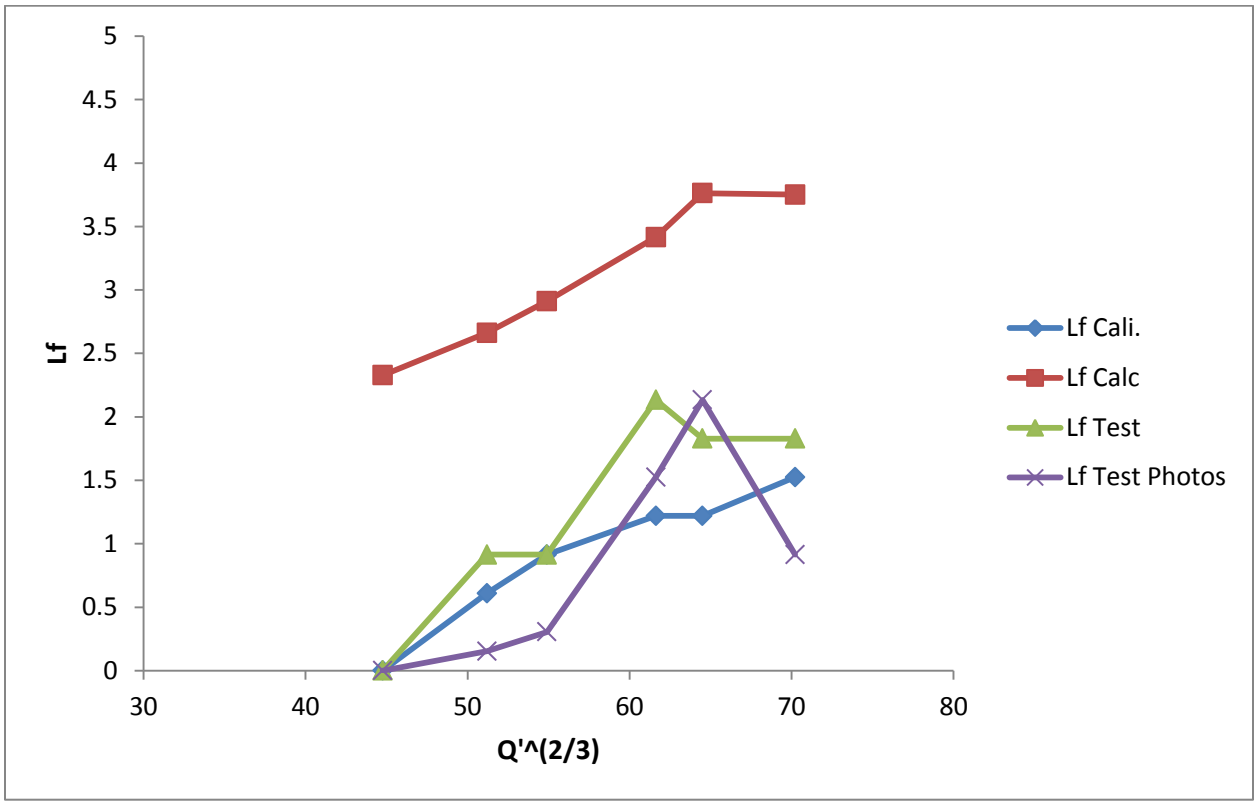

Figure 1: Theoretically calculated flame heights, actual calibration and test flame heights based on temperature and visual data from test report.

This graph shows the results of the flame height estimation method described above in comparison to the estimated flame height based on other information. The blue line shows the flame height estimated during calibration, which is based on the calibration temperature data at various wall heights provided in the test report. The purple line shows the flame height during the test, and is based solely on visual observations from the photos taken during the 285 test. The green line shows the flame height during the test, estimated based on the temperature data collected with thermocouples that was provided in the test report. As is visible in the graph above, the purple line demonstrates a significantly lesser flame height in the first three time steps of the test than the green line shows. This suggested to us that the temperature data may not accurately reflect the flame height during the test, and that perhaps the plume temperatures up the wall reach 1000°F before the flames actually reach that height on the wall. Finally, the red line shows the flame height during the test calculated using the equation previously described. In this calculation the heat release rate per unit length includes the heat release rate coming from the burning wall. This was estimated as described above, using the heat release rate per unit area from the Cone, which is multiplied by the estimated pyrolysis height, x_p.

However, the results shown in the graph above were considered less than desirable, as the theoretical flame heights shown by the red line did not appear to accurately depict the flame height in the test

according to either the temperature data or the visual observations. The next step taken was to try a different approach to determining the pyrolysis height. This new approach was developed with the intention of more accurately estimating the pyrolysis height, and would also involve using the pyrolysis area in order to calculate the heat release rate per unit length of the burning wall.

In our second attempt to use the correlation created by Delichatsios (SFPE, 2002), we used a different approach to calculating the heat release rate per unit length during each step of the test. In this new method, we used a different approximation of the pyrolysis length. These values were estimated based on knowledge of the heat fluxes applied to the wall by the burners during calibration, which are given in the test report at heights of 2 feet, 3 feet, and 4 feet above the window opening. These heat fluxes are as follows:

Table 3: Heat fluxes recorded during calibration from test report.

Calibration Heat Fluxes [kW/m^2]							
Time [minutes]							
Height [ft]	Height [m]	0 to 5	5 to 10	10 to 15	15 to 20	20 to 25	25 to 30
2	0.6096	9	22	25	29	32	37
3	0.9144	10	23	27	32	36	40
4	1.2192	8	17	21	25	28	32

Based on the results from the Cone testing we performed, we knew that the critical heat flux for ignition of the wall material was 25 kW/m^2. Using this knowledge, we established that ignition did not likely occur during the first three time steps of the test, since the heat fluxes during these steps did not significantly exceed 25 kW/m^2. We then established that based on these heat fluxes, the pyrolysis height was likely 3 feet above the window during the fourth time step, and at least 4 feet above the window during the fifth and sixth time steps. This provided the following values of x_p:

Table 4: Pyrolysis heights based on the calibration heat flux data and critical heat flux for ignition.

Xp Based on Cal. Q" (Q"cr = 25 kW/m^2)		
Time [min]	Xp [ft]	Xp [m]
0 to 5	0	0
5 to 10	0	0
10 to 15	0	0
15 to 20	3	0.9144
20 to 25	4	1.2192
25 to 30	4	1.2192

Next, using the photos of the NFPA 285 test from the test report, taken at various times throughout the test, a width of the base of the pyrolysis zone (w_p) was estimated. Since it was established that the wall was only considered to be burning during the fourth, fifth, and sixth time steps, a base width was estimated only for these steps. The widths are as follows:

Table 5: Estimated widths of base of pyrolysis zone based on test photos from test report.

Width of Base of Pyrolysis Zone (Wp)		
Time [min]	Wp [ft]	Wp [m]
0 to 5	0	0
5 to 10	0	0
10 to 15	0	0
15 to 20	2.5	0.762
20 to 25	3	0.9144
25 to 30	3.5	1.0668

Using these widths, and the pyrolysis heights previously mentioned, the area of pyrolysis, A_p, was calculated. From the test photos, it was determined that the shape of the pyrolysis zone could most nearly be approximated as a triangle. Therefore, A_p was calculated using the basic equation for the area of a triangle:

$$A_p = \tfrac{1}{2}(x_p w_p)$$

This calculation yielded the following results:

Table 6: Calculated areas of pyrolysis based on identified pyrolysis dimensions.

Area of Pyrolysis		
Time [min]	Ap [ft^2]	Ap [m^2]
0 to 5	0	0
5 to 10	0	0
10 to 15	0	0
15 to 20	3.75	0.348375
20 to 25	6	0.5574
25 to 30	7	0.6503

However, it was also determined from the data gathered during the Cone testing that the material would burn for about 8 minutes. This suggests that each pyrolysis area would actually burn for two time steps and not one, but that the area burning during time step four would no longer be burning during time step six. Therefore, the area calculated for the fourth time step must be subtracted from the sixth, resulting in the following pyrolysis areas:

Table 7: Calculated areas of pyrolysis based on fuel burnout time.

Area of Pyrolysis		
Time [min]	Ap [ft^2]	Ap [m^2]
0 to 5	0	0
5 to 10	0	0
10 to 15	0	0
15 to 20	3.75	0.348375
20 to 25	6	0.5574
25 to 30	3.25	0.301925

These areas were then used to find the heat release rate, in kW, of the burning wall during time steps 4 through 6 by multiplying the average heat release rate per unit area from Cone testing by the areas of pyrolysis. The average heat release rate per unit area from the Cone Calorimeter was found to be 65 kW/m^2. The calculated heat release rates were then divided by the width of the pyrolysis zone, w_p, in order to find the heat release rate per unit length, Q', for each step. The following values of Q' due to the burning wall were found:

Table 8: Estimated heat release rate per unit length of the burning wall.

Q' Wall [kW/m]						
Height [m]	0 to 5	5 to 10	10 to 15	15 to 20	20 to 25	25 to 30
0.6096	0	0	0	29.71703	39.6227	18.39626
0.9144	0	0	0	29.71703	39.6227	18.39626
1.2192	0	0	0	29.71703	39.6227	18.39626

These values were then added to the heat release rates per unit length of the burners and used in the flame height equation, Equation (1), from Delichatsios:

$$L_f = 0.052\dot{Q}'^{\frac{2}{3}}$$

The results are shown in the following graph:

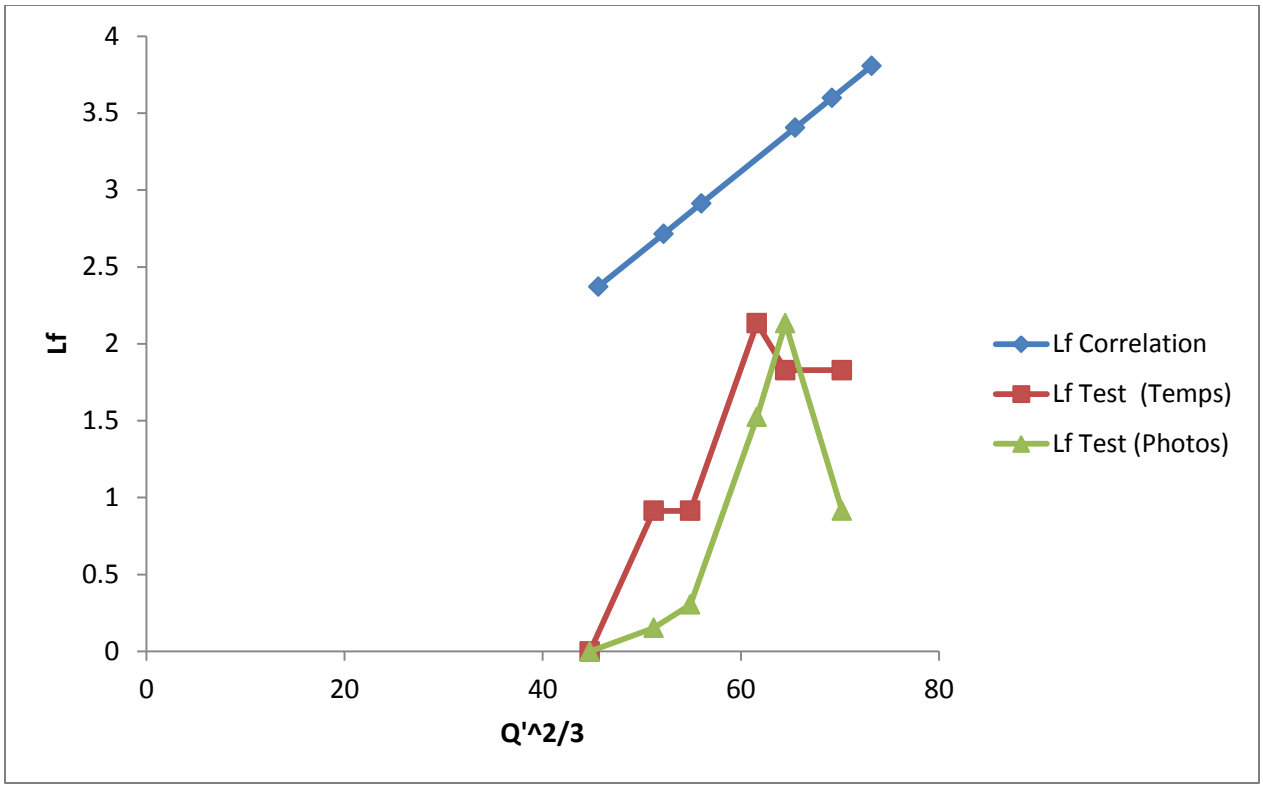

Figure 2: Theoretically calculated flame heights and test flame heights based on test temperature data and visual data from test report.

The results shown in the graph above are not significantly more desirable than the results shown for the previous method. The red line shows the flame height from the test based on temperature data from the test report, the green line shows the flame height during the test based on visual observations from the photos provided in the test report, and the blue line shows the calculated flame lengths based on Equation (1). Even when the changing area of pyrolysis was accounted for, the result was still that the correlation greatly overestimates the flame height throughout the test.

The team performed further modifications to our methods by changing the constant, which is given by Delichatsios in the equation to be equal to 0.052, and also changing the exponent. However, no combinations of constant and exponent values were found to yield desirable results. At this time, we were forced to conclude our research and development of this portion of the project due to time constraints. However, it is possible that in the future other students may be able to continue working on this portion of our project to improve the use of this correlation method or to create a better method for predicting flame heights in the NFPA 285 test.

Development of Plume Temperature Equations

A method that was explored for predicting the results of the NFPA 285 Test involves the use of an enthalpy equation to predict the fire plume temperature, T_s, at various heights above the top of the window, based on the mass flow rate of the plume smoke (in kg/s) and heat release rate (in kW). Estimating the temperature at various heights in the fire plume is useful for predicting the pass/fail status of a material in the NFPA 285 Test because, again, the test standard defines the presence of flame as a temperature of at least 1000°F (538°C). Therefore, predicting the temperature of the plume going up the wall assembly at various heights would allow the height that the flames will extend up the wall to be determined. However, before this equation for T_s could be put to use, several other calculations were performed, and other values needed to be determined. The quantities that were gathered or solved for in our calculations are defined as follows:

T_o = ambient temperature (given in the 285 Test Report to be 302.5 K)

T_{max} = maximum temperature (measured during testing using thermocouples [K])

T_s = average plume smoke layer temperature [K]

g = acceleration due to gravity (a known value of 9.81 m/s^2)

ρ_∞ = density of the ambient air (known to be 1.2 kg/m^3)

c_p = specific heat of the ambient air (known to be 1 kJ/kgK)

W = width of the window opening, or spill edge (known to be 1.98 m)

w_p = width of the base of pyrolysis of the burning wall [m]

w_p' = fraction of the width of the base of pyrolysis of the burning wall [m]

d_w = depth of gas layer evaluated horizontally at the window opening [m]

C_m = dimensionless entrainment coefficient (estimated in Harrison and Spearpoint's *A Review of Simple Entrainment Calculation Methods for the Thermal Spill Plume* to be 0.44 for a spill plume)

$C = 0.3C_m \rho_\infty$

K_s = fraction of convective heat release contained in smoke layer (assumed to be 1.0)

Q_t = total heat release rate, including room burner and window burner [kW]

Q_c = convective fraction of heat release rate [kW]

Q' = total heat release rate per unit length [kW/m]

Q'_s = heat release rate per unit length (based on the width of the window opening) from the source fires [kW/m]

Q'_w = heat release rate per unit length of the burning wall [kW/m]

$\dot{m}_s$ = mass flow rate of gases in the smoke layer flow below the spill edge [kg/s]

$\dot{m}_p$ = mass flow rate of gases in plume at an arbitrary height of rise, z [kg/s]

z = height of rise above the top of the window opening [m]

z_o = virtual origin (estimated value used to shift theoretical values to better match experimental values, see calculation procedure for further explanation)

In order to determine which of the existing correlations developed through fire plume research and experimentation were applicable to the conditions that exist during the NFPA 285 Test, we performed calculations using the equations we found in our research and then compared these theoretical results to the NFPA 285 test results from the test report. This allowed us to determine which existing correlations most closely matched the data collected during the test, after which any necessary manipulations to these equations were performed in order to tailor them to the specific test conditions and configuration of the 285 test. Our comparison of the theoretical and experimental results was completed by performing calculations using Excel spreadsheets, and then graphing those theoretical results against the experimental values measured during test calibration. We compared three correlations for estimating the mass flow rate of the plume smoke, $\dot{m}_p$, which was then used to find the plume temperature at various heights on the wall above the window opening. We found through comparison of all three equations to the experimental values that none of the equations would adequately match the experimental results without the addition of a virtual origin term, z_o, to the height term, z, in each of the three mass flow rate equations, and perhaps even further manipulations in some cases. However, the addition of a virtual origin term was justifiable based on the differences between the situations that the mass flow equations were created to model and the actual conditions that exist during the

NFPA 285 test. The mass flow equations were meant to model a two-dimensional spill plume. However, in the 285 test, the geometry of the wall assembly acts more as a quasi-two-dimensional spill plume as the wall assembly is not infinitely wide. Therefore, the z_o term was added to the equations in order to account for the different conditions. The calculation steps and comparison of the theoretical results of the three correlations can be found below (full sample calculations can be found at the end of Appendix C).

It is important to note that all of the equations that were considered were intended for use in evaluating two-dimensional spill plumes. It was reasonable to simplify the conditions of the test and consider the spill plume in the NFPA 285 test to be nominally two-dimensional because, as will be seen in the calculations that follow, the heat release rates were expressed in terms of unit length. In this case, the unit length for the heat release rates produced by the burners will be the width of the window, W, and the unit length for the heat release rates produced by the burning wall will be a portion of the width of the pyrolysis area, w_p. This normalization of the heat release rates allowed us to assume that the line fire source is infinitely wide, resulting in expected two-dimensional plume behavior (Yuan, Cox 126).

The first step in performing the necessary calculations to predict the plume temperature was to determine the average total heat release rate, Q_t, at each five minute time interval using the calibration data provided in the 285 test report. The total heat release rate during calibration is simply the sum of the heat release rates of the room and window burners:

Table 9: Heat release rates of the source burners from calibration data from test report.

Minutes	Room Burner	Window Burner	Combined HRR [kW]
0-5	770	0	770
5-10	772	170	942
10-15	776	270	1046
15-20	880	364	1244
20-25	907	425	1332
25-30	946	567	1513

We also needed to collect the average temperatures during calibration from the test report for each time step at various heights above the window opening for use in later calculations:

Table 10: Temperatures at various heights during calibration, from test report.

Minutes	T [K] at 0.61 m	T [K] at 0.91 m	T [K] at 1.22 m	T [K] at 1.52 m	T [K] at 1.83 m
0-5	631.4	591.4	545.8	516.3	490.2
5-10	845.5	789.2	719.4	658.0	604.7
10-15	877.4	838.9	772.9	714.4	656.3
15-20	919.8	891.7	830.5	771.2	709.2
20-25	943.0	920.4	864.4	807.5	743.2
25-30	981.3	954.9	900.8	842.5	773.6

Next, the heat release rate per unit length, Q', can be calculated. This is done by simply dividing the total heat release rate of the burners by the width of the window opening, W, which was considered to be the width of the fire produced by the burners and is defined in the NFPA 285 Test Standard and is equal to 1.98 m:

$$\dot{Q}' = \frac{\dot{Q}}{W} \qquad (2)$$

Table 11: Calculated heat release rates per unit length of the source burners.

Combined HRR [kW]	Q' [kW/m]
770	388.8888889
942	475.7575758
1046	528.2828283
1244	628.2828283
1332	672.7272727
1513	764.1414141

Then, the convective portion of the total heat release rate could be estimated as a fraction of the total heat release rate per unit length using the following equation from Guigard et al., which states that Q_r, the radiative heat release fraction, is approximately 0.23 for natural gas, which is the fuel that is used to fuel the burners in the NFPA 285 test (Guigard 2000). The convective heat release fraction is therefore the other portion of the total heat release rate, or total heat release rate per unit length, yielding the following equations for Q_c, or in the latter case, Q'_c:

$$\dot{Q}_c = 0.77\dot{Q}$$

$$\dot{Q}'_c = 0.77\dot{Q}' \qquad (3)$$

From this point forward, all heat release rates, expressed both as a heat release rate or a heat release rate per unit length, will be taken as the convective portion. This was reasonable for our calculations because the radiative fraction of the heat release rate is the portion that will be lost almost immediately to the surroundings, and the convective fraction of the heat release will be what remains and contributes to the spill plume temperature.

Next, the mass flow rate of the smoke layer at the spill edge, $\dot{m}_s$ was calculated for each of the six time steps of the test, which was done using the following equation from Harrison and Spearpoint's *A Review of Simple Entrainment Calculation Methods for the Thermal Spill Plume* (Equation 5) (Harrison, 2007):

$$\dot{m}_s = 0.025(\dot{Q}'_t W^2)^{1/3} \qquad (4)$$

We also needed to make an estimation of d_w, the depth of the gas layer evaluated horizontally at the window opening, for some of the calculations that follow. This was estimated under the assumption that the gas layer would extend from the ceiling to about halfway down the height of the window opening. The height of the window opening in the test is 30 inches, or 0.762 m, and the depth of the downstand above the opening is also 30 inches, so the gas layer depth, in meters, is estimated as follows:

$$d_w = 0.762 + \frac{1}{2}(0.762)$$

$$d_w = 1.143\ m$$

The temperature of the plume smoke layer at a chosen height was calculated using a form of the following enthalpy equation from NFPA 92B (Equation 6.2.5b)(NFPA 92B, 2009):

$$T_s = T_o + \frac{K_s \dot{Q}_c}{c_p \dot{m}_p} \qquad (5)$$

This equation was first manipulated in order to better account for the reality that there are three dimensions to the plume, even though we considered the plume to be nominally two-dimensional in our correlations. The equation, after modification and in combination with the chosen equation for the mass flow rate of the plume at height z, becomes the following:

$$\Delta T = \beta \left(\frac{Z + Z_o + C}{\dot{Q}'^{2/3}}\right)^{\alpha} \qquad (5a)$$

This equation, whose constants are defined later in this brief, along with the full explanation of the modifications made in order to create it, will become quite useful in later steps of developing the final correlation for predicting plume temperatures. However, the modifications of the temperature equation and temperature calculations that will follow could only be performed after the mass flow rate of gases in the plume had been calculated at a given height on the wall assembly. In order to choose the best spill plume mass flow rate equation to model the NFPA 285 test situation, we explored several options, comparing the theoretical and experimental test results through graphs. The potential equations and comparison process are detailed in the explanations that follow.

The mass flow rate of the plume, $\dot{m}_p$, can be calculated at any chosen height of rise above the top of the window, z, using the one of the following equations, the first of which is from Harrison and Spearpoint's *Physical Scale Modelling of Adhered Spill Plume Entrainment* (Harrison, 2010):

$$\dot{m}_p = 0.08\dot{Q}_c^{\frac{1}{3}}W^{\frac{2}{3}}z + 1.34\dot{m}_s \qquad (6)$$

However, with the addition of the virtual origin term, the equation becomes:

$$\dot{m}_p = 0.08\dot{Q}_c^{\frac{1}{3}}W^{\frac{2}{3}}(z + z_o) + 1.34\dot{m}_s \qquad (6a)$$

When used in the equation for T_s, graphed, and compared to the experimental values from calibration found in the test report, this equation yielded a result that is satisfactorily close to the calibration results. The comparison looked promising because, with the use of the virtual origin term, the theoretical results not only delivered results that remain very tight to one another throughout, but they also were quite similar in curvature to the experimental calibration results, and show a large amount of overlap. The graph below depicts the comparison of the theoretical and experimental results, with the virtual origin set at a constant value of 0.2 m. Since it may not be clear from the legend on the chart, the longer, sweeping lines that are close together display the theoretical results, and the shorter lines are the experimental calibration results:

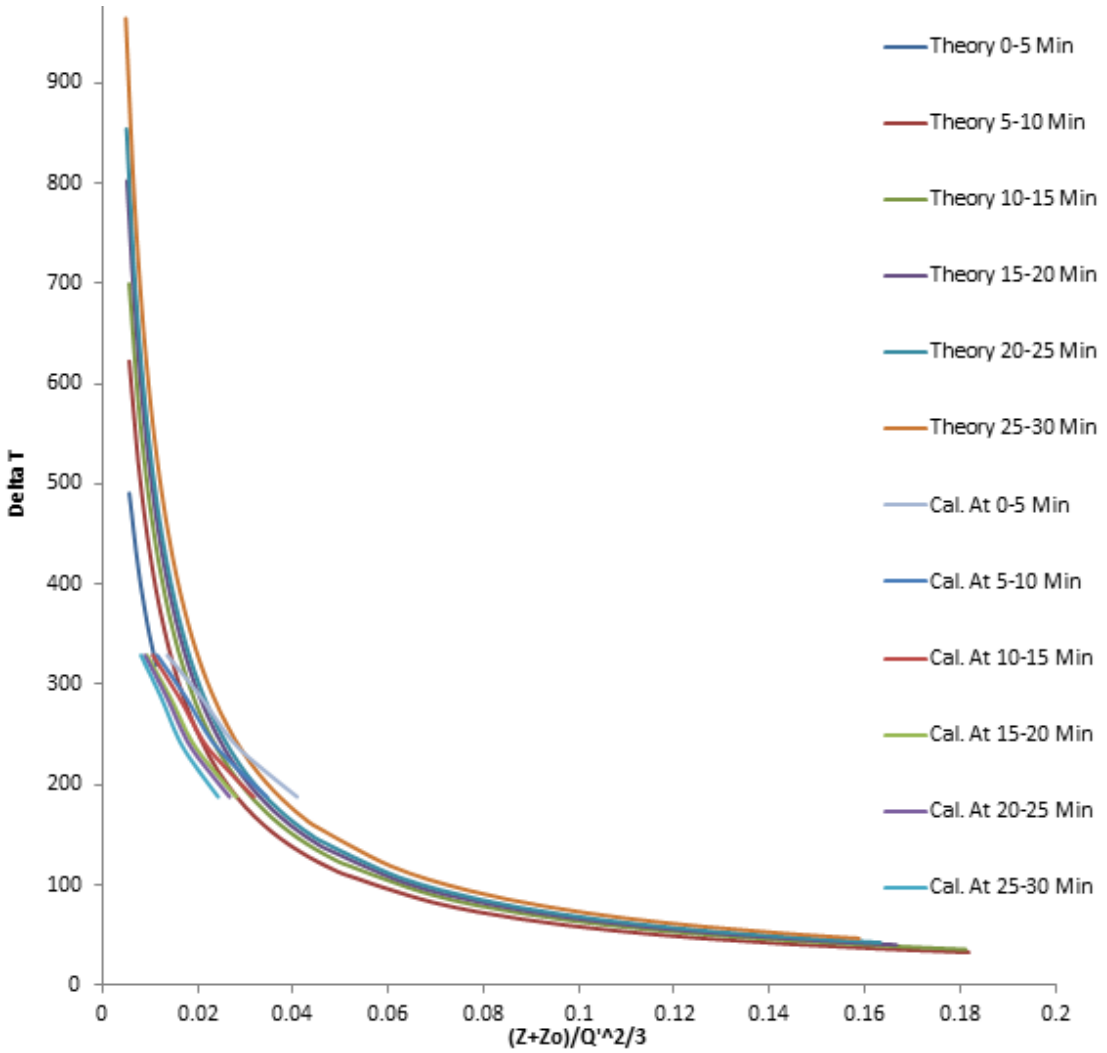

Figure 3: Graphical results of calculated theory compared to actual calibration data using plume mass flow rate equation (6a).

Another equation for $\dot{m}_p$ which yields a noticeably different result to that of the previous equation is the following, from Harrison and Spearpoint's *A Review of Simple Entrainment Calculation Methods for the Thermal Spill Plume* (Equation 27)(Harrison, 2007):

$$\dot{m}_p = 0.16\dot{Q}_c^{\frac{1}{3}}W^{\frac{2}{3}}z + 1.4\dot{m}_s + 0.0014\dot{Q}_c \qquad (7)$$

However, with the addition of the virtual origin term, the equation becomes:

$$\dot{m}_p = 0.16\dot{Q}_c^{\frac{1}{3}}W^{\frac{2}{3}}(z + z_o) + 1.4\dot{m}_s + 0.0014\dot{Q}_c \qquad (7a)$$

When used in the equation for T_s, graphed, and compared to the experimental calibration values, this equation yielded a result that is not as close to the calibration results as the previous equation. Even with adjustments using a virtual origin term, the graph did not align with the experimental calibration values as closely as what we would hope to see for the equation that is chosen. The graph below depicts the comparison of the theoretical and experimental results, with the virtual origin set at a

constant value of 0.8 m. In case it is not clear from the legend on the chart, the longer, sweeping lines that are close together are the theoretical results, and the shorter lines that generally lie higher on the plot are the experimental calibration results:

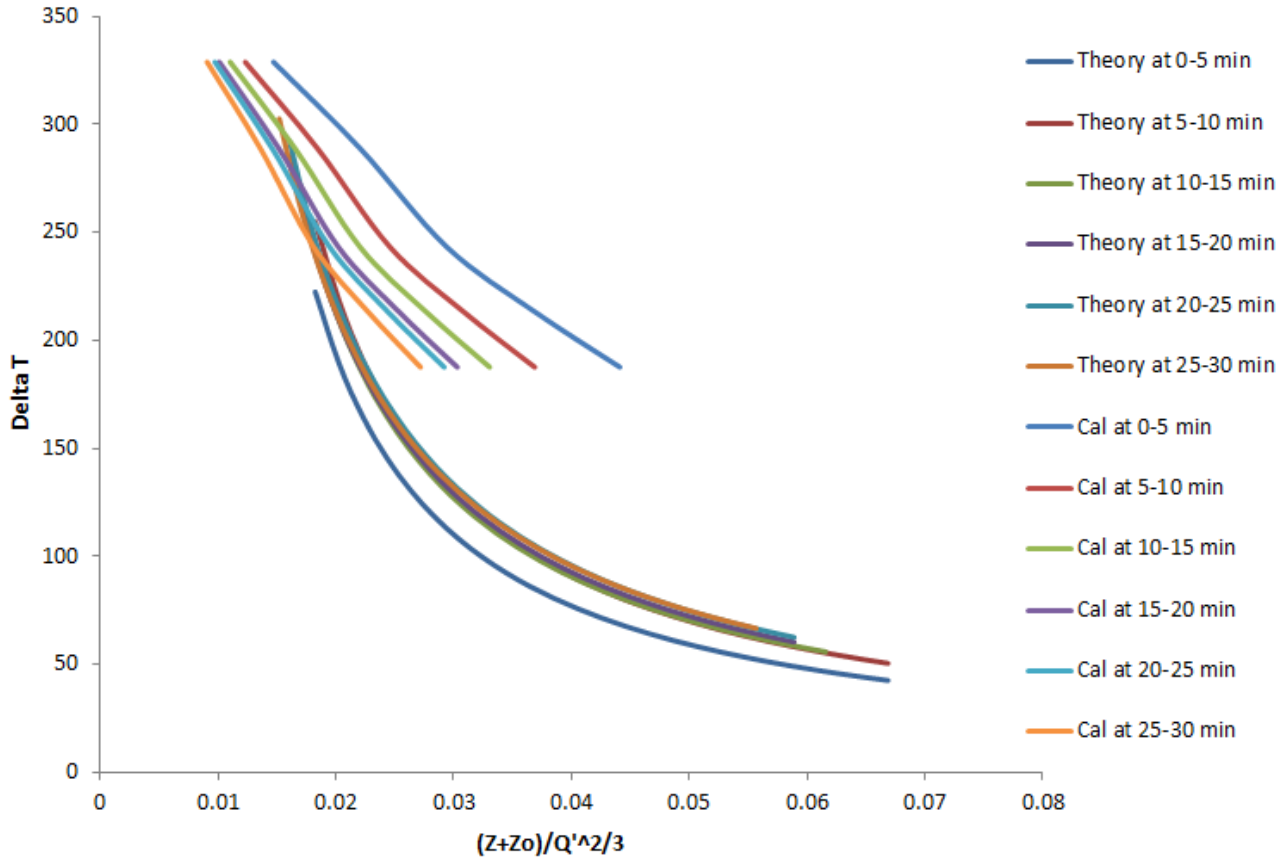

Figure 4: Graphical results of calculated theory compared to actual calibration data using plume mass flow rate equation (7a).

The third potentially useful equation for calculating $\dot{m}_p$ is the following, created by Poreh, Morgan, Marshall and Harrison, and also found in Harrison and Spearpoint's *A Review of Simple Entrainment Calculation Methods for the Thermal Spill Plume* (Equation 20). This equation again yielded different results from the first two options (Harrison, 2007):

$$\dot{m}_p = C\dot{Q}_c^{\frac{1}{3}}W^{\frac{2}{3}}\left[z + d_w + \left(\frac{\dot{m}_s}{C\dot{Q}_c^{\frac{1}{3}}W^{\frac{2}{3}}}\right)\right] \qquad (8)$$

However, with the addition of the virtual origin term, the equation becomes:

$$\dot{m}_p = C\dot{Q}_c^{\frac{1}{3}}W^{\frac{2}{3}}\left[(z + z_o) + d_w + \left(\frac{\dot{m}_s}{C\dot{Q}_c^{\frac{1}{3}}W^{\frac{2}{3}}}\right)\right] \qquad (8a)$$

When used in the equation for T_s, graphed, and compared to the experimental values from calibration, this equation yielded a result that is somewhat close to the calibration results, but its line were not as tight to each other as those in the first two graphs, which suggested to us that this may not be the best correlation to choose for our purposes. The graph below depicts the comparison of the theoretical and experimental results, with the virtual origin set at a constant value of 1 m. As it may not be clear from the legend on the chart, the longer, more curved lines are the theoretical results, and the slightly shorter and straighter lines are the experimental calibration results:

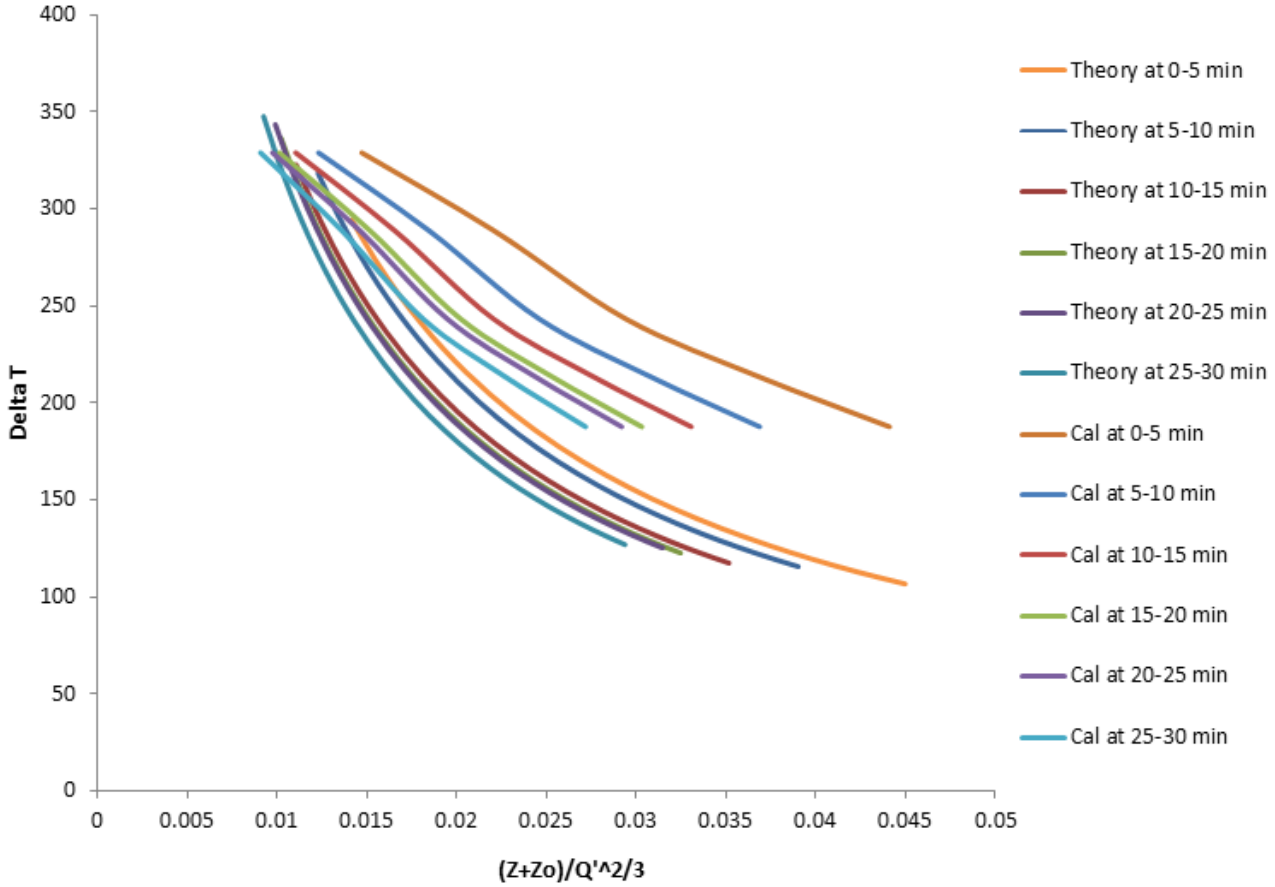

Figure 5: Graphical results of calculated theory compared to actual calibration data using plume mass flow rate equation (8a).

The temperatures in the three graphs above were, again, found using the following equation:

$$T_s = T_o + \frac{K_s \dot{Q}_c}{c_p \dot{m}_p} \qquad (5)$$

Once the temperatures were graphed, with the virtual origin terms included in the mass flow rate equations, a choice could be made as to which of the three mass flow rate equations under consideration would best model the results of the NFPA 285 test calibration, and therefore would be the best choice for moving forward in making further adjustments and creating a model for the results of the actual NFPA 285 test.

After examining the three graphs previously shown, the choice was made that the first mass flow rate equation was the best option. Again this equation was as follows:

$$\dot{m}_p = 0.08\dot{Q}_c^{\frac{1}{3}}W^{\frac{2}{3}}(z + z_o) + 1.34\dot{m}_s \qquad (6a)$$

This equation was chosen for several reasons. The first and perhaps most obvious reason is that when plotted against the experimental calibration results, the graphs lined up the most favorably of the three options that were considered. The equation also provided the tightest theoretical data points of the three, with the lines for each time step almost collapsing onto each other. This was a favorable result because it did not show a great deal of variance between the six different time steps of the NFPA 285 test. This equation was also chosen, however, because it was intended to be used for a situation that is arguably quite similar to that which the NFPA 285 test is designed to simulate. The assumption that the spill plume in the NFPA 285 test will behave as a two-dimensional plume has already been discussed, and the chosen mass flow equation was intended to model the mass flow of a two-dimensional spill plume. This equation was also designed to model an adhered spill plume, which means that the plume smoke remains close to the wall above the spill edge as it rises past the spill edge and up the wall. This was also quite similar to the plume in the NFPA 285 test, which does have a tendency to come outward from the wall just above the spill edge, but then curves back toward the wall and can be considered adhered to the wall from that point upward.

After the mass flow rate equation was chosen, the temperature equation modifications that were previously mentioned could be performed. These manipulations began with the original mass flow rate and enthalpy equations:

$$\dot{m}_p = 0.08\dot{Q}_c^{\frac{1}{3}}W^{\frac{2}{3}}(z + z_o) + 1.34\dot{m}_s$$

$$\dot{m}_s = 0.025(\dot{Q}_t W^2)^{1/3}$$

$$T_s = T_o + \frac{K_s\dot{Q}_c}{c_p\dot{m}_p}$$

The mass flow rate equations could become the following by replacing the constants 0.08, 1.34, and 0.025 with variables C_1, C_2, and C_3:

$$\dot{m}_p = C_1\dot{Q}_c^{\frac{1}{3}}W^{\frac{2}{3}}(z + z_o) + C_2\dot{m}_s$$

$$\dot{m}_s = C_3(\dot{Q}_t W^2)^{1/3}$$

This new equation for $\dot{m}_s$ could then be substituted into the $\dot{m}_p$ equation, which will become the following after combining the C values to make a new C value and distributing the exponent:

$$\dot{m}_p = C_1\dot{Q}_c^{\frac{1}{3}}W^{\frac{2}{3}}(z + z_o) + C_4\left(\dot{Q}_t^{\frac{1}{3}}W^{\frac{2}{3}}\right)$$

This then became,

$$\dot{m}_p = C_1\dot{Q}_c^{\frac{1}{3}}W^{\frac{2}{3}}(z + z_o) + C_4\left(\frac{\dot{Q}_c}{\chi_{conv}}\right)W^{\frac{2}{3}}$$

Now, combining C_4 with χ_{conv} to again make a new C value, the equation becomes:

$$\dot{m}_p = C_1 \dot{Q}_c^{\frac{1}{3}} W^{\frac{2}{3}} (z + z_o) + C_5 \dot{Q}_c^{\frac{1}{3}} W^{\frac{2}{3}}$$

Then, through factoring, the following was obtained:

$$\dot{m}_p = (\dot{Q}_c^{\frac{1}{3}} W^{\frac{2}{3}})(C_1(z + z_o) + C_5)$$

The enthalpy equation, after dropping the constant K_s, which was assumed to be equal to 1.0, could be rearranged to become:

$$\dot{m}_p = \frac{\dot{Q}_c}{c_p \Delta T}$$

Now, substituting for $\dot{m}_p$, the equation below was created:

$$\frac{\dot{Q}_c}{c_p \Delta T} = (\dot{Q}_c^{\frac{1}{3}} W^{\frac{2}{3}})\big(C_1(z + z_o) + C_5\big)$$

Next, the equation above could be rearranged to be in terms of change in temperature, which will ultimately be the form that will be used:

$$\Delta T = \frac{\dot{Q}_c}{c_p} (\dot{Q}_c^{\frac{1}{3}} W^{\frac{2}{3}})^{-1} (C_1(z + z_o) + C_5)^{-1}$$

With additional rearranging, the equation above becomes:

$$\Delta T = c_p \dot{Q}_c^{\frac{2}{3}} W^{\frac{-2}{3}} (C_1(z + z_o) + C_5)^{-1}$$

Next, creating a new constant, C_6, by adding c_p into the constant, as this is a constant throughout the test, and then with further rearranging:

$$\Delta T = C_6 [\left(\frac{\dot{Q}_c}{W}\right)^{\frac{2}{3}} / (C_1(z + z_o) + C_5)$$

Next, the equation is put into a form with an exponent governing the full equation besides the constant C_6:

$$\Delta T = C_6 [(C_1(z + z_o) + C_5) / \left(\frac{\dot{Q}_c}{W}\right)^{\frac{2}{3}}]^{-1}$$

Again combining constants we get the following:

$$\Delta T = C_8 [((z + z_o) + C_7) / \left(\frac{\dot{Q}_c}{W}\right)^{\frac{2}{3}}]^{-1}$$

The next step in creating a correlation to model the NFPA 285 test results was to attempt to separate the temperature data into multiple regions, with C_7 being a culmination of all of the constants from the original equations, and equal to 0.46, different values for C_8 corresponding to each region, as well as adjustments to the -1 exponent for each region. We created this procedure based on that found in Yuan and Cox's *An Experimental Study of Some Line Fires*. In this study by Yuan and Cox, line fires were simulated by burning natural gas on long, narrow burners, not unlike the window burner found in the NFPA 285 test, which made this a valid case study to model our own processes and correlations from.

Based on Yuan and Cox's experiments, which assume that the fire can be broken into three different regions, we also began our adjustments of the constants and exponents based on the assumption that three regions are present. These three regions are classified as continuous flame, intermittent flame, and thermal plume. We first attempted to fit the correlation to the three regions of the calibration data, and adjust the equation above by changing the -1 exponent to be a variable represented by α, following the ideas of Yuan and Cox. This change of the exponent allows for variation in the slope of the fit lines for each region. The other constants, C_8 and C_7 are also renamed to be β and C, respectively. The equation then becomes the following:

$$\Delta T = \beta \left(\frac{Z + Z_o + C}{\dot{Q}'^{2/3}} \right)^{\alpha} \qquad (7)$$

Using this equation with z_o varying at each time step, three lines (one for each region) could be graphed and fit to the calibration data by changing the constants and the value of n for each region. The values to create the best model were found through extensive trial and error, and many adjustments. The best fit was determined to occur with the use of the following values set for the variables:

Table 12: Values corresponding to the 3 regions of the calibration model.

	Beta	Alpha	C
Continuous	575	0	0.46
Intermittent	42	-0.6	0.46
Plume	8.46	-0.998	0.46

These values yielded the following graph:

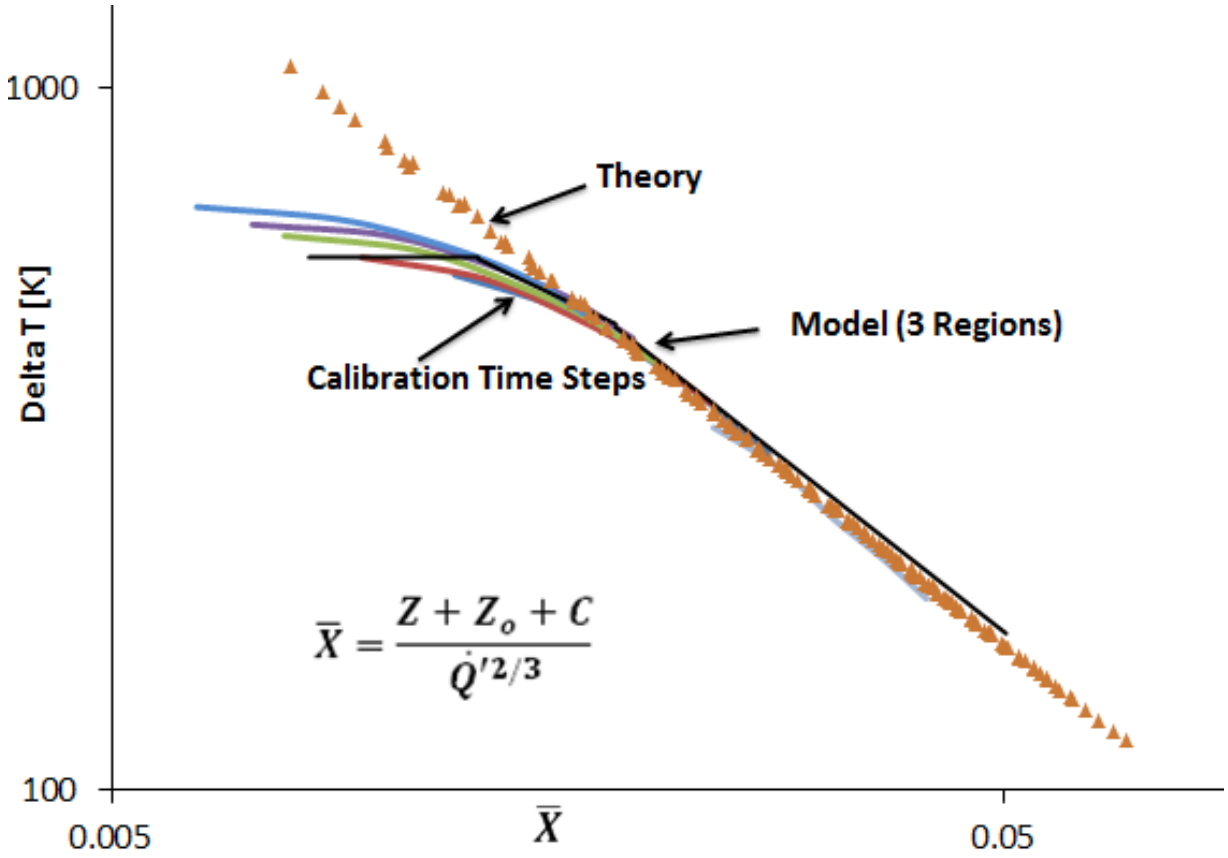

Figure 6: Graph comparing the theoretically calculated results, calibration data, and calibration model that was developed.

The graph above shows the theoretically calculated change in temperature versus $(Z+Zo+C)/Q'^{2/3}$, the experimental calibration results, and the three black lines that have been fit to the continuous flame, intermittent flame, and plume regions. The bottom black line correlates to the plume region, the middle line correlates to the intermittent flame, and top horizontal line correlates to the continuous flame region.

The virtual origin term was used to make the six multi-colored lines representing the data from the six time steps during calibration was used to make the lines collapse onto each other as closely as possible. The values of z_o were different for each time step, as mentioned above, and were determined through trial and error. The virtual origin values for each step were found to be as follows (with units of meters):

Table 13: Values of virtual origin for each time step of the calibration, with corresponding heat release rate per unit length.

Time Step [min]	Zo [m]	Q's [kW/m]
0-5	0.6	299.44
5-10	-0.088	366.33
10-15	-0.241	406.78
15-20	-0.308	483.78
20-25	-0.335	518
25-30	-0.377	588.39

Modeling the Burning Wall of the NFPA 285 Test

Once the data correlation for the test calibration was complete, the next step in the process of creating a model for predicting the results of the NFPA 285 test was to add the burning wall aspect of the test into the correlation. This would be accomplished using knowledge and data collected during the Cone testing.

Using similar methods to those used in the creation of the calibration correlation, the test data from the test report was graphed. Assuming that the burners produced the same heat release rates during the test as during the calibration, we were able to simply add the heat release rate per unit length of the burning wall to that of the burners. However, the most challenging aspect of this was accurately estimating the heat release rate of the burning wall, as the test report did not provide any heat release rate data for the test.

The heat release rate per unit length of the burning wall was estimated through an iterative trial and error process. The same axes were used as in the procedure for the calibration model, with the x axis being $(Z+Zo+C)/Q'^{2/3}$ and the y axis being change in temperature. However, the x axis values now include the heat release rate per unit length of the source as well as the burning wall (which are initially set to 0 kW/m,) and the y axis values are now based on the temperature data gathered throughout the NFPA 285 test using thermocouples, rather than those from calibration. With the heat release rate values of the burning wall set to 0 kW/m, the following graph of the six time steps from the test was produced:

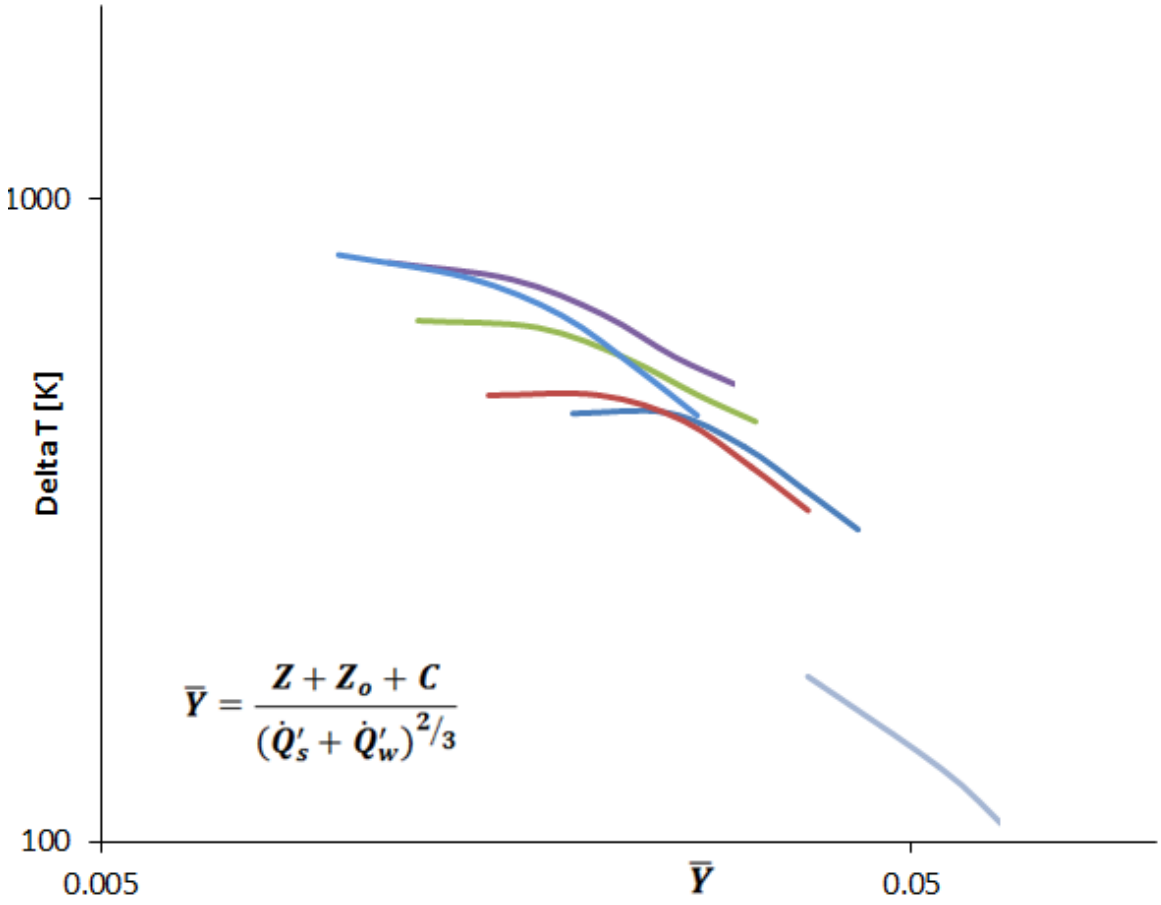

Figure 7: Graph of the test data for the 6 time steps before the heat release rates per unit length of the burning wall are estimated and added to the total heat release rate per unit length.

The same principal used to determine which time steps included pyrolysis of the wall as were used in the attempted flame height correlation was applied to estimating Q'_w for this model.

The pyrolysis heights were again estimated based on knowledge of the heat fluxes applied to the wall by the burners during calibration, which are given in the test report at heights of 2 feet, 3 feet, and 4 feet above the window opening. These heat fluxes were as follows:

Table 14: Heat fluxes recorded at several heights on the wall during calibration.

Calibration Heat Fluxes [kW/m^2]							
Time [minutes]							
Height [ft]	Height [m]	0 to 5	5 to 10	10 to 15	15 to 20	20 to 25	25 to 30
2	0.6096	9	22	25	29	32	37
3	0.9144	10	23	27	32	36	40
4	1.2192	8	17	21	25	28	32

Based on the results from the Cone testing we performed, we knew that the critical heat flux for ignition of the wall material was 25 kW/m^2. Using this knowledge, we established that ignition did not likely occur during the first three time steps of the test, since the heat fluxes during these steps did not significantly exceed 25 kW/m^2.

Knowing that the wall would only contribute to the heat release rate during the fourth, fifth, and sixth steps of the test, we concluded that the best approach to estimating the heat release contribution of the burning wall was to simply use trial and error methods to find heat release rate per unit length values that would make the six lines on the graph better align. Once this was completed, the other characteristics of the fire such as the area of pyrolysis could be better estimated and to some extent reverse engineered based on the Q'_w values that were found. From the trial and error type of experimentation that was performed in our excel spreadsheets, it was determined that the data lines for the six time steps would line up best when the heat release rate per unit length of the wall was estimated to be 125 kW/m in the fourth time step, 300 kW/m in the fifth time step, and 130 kW/m in the sixth time step. This yielded the following total heat release rate values per unit length:

Table 15: Heat release rates per unit length of the source burners and the burning wall.

Heat Release Rate Per Unit Length			
Time	Q's	Q'w	Q'total
0-5	299.44444	0	299.4444
5-10	366.33333	0	366.3333
10-15	406.77778	0	406.7778
15-20	483.77778	125	608.7778
20-25	518	300	818
25-30	588.38889	130	718.3889

The following graph was produced when the heat release rates per unit length of the burning wall were added to the heat release rates per unit length of the source burners. The values of z_o for each time step remained the same as those from the calibration correlation:

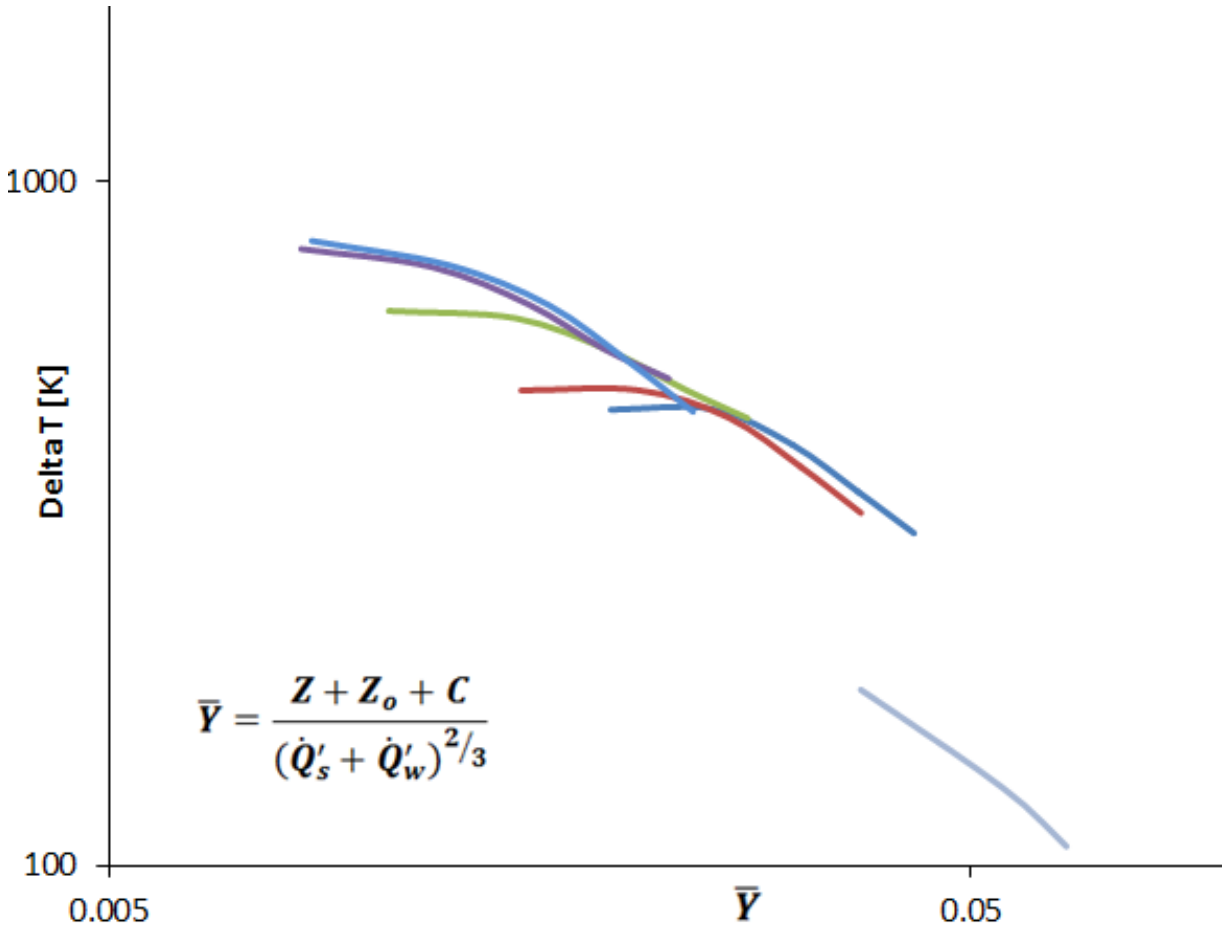

Figure 8: Graph of the test data for the 6 time steps after the heat release rates per unit length of the burning wall are estimated and added to the total heat release rate per unit length.

Although these results did not appear to be as well-aligned as the calibration results were, the plume regions of the lines did collapse satisfactorily onto one another. The other regions did not collapse as well as the plume region did, but a possible explanation for this is that, as explained previously, the equations used to plot the calibration and test data were intended to be used to predict the plume temperatures for a far-field two-dimensional spill plume situation. The NFPA 285 test involves a burning wall in addition to the gas burners, which poses a challenge because the temperatures on the wall in the test are no longer due to a far-field plume, but in the fourth through sixth time steps are due to actual flames. This likely caused the significant difference in the ΔT values between the time steps and causes the intermittent and continuous regions of the lines to be so far apart. However, these imperfect results are to be expected as the equations used were intended for simpler configurations than that which exists in the NFPA 285 test.

Although the same form of the enthalpy equation was used to create the model for the test, different values were used for the constants in order to obtain the best fit to the test data. In theory, the calibration model should have also worked to model the test results. However, this was not the case and we believed that the need for the adjustments was, in addition to the challenge of adding the burning wall into the correlations, largely due to a discrepancy between the heat release rates produced by the gas burners during the calibration versus those produced during the test. After examining the

temperature data from the calibration and test portions of the 285 test report, it became clear that the temperatures at various heights on the wall from the test significantly differed from those recorded during calibration.

The test temperatures were significantly less than those from calibration, and this was especially noticeable during the first three time steps of the test, when there is no burning wall to contribute heat and raise the temperatures. The temperatures should have been approximately the same during calibration and testing, but they were not. This suggests that the source burners were not producing the same heat release rates during the test as were produced during calibration, which would cause the model to change from that used to model the calibration results in order to accurately model the test results. The following values were used for the test model:

Table 16: Values corresponding to the 3 regions of the test model.

	Beta	Alpha	C
Continuous	670	0	0.46
Intermittent	51.5	-0.6	0.46
Plume	10.4	-0.998	0.46

These new values produced the following model for the NFPA 285 test results:

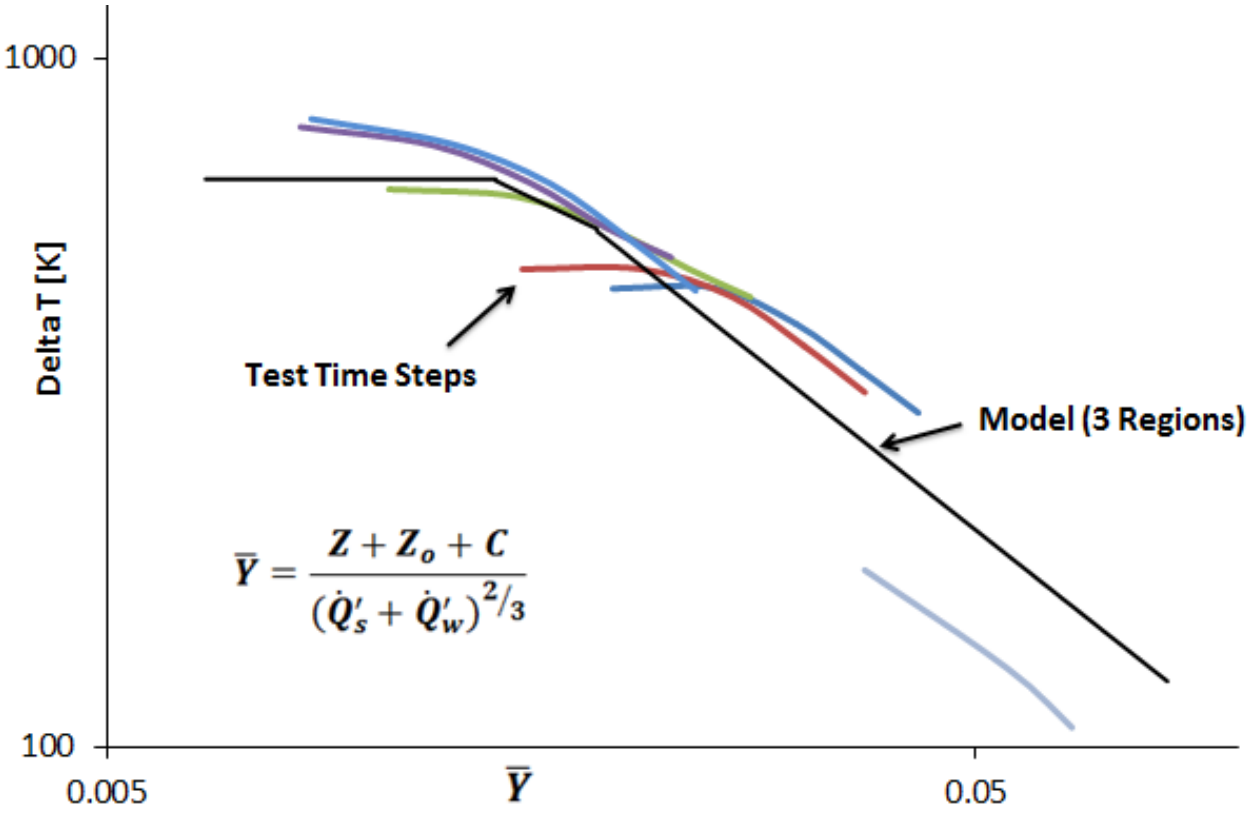

Figure 9: Graph comparing the test data and test model that was developed.

The next step in our process was then to reverse engineer some of the characteristics of the pyrolysis zone of the fire for use in future correlations. We established that based on the heat fluxes from the

calibration, the pyrolysis height was likely 3 feet above the window during the fourth time step, and at least 4 feet above the window during the fifth and sixth time steps. However, we estimated the pyrolysis height during the sixth time step to be higher than 4 feet based on the measured heat flux during this step being much greater at 4 feet than the critical heat flux for ignition. The pyrolysis height during the sixth time step was therefore estimated to be 4.5 feet. This provided the following values of x_p:

Table 17: Pyrolysis heights based on calibration heat flux data and critical heat flux for ignition.

Xp Based on Cal. Q" (Q"cr = 25 kW/m^2)		
Time [min]	Xp [ft]	Xp [m]
0 to 5	0	0
5 to 10	0	0
10 to 15	0	0
15 to 20	3	0.9144
20 to 25	4	1.2192
25 to 30	4.5	1.3716

Next, using the photos of the test from the test report and also knowledge of what the final heat release rates per unit length of the burning wall should be, a width of the base of the pyrolysis zone (w_p) was estimated. Since it was established that the wall was only considered to be burning during the fourth, fifth, and sixth time steps, a base width was estimated only for these steps. The widths are as follows:

Table 18: Widths of base of pyrolysis zone based on test photos from test report.

Width of Base of Pyrolysis Zone (Wp)		
Time [min]	Wp [ft]	Wp [m]
0 to 5	0	0
5 to 10	0	0
10 to 15	0	0
15 to 20	2.25	0.686
20 to 25	3.75	1.143
25 to 30	3	0.914

Using these widths, and the pyrolysis heights previously mentioned, the area of pyrolysis, A_p, was calculated. From the test photos, it was determined that the shape of the pyrolysis zone could most nearly be approximated as a triangle. Therefore, A_p was calculated using the basic equation for the area of a triangle:

$$A_p = \tfrac{1}{2}(x_p w_p)$$

This calculation yielded the following results:

Table 19: Calculated areas of pyrolysis.

Area of Pyrolysis		
Time [min]	Ap [ft^2]	Ap [m^2]
0 to 5	0	0
5 to 10	0	0
10 to 15	0	0
15 to 20	3.375	0.314
20 to 25	7.5	0.697
25 to 30	6.75	0.627

However, it was also determined from the data gathered during the Cone testing that the material would burn for about 8 minutes. This suggested that each pyrolysis area would actually burn for two time steps and not one, but that the area burning during time step four would no longer be burning during time step six, as each time step is 5 minutes long. Therefore, the area calculated for the fourth time step must be subtracted from the sixth, resulting in the following pyrolysis areas:

Table 20: Calculated areas of pyrolysis based on fuel burnout time.

Area of Pyrolysis		
Time [min]	Ap [ft^2]	Ap [m^2]
0 to 5	0	0
5 to 10	0	0
10 to 15	0	0
15 to 20	3.375	0.314
20 to 25	7.5	0.697
25 to 30	3.375	0.314

These areas were then used to find the heat release rate, in kW, of the burning wall during time steps four through six by multiplying the peak heat release rate per unit area from Cone testing by the areas of pyrolysis. The peak heat release rate per unit area from the Cone Calorimeter was found to be 80 kW/m^2. The calculated heat release rates were then divided by a constant width of the pyrolysis, w_p', in order to find the heat release rate per unit length, Q'. The value of w_p' was found through trial and error. This value was used in place of w_p, which was used in the attempted flame height estimation methods because it was believed to be a more accurate representation of the width of pyrolysis zone of the wall. Since the pyrolysis area was considered to be an approximate triangle in shape, the width of the pyrolysis varies with the height of the triangle. Through trial and error iterations, the value of w_p' that would result in values of Q'_w that were nearest to those previously estimated for the fourth, fifth, and sixth time steps, 125, 300, and 130 kW/m, respectively, was 0.6 feet, or 0.183 m. This width is approximately 1/5 of the width of the base of the pyrolysis zone on the wall. The following values of Q' due to the burning wall were found using w_p':

Table 21: Calculated heat release rates per unit length of the burning wall.

Q' Wall [kW/m]						
Height [m]	0 to 5	5 to 10	10 to 15	15 to 20	20 to 25	25 to 30
0.6096	0	0	0	137.16	304.79	137.16
0.9144	0	0	0	137.16	304.79	137.16
1.2192	0	0	0	137.16	304.79	137.16

Although these heat release rate per unit length values for the burning wall do not exactly match those found in the previous steps of this method (125, 300, and 130 kW/m), they were considered to be a satisfactory approximation. In the future, the heat release rate per unit length of a burning wall in the NFPA 285 test could be approximated using the methods just described in this brief, with the value of w_p' assumed to be a fixed value that is approximately 1/5 the width of the base of a triangular pyrolysis area.

To conclude, throughout this project we have developed methods for modeling material fire performance in the NFPA 285 test, and for estimating the heat release rate per unit length of a burning wall and dimensions of pyrolysis on that wall. We believe that the NFPA 285 test models and calculation methods created in this project are a satisfactory representation of the data that was available at the time the project was completed. However, a significant limitation of this project was the minimal NFPA 285 test data used to develop the models. If more data had been available, such as reports from several NFPA 285 tests instead of just one, the model could likely be improved. This is one opportunity that was identified for future students to improve the NFPA 285 test model.

Appendix C Sample Calculations:

The following sample calculations show one iteration of the calculations that must be performed for all of the correlations discussed in this brief. All of the sample calculations shown will be for the 5-10 minute time interval of the test, unless otherwise stated.

Flame Height Equations:

Known Values:

Q' = 475.8 kW/m

$$L_f = 0.052Q_l^{2/3}$$

$$L_f = 0.052(475.8)^{2/3}$$

$$L_f = 3.16 \text{ m}$$

Plume Temperature Equations:

Known Values:

T_o = 302.5 K | g = 9.81 m/s^2 | ρ_∞ = 1.2 kg/m^3

c_p = 1 kJ/kgK | W = 1.98 m | d_w = 1.143 m

C_m = 0.44 | $C = 0.3C_m \rho_\infty$ | K_s = 1.0

Q_t = 942 kW

For the purposes of these calculations, we will arbitrarily assume a height z of 1 m.

Heat release rate per unit length:

$$Q' = Q_t/W$$

$$Q' = 942/1.98$$

$$Q' = 475.8 \text{ kW/m}$$

Convective Portion of Heat Release Rate:

$$Q_c = 0.77Q_t$$

$$Q_c = 0.77(942)$$

$$Q_c = 725.3 \text{ kW}$$

$$Q_c' = 0.77Q'$$

$$Q_c' = 0.77(475.8)$$

$$Q_c' = 366.4 \text{ kW/m}$$

Mass flow rate of the smoke layer at the spill edge:

$$\dot{m}_s = 0.025(Q_t W^2)^{1/3}$$

$$\dot{m}_s = 0.025(942*1.98^2)^{1/3}$$

$$\dot{m}_s = 0.386 \text{ kg/s}$$

Mass flow rate of the plume using the chosen equation, with z_o = 0.1:

$$\dot{m}_p = 0.08 Q_c'^{1/3} W^{2/3} (z+z_o) + 1.34\dot{m}_s$$

$$\dot{m}_p = 0.08(366.4)^{1/3}(1.98)^{2/3} (1-0.088) + 1.34(0.386)$$

$$\dot{m}_p = 1.34 \text{ kg/s}$$

Plume smoke temperature at the given height of 1 m, using the initial equation:

$$T_s = T_o + (K_s Q_c / \dot{m}_p c_p)$$

$$T_s = 302.5 + [(1.0*366.4)/ (1.34*1)]$$

$$T_s = 575.9 \text{ K}$$

Change in plume temperature using the test model equation in the intermittent region:

$$\Delta T = \beta [((z+z_o) + C)/(Q_c /W)^{2/3})]^{\alpha}$$

In this region, $\beta = 51.5$, $\alpha = -0.6$, and $C = 0.46$, yielding a change in temperature of:

$$\Delta T = 51.5[((1-0.088) + 0.46)/(725.3 /1.98)^{2/3})]^{-0.6}$$

$$\Delta T = 463.6 \text{ K}$$

APPENDIX D: BUILDING CODE MODIFICATIONS BRIEFING

The International Building Code (IBC) currently does not provide its users with prescriptive tools regarding the acceptance criteria of the NFPA 285 test. However, compliance with the criteria of NFPA 285 is mandated by the IBC for exterior wall assemblies. Using the knowledge that NFPA 285 requires flames to maintain a height of less than 10 feet above the window opening throughout the test and that the presence of flame is defined in the test standard as a temperature greater than 1000°F, a simple prescriptive tool was developed that, if added to the IBC, would allow users of the code to predict whether their material would comply with NFPA 285 based on knowledge of the heat release rate per unit area and pyrolysis height produced by the material.

The prescriptive tool was created by determining the heat release rate per unit length of the burning wall ($\dot{Q}'_w$) that would result in a temperature of 1000°F at a height of 10 feet above the window using the following equation created for the NFPA 285 test model:

$$\Delta T = \beta \left(\frac{Z + Z_o + C}{(\dot{Q}'_s + \dot{Q}'_w)^{2/3}} \right)^{\alpha} \qquad (1)$$

Using equation (1), the heat release rate per unit area that would result in a wall temperature of 1000°F at a height of 10 feet (3.05 m) above the window could be determined by setting $\dot{Q}'_s$, z_o, β, C, and α to be the values associated with the plume region of the model during the sixth time step of the test. Therefore, the following values were used based on the model and known heat release rate of the source:

$\dot{Q}'_s$ was set to the heat release rate per unit length of the source burners during the sixth time step of the test according to the calibration data, which was 588.4 kW/m.

z_o was set to the value of z_o that was determined during the model development process, which was -0.38 m.

β was set to the plume region value determined for the test model, which was 10.4.

C was also set to the plume region value determined for the test model, which was 0.64.

α was set to the plume region value determined for the test model, which was -0.998.

ΔT was set to the maximum allowable difference between the ambient and wall temperature that would result in the wall temperature reaching 1000°F, or 537.8°C. This value was found by subtracting the ambient temperature, known from the report to be 29.5°C, from the maximum allowable wall temperature of 537.8°C. This resulted in a maximum allowable ΔT value of 508.3°C.

Using all of these values, equation (1) becomes:

$$508.3 = 10.4 \left(\frac{3.05 - 0.38 + 0.64}{(588.4 + \dot{Q}'_w)^{2/3}} \right)^{-0.998}$$

The equation was then solved for the heat release rate per unit length of the burning wall, and the value of $\dot{Q}'_w$ was found to be 1488.5 kW/m. This value of $\dot{Q}'_w$ represents the pass/fail threshold heat release rate per unit length of the burning wall during the test.

From the threshold value for the heat release rate per unit length of the burning wall, pairs of heat release rate per unit area (Q") and pyrolysis height (x_p) were identified to create a pass/fail curve to be used as a screening tool for exterior building materials. These data pairs were found using a similar method to that used in developing the process for estimating characteristics of the pyrolysis zone in the test. Before the data pairs could be found, the value of $\dot{Q}'_w$ had to be normalized using the pyrolysis width, w_p'. The following derivation was performed in order to do so.

First, a simple relation between heat release rate and heat release rate per unit area was identified:

$$\dot{Q} = A_p \dot{Q}^{"} \tag{2}$$

We know from test photos that the shape of the area of pyrolysis, A_p, can be approximated as a triangle. Next, the equation becomes:

$$\dot{Q} = (\tfrac{1}{2} w x_p)\dot{Q}^{"} \tag{2a}$$

Then, in order to convert heat release rate to heat release rate per unit area, we divided both sides of the equation by the width of pyrolysis, w_p':

$$\frac{\dot{Q}}{w'_p} = \frac{(\frac{1}{2} w x_p)\dot{Q}^{"}}{w'_p} \tag{2b}$$

This was equivalent to the following equation:

$$\dot{Q}'_w = \frac{(\frac{1}{2} w x_p)\dot{Q}^{"}}{w'_p} \tag{2c}$$

Rearranging the equation above produced the following:

$$\frac{\dot{Q}'_w w'_p}{\frac{1}{2} w} = x_p \dot{Q}^{"} \tag{3}$$

Next, knowing from previous calculations (see Appendix C) that w is equal to 3 feet, or 0.91 m, and w_p' is about 1/5 of that, or 0.18 m, the left side of the equation was solved and the value that $x_p \dot{Q}^{"}$ needs to equal to was revealed:

$$\frac{1488.5(0.18)}{\frac{1}{2}(0.91)} = x_p \dot{Q}^{"}$$

$$595.4 = x_p \dot{Q}^{"}$$

The knowledge of this value was then used to create the pyrolysis height and heat release rate per unit area data pairs. This was accomplished by fixing a series of values of x_p, ranging from 0.1 m to 3.1 m, as any greater values than 3.1 would far surpass the flame height limit of 3.05 m, and then dividing the calculated value 595.4 kW by the various x_p values to obtain the corresponding Q" value. These values were then graphed to produce a pass/fail curve.

If added to the IBC, the pass/fail curve could aid users in predicting whether a material would comply with the criteria of NFPA 285 based on knowledge of Q" and x_p. The curve is shown in Figure 1 below.

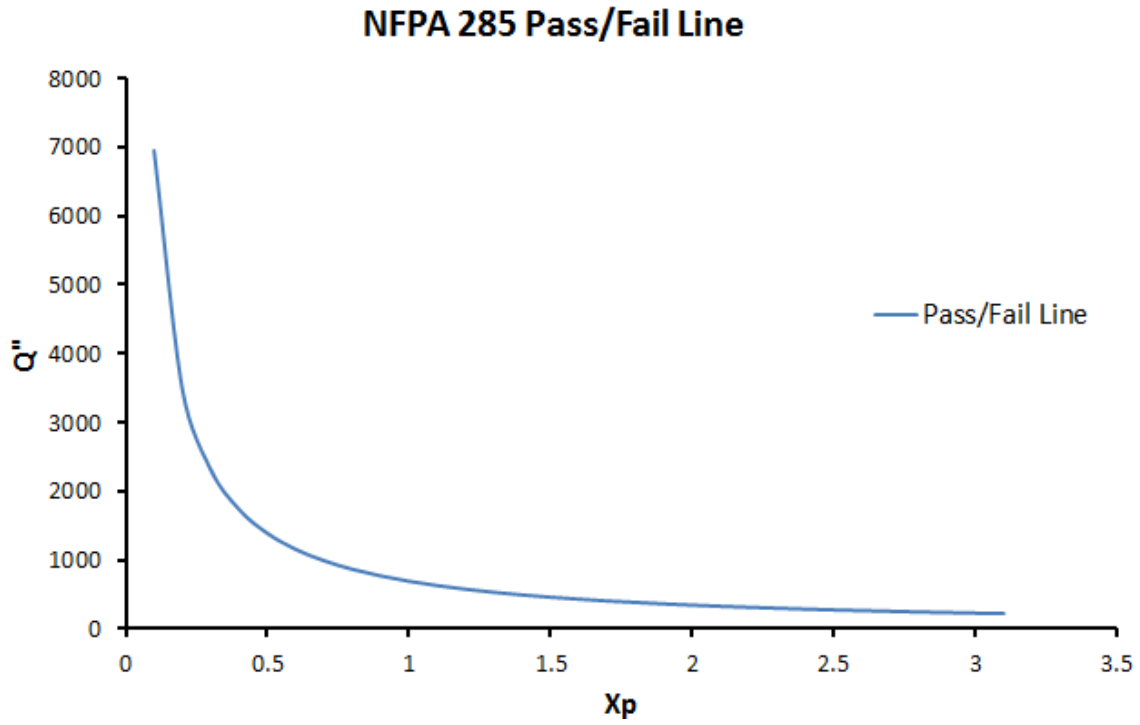

Figure 1: This graph demonstrates the prescriptive tool created to show the pass/fail curve for the NFPA 285 test. All combinations of Q" and x_p that fall below the curve indicate that the material would meet the acceptance criteria of NFPA 285, while pairs falling above the curve are not likely to comply.

APPENDIX E: RAW CONE DATA

Kreysler 1

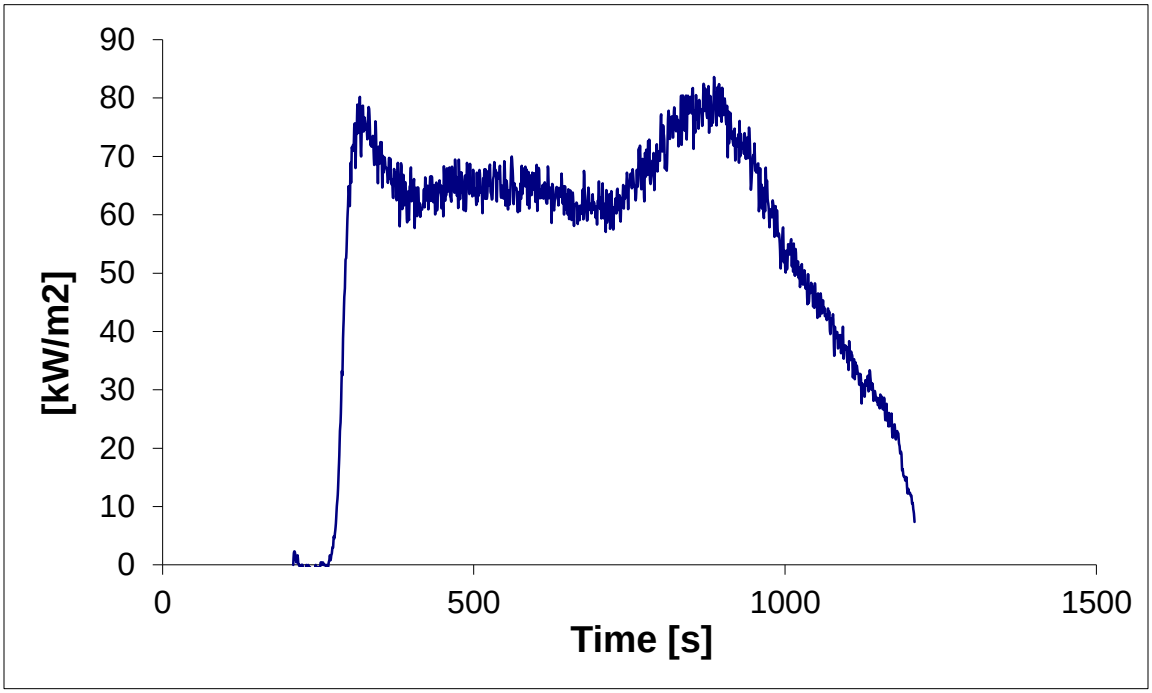

Figure 6: Heat Release Rate per Unit Area Kreysler 1, Test 1

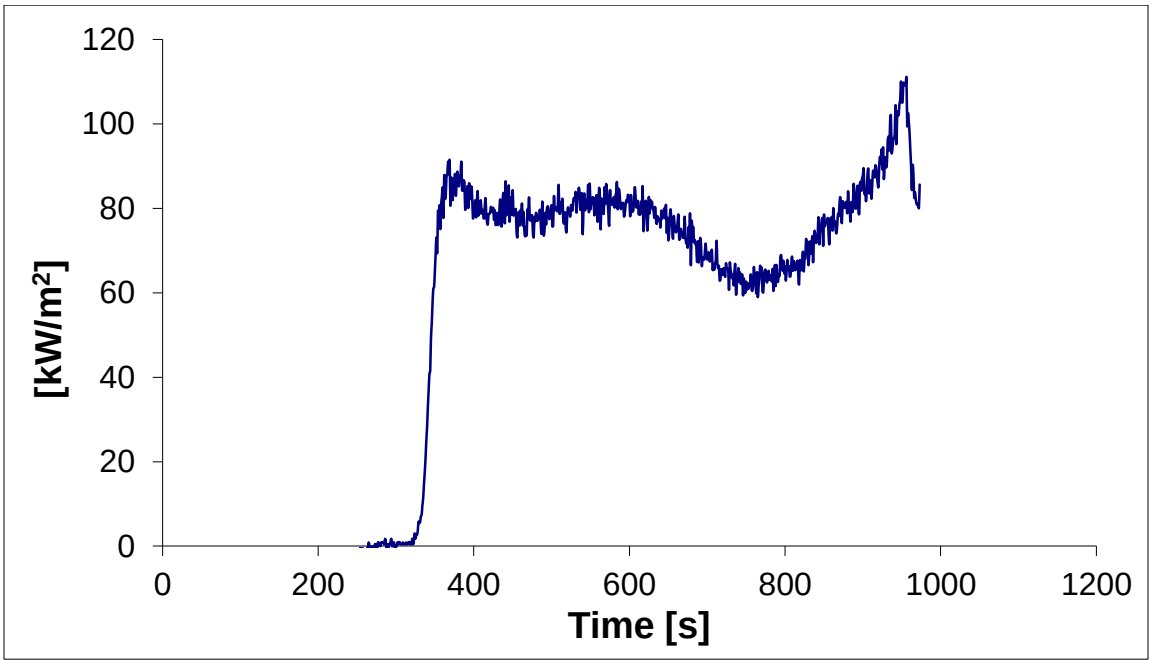

Figure 7: Heat Release Rate per Unit Area Kreysler 1, Test 2

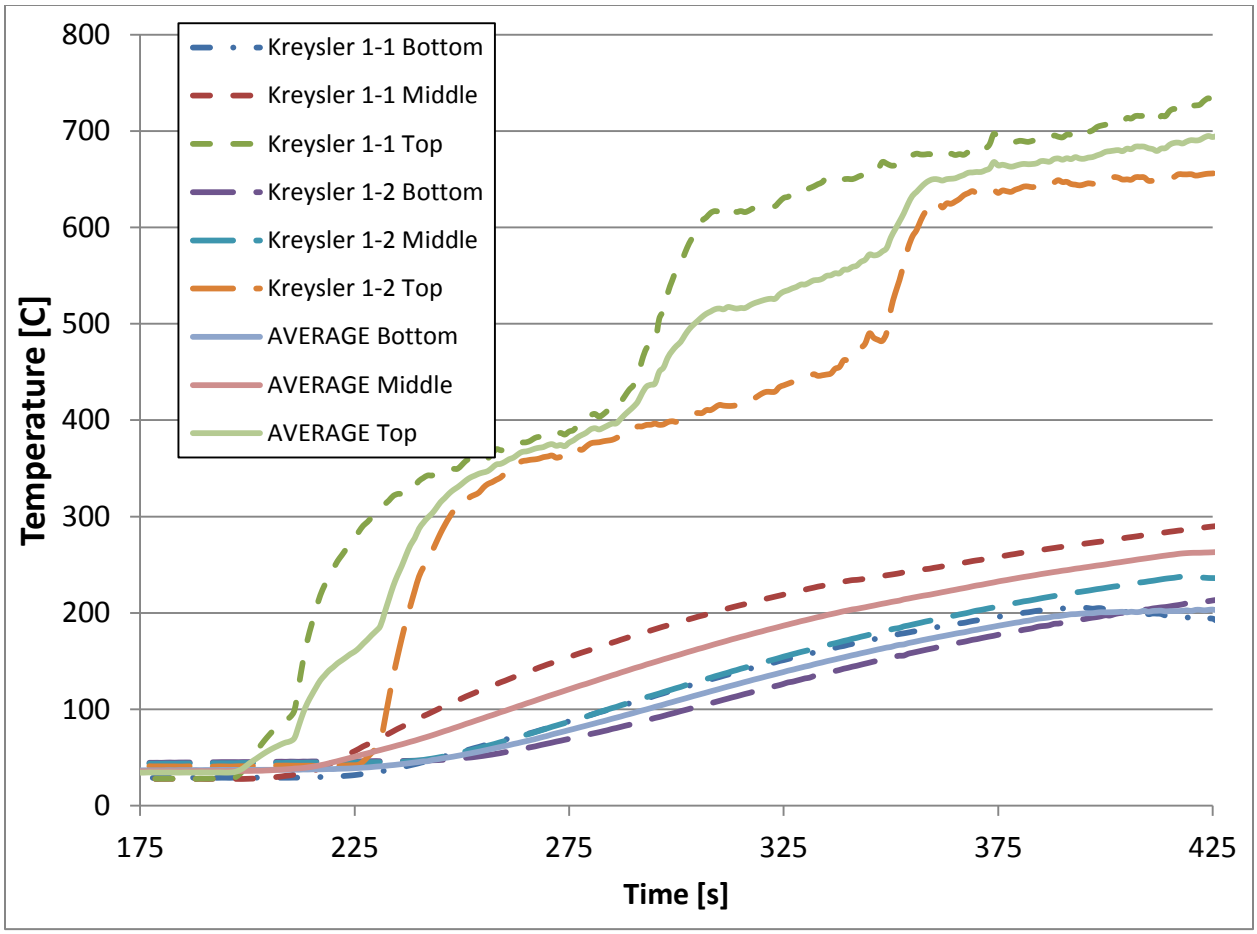

Sample 1 092412-1 (1) 50 kW 10-3-12
9 mm 156.17 g 4inx4in photo 365
296 – white smoke
330 – flash
342 – flash
354 – brown
379 – bubbling
385 – flash
420 – charring
445 – black smoke
502 – flickering, cellular flame
655 – edges
736 – thick black smoke at surface
770 – only edge
952 – edge with dancing surface
1132 – burning underneath frame
1320 – dripping

Sample 1 092412-1 (2) 50 kW 10-3-12
8 mm 152.46 g 4inx4in photo 367

237 – white smoke
295 – smoke increase
306 – browning
318 – bubbling of surface
328 – blackening surface
334 – flashes
348 – ignition, cellular flame on surface
372 – black smoke
412 – flame “dancing”, seems to be some edge burning
435 – more surface blackening and intumescence
464 – flame flashing in and out on surface
520 – some signs of edge burning
582 – mostly edge burning 617 – dying down and flickering, small flame, still mostly edge burning
677 – white smoke out of edge frame holes
740 – flame increasing from edge burning, minimal to no surface burn
814 – cellular flames on surface – small predominantly edge burn
936 – increased black smoke
1015 – flame out of hole in edge frame
1044 – flame out of bottom of edge frame, char
1107 – black particles in smoke
1136 – surface seems to be flashing a bit, also edge burn
1217 – more char in air
1239 – only edge burn
1310 – glowing parts of surface

Kreysler 2

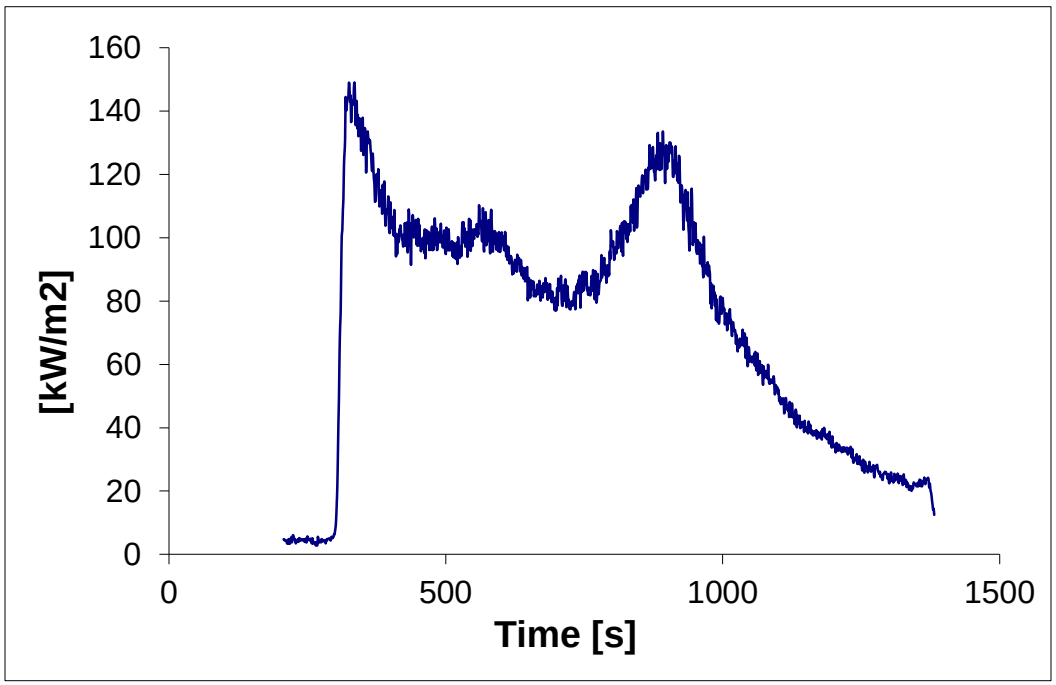

Figure 8: Heat Release Rate per Unit Area Kreysler 2, Test 1

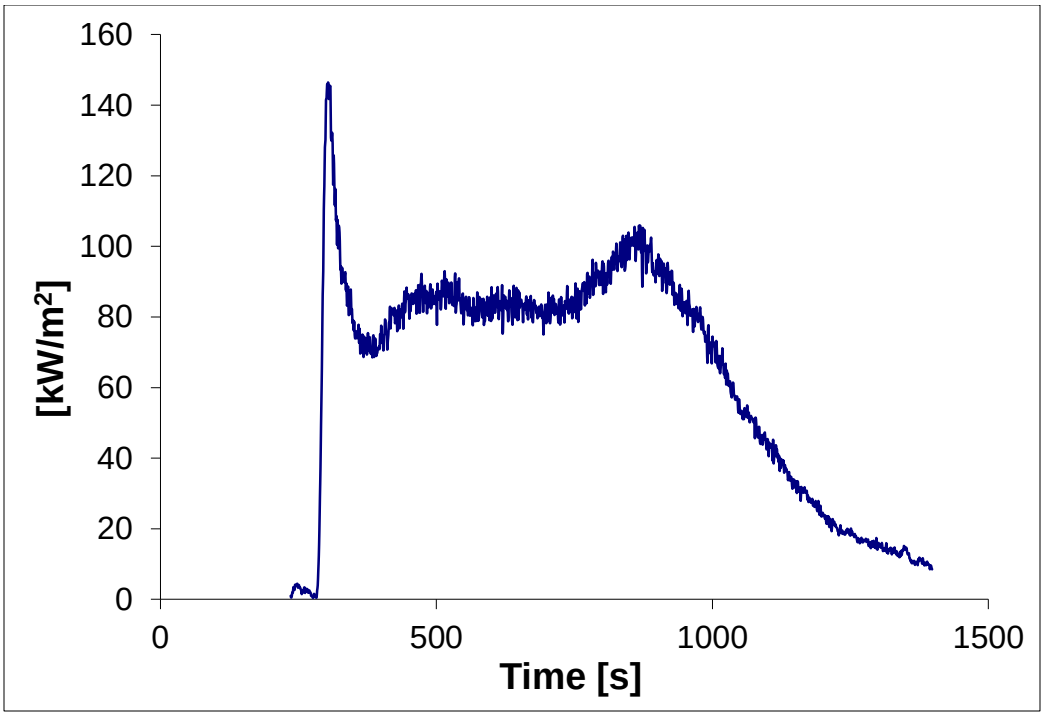

Figure 9: Heat Release Rate per Unit Area Kreysler 2, Test 2

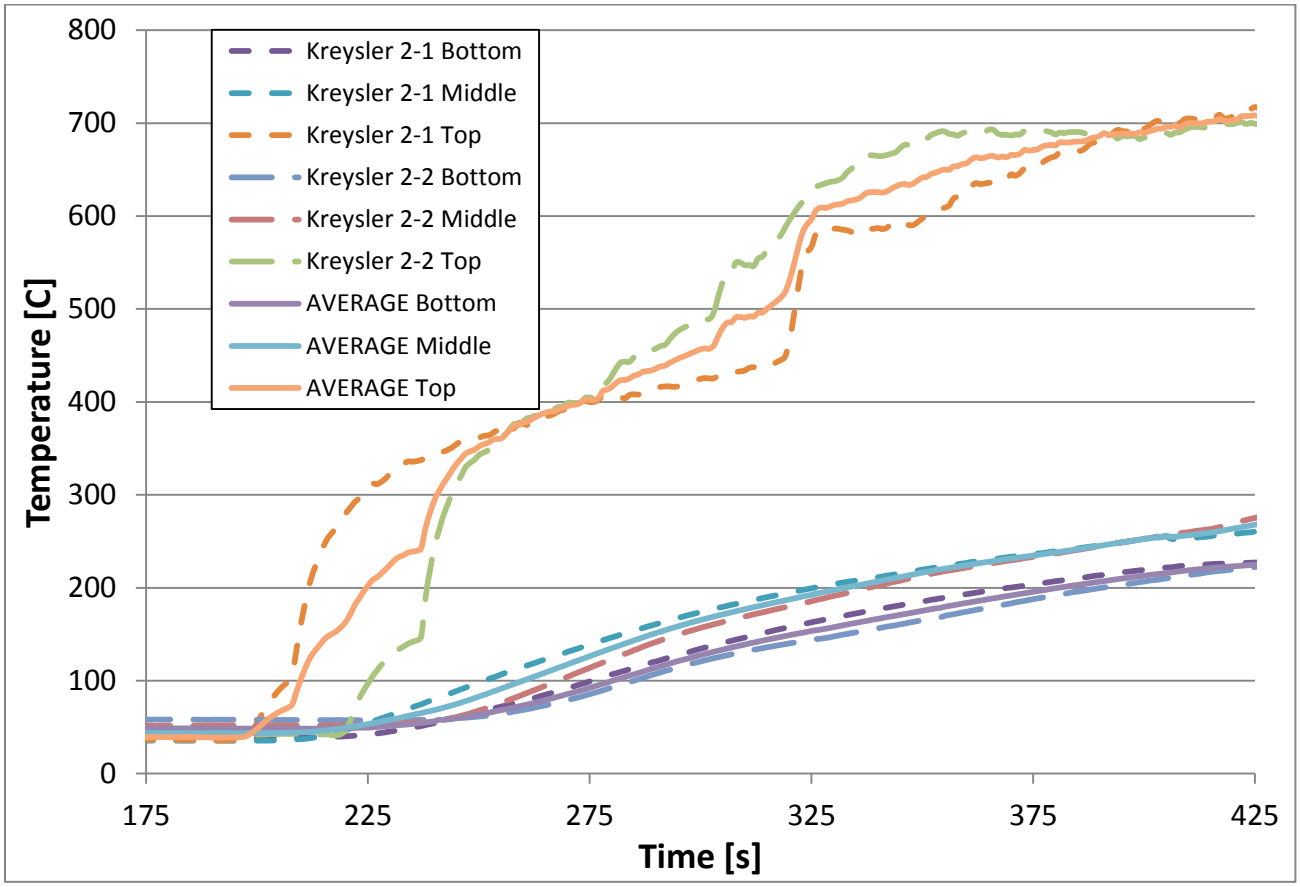

Kreysler 2-1 50 kW/m^2 Top Top 1, E6 Middle 3, L29 Bottom 2
7.94 mm 152.12 g 4inx4in 1/24/13
215 – white smoke
267 – popping sound
309 – surface browning
320 – ignition
343 – cellular flame @ 9 inches above the cone
396 – slight edge burn
489 – smoke coming out of the side of edge frame
653 – mostly edge burn occurring
668 – flame is barely above the cone
828 – flame coming out of side hole
887 – flames flashing from side holes and underneath
1113 – cellular flames surrounding edge of frame

Kreysler 2-2 50 kW/m^2 21 Top 3, E22 Middle 2, S10 Bottom 1
7.72 mm 146.27 g 4inx4in 1/24/13
260 – smoke
280 – cracking surface → lifting TC
305 – ignition
315 – TC back down to surface, flames 6-8 inches above cone
550 – smoke out side holes of frame
630 – edge burning
900 – flames out frame holes on right side
952 – flames out holes on both sides
1160 – all edge burning; flames dwindling

CP 802

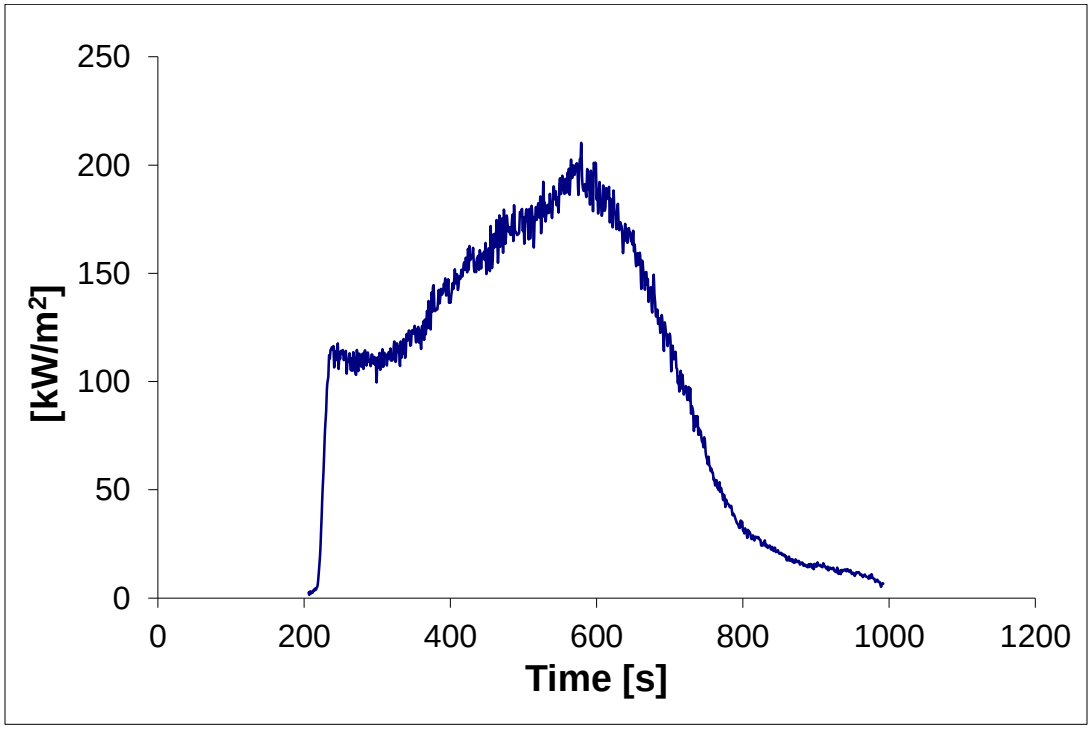

Figure 10: Heat Release Rate per Unit Area CP 802, Test 1

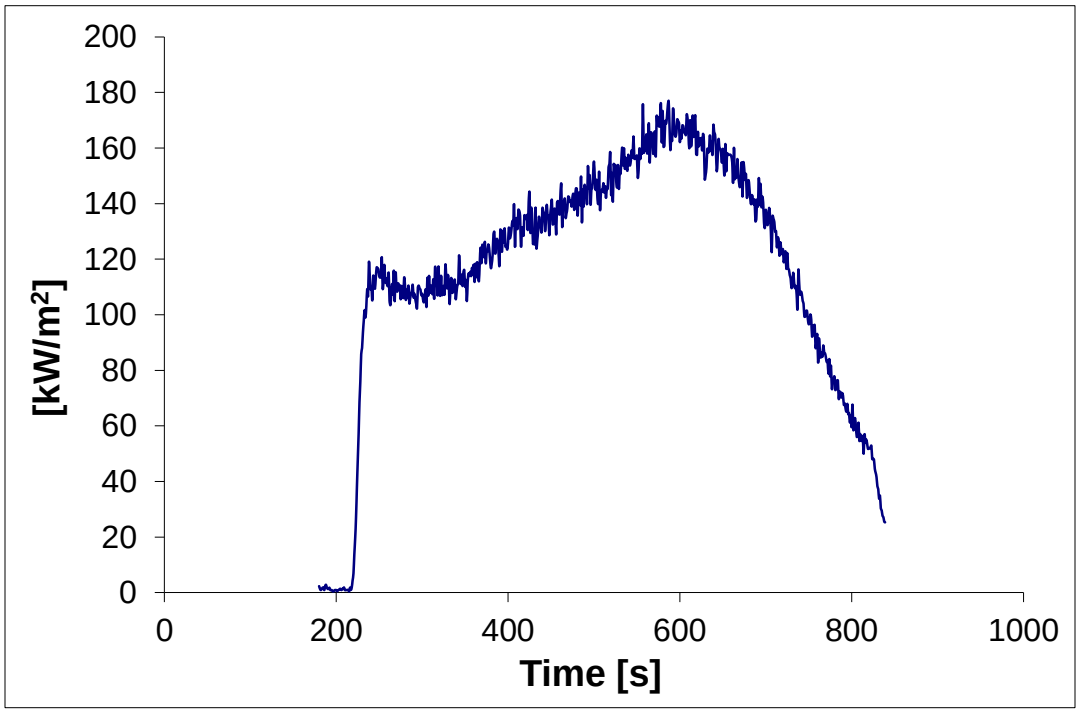

Figure 11: Heat Release Rate per Unit Area CP 802, Test 2

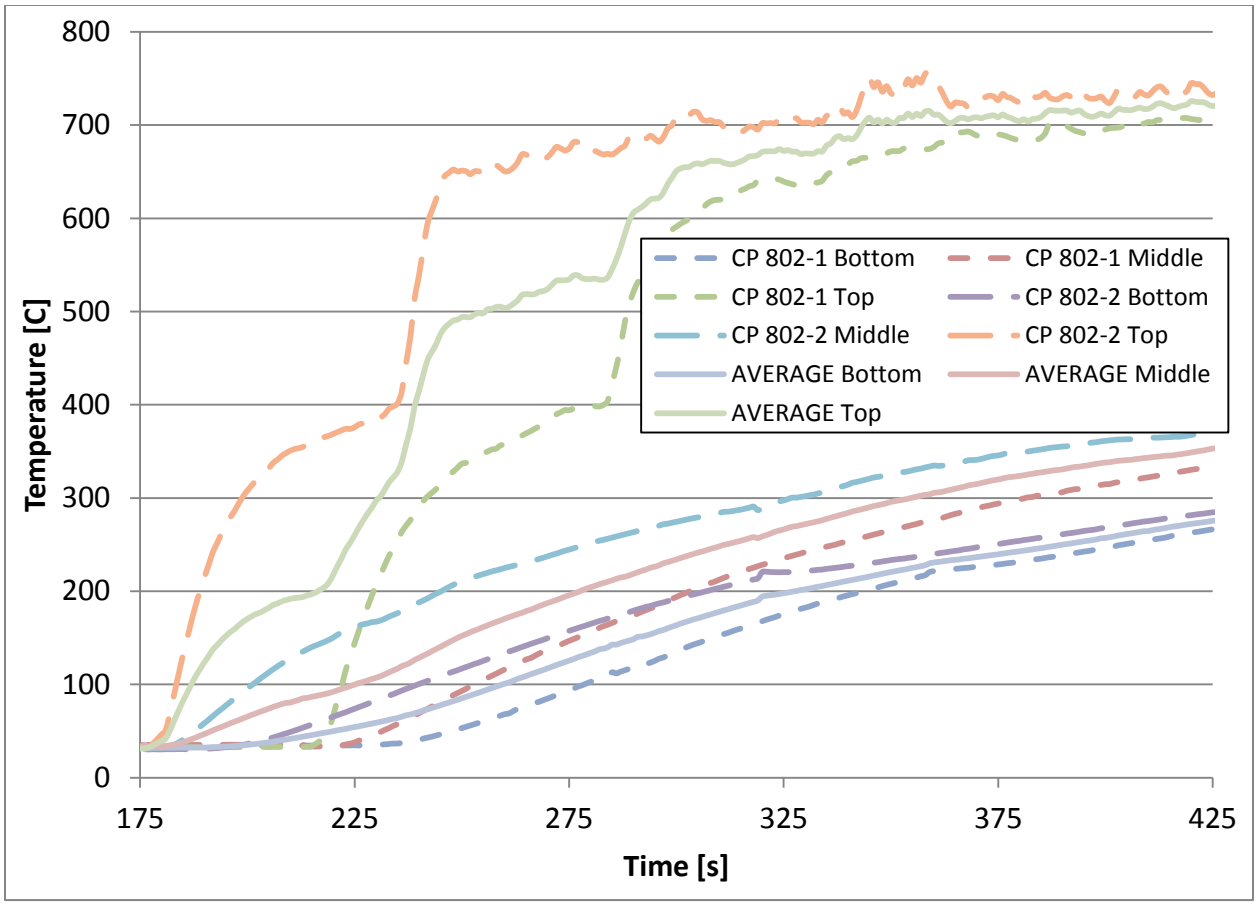

Creative Pultrusion Skin 802 Test 1 50 kW/m^2 10-25_Sample4-1_802_50kW.txt
6.2 mm 112.67 g 4inx4in
200 – white smoke
220 – crackling
230 – flashing until 240\245 – candle flames, black smoke
260 – cellular, then cone flame
270 - ~6-8 inches above cone
420 – flames out sides (off gassing)
500 – a lot of off gassing (side and bottom)
590 – dripping out bottom (where off gassing is)
620 – off gassing on other side too, and bottom all around
650 – flame lower ~3-5 inches
714 – below cone
760 – edge burning (and outside still)
830 – corners, outside holes, small dancing blue flames on edges
899 – top out, little flames from holes, out right after

Creative Pultrusion Skin 802 Test 2 50 kW/m^2 10-25_Sample4-2_802_50kW.txt
6.2 mm 113.70 g 4inx4in
200 – white smoke

220 – crackling
230 – flashing until 240
240 – candle flames
260 – conical ~9-10 inches above cone
440 - ~ a foot
670 – cellular
750 – lower flame ~2-3 inches
880 – corners only, mostly front right
920 – 3 corners, some flickering on edges
950 – 2 corners
990 – 1 corner
1010 – flame out (slight delay in pushing button)

CP 702

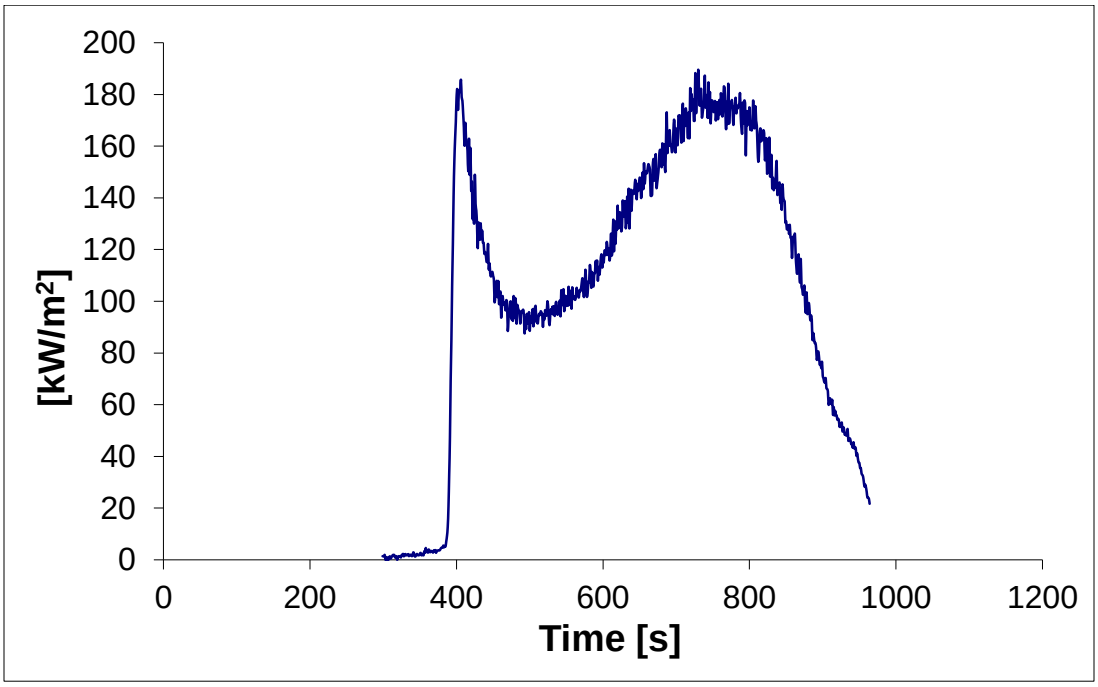

Figure 12: Heat Release Rate per Unit Area CP 702, Test 1

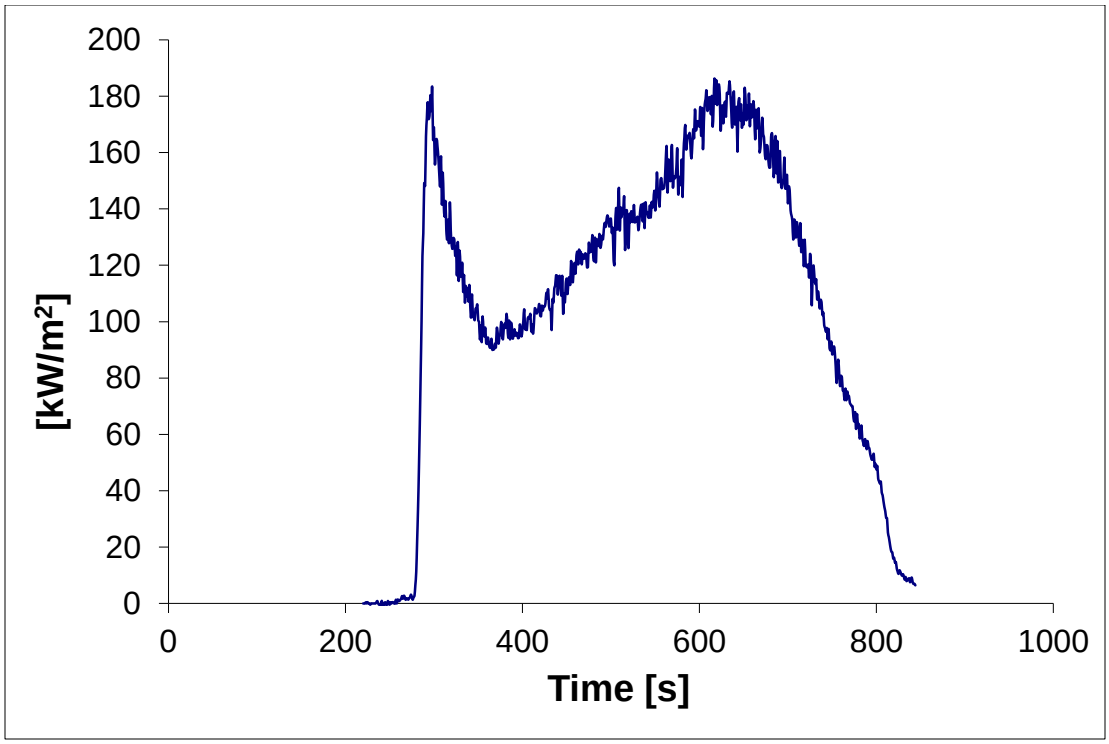

Figure 13: Heat Release Rate per Unit Area CP 702, Test 2

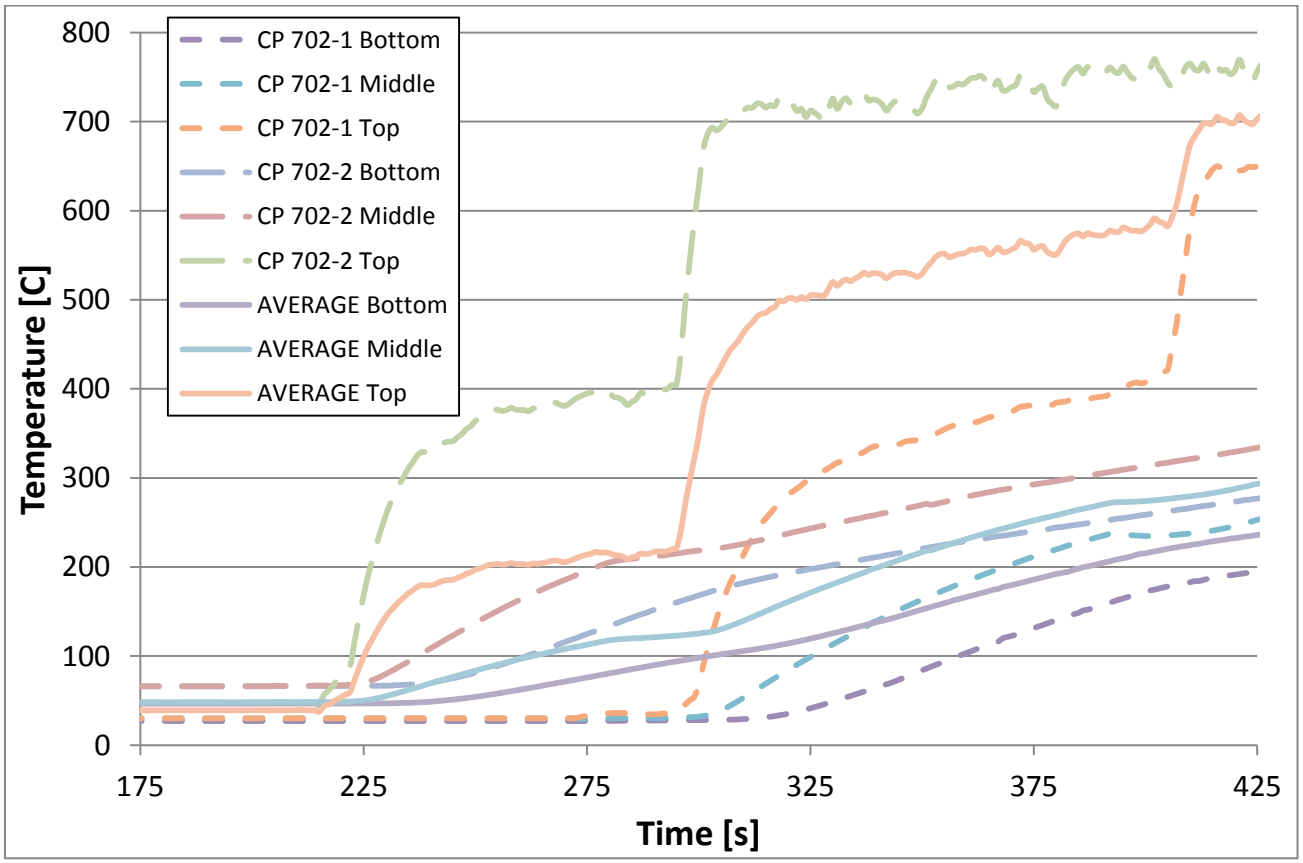

Creative Pultrusion Skin 702 Test 1 50 kW/m^2 10-25_Sample3-1_702_50kW.txt
6.2 mm 114.88 g 4inx4in changed to 10-25_Sample5-1_702_50kW.txt
sparker not in place until ~210 seconds (sorry!)
230 – white smoke
235 – crackling sound
245 – surface blackening a little
265 – flashes until ignition
286 – black smoke, tall flame ~ 8 inches above
290 – conical flame
360 – lower flame ~ 4-6 inches
670 – still the same
770 – lower ~2-4 inches
800 - ~1 inch
815 – left edge and front edge burning, not much else, edge flashing back right
1000 – edge burning in front corners only

Creative Pultrusion Skin 702 Test 2 50 kW/m^2 10-25_Sample3-2_702_50kW.txt
6.2 mm 115.11 g 4inx4in changed to 10-25_Sample5-2_702_50kW.txt
250 – white smoke
265 – crackling noise
280 – flash
295 – flash
317 – cellular (candle flames) (thick black smoke)
340 – conical flame (thick black smoke)
375 – 10” flame (thick black smoke)
418 – becoming cellular (thick black smoke)
432 – conical again (thick black smoke)
470 – side/edge burning
645 – 12” flame, all edges burning
680 – side off gassing
700 – large flame cone
770 – cellular 6” flame
805 – 4 corner edge burning (2” flame)
858 – 3 corner edge burning
895 – black dripping
965 – 2 corner edge burning

CP 286

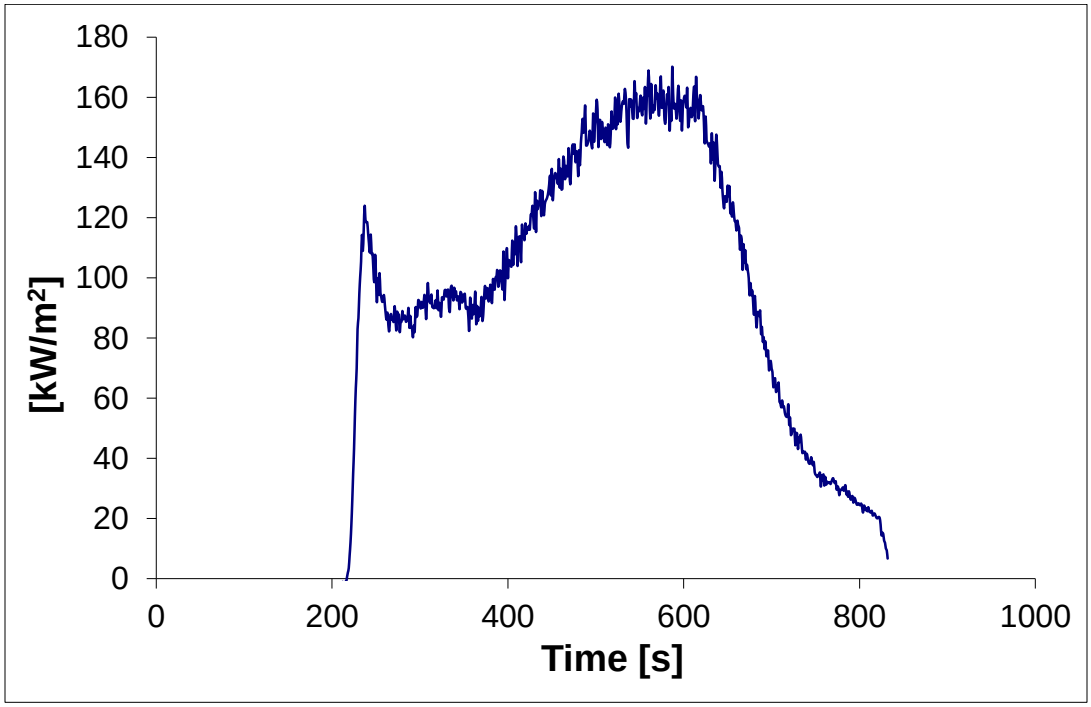

Figure 14: Heat Release Rate per Unit Area CP 286, Test 1

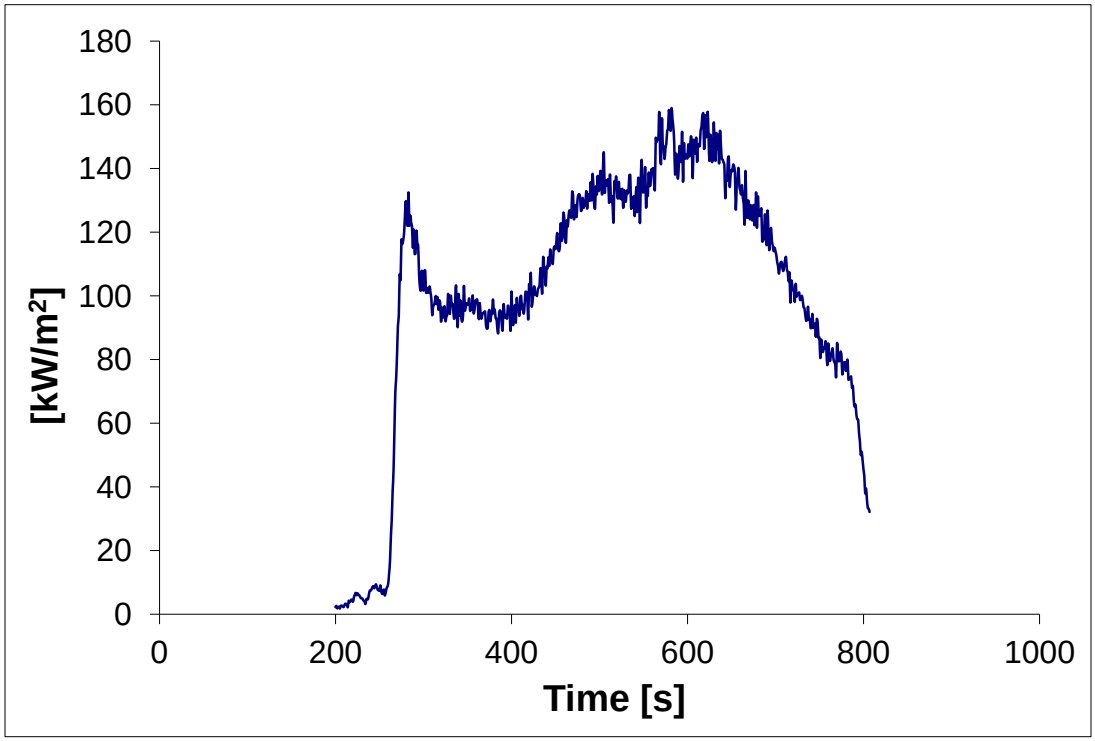

Figure 15: Heat Release Rate per Unit Area CP 286, Test 2

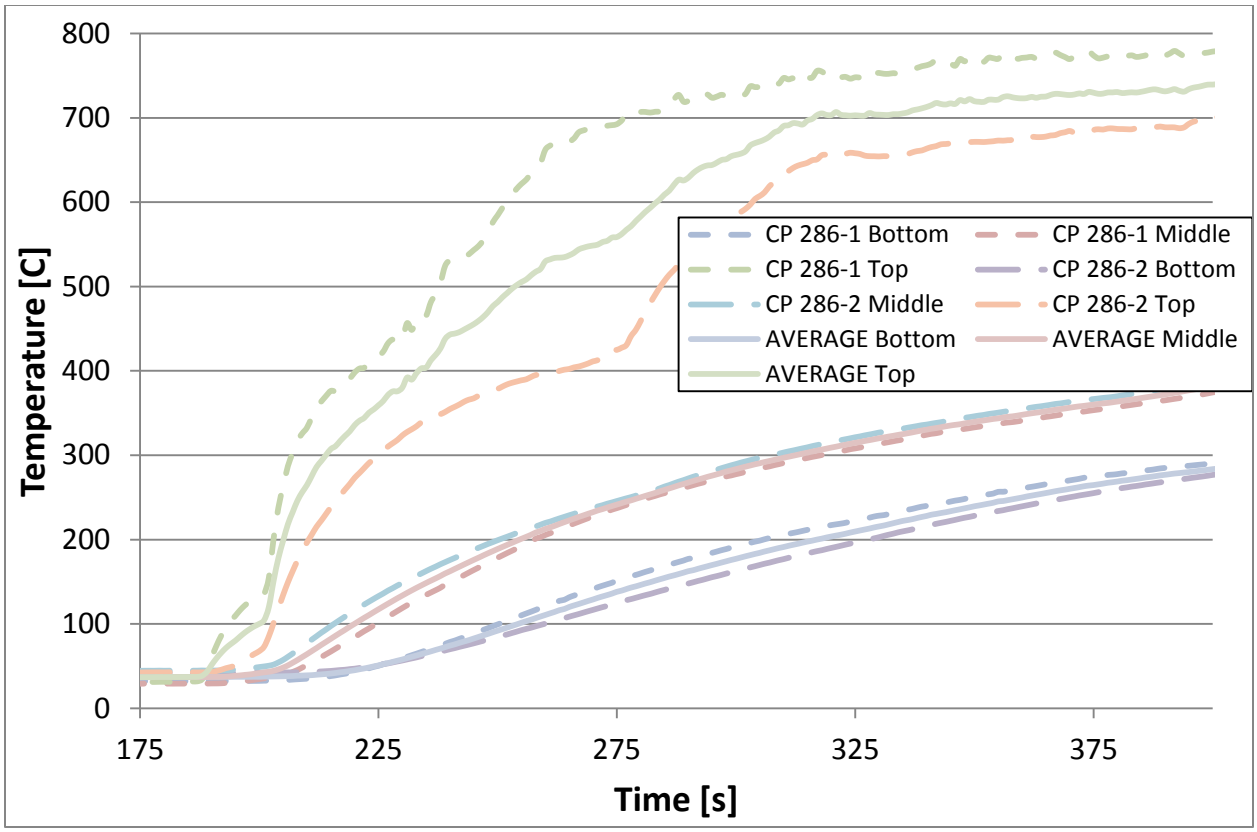

Creative Pultrusion Skin 286 Test 1 50 kW/m^2 10-24_Sample3-1_286_50kW.txt
6.3 mm 116.8 g 4inx4in in CP folder
216 – white smoke
230 – small bubbles in grid form
253 – flashes (very bright)
274 – 8 inch flame above cone top then quickly lowers to 3 inches above cone, also has uniform flame cone, black smoke
334 – some edge burn
464 – smoke from bottom of edge frame
626 – dripping from holder
719 – mostly edge burning, flame even with top of cone
800 – all edge burning

Creative Pultrusion Skin 286 Test 2 50 kW/m^2 10-24_Sample3-2_286_50kW.txt
6.3 mm 116.49 g 4inx4in
250 – white smoke
275 – bubbles over surface (grid)
296 – big bubbles and flashing
319 – uniform flame cone ~ 8 inches above cone and drops to 3 inches quickly
370 – frame lifted up and some edge bunring
550 – white smoke from bottom of edge frame
630 – more edge burning
701 – mostly edge burning, flame still ~ 3 inches above cone
820 – all edge burning